REPORT DOCUMENTATION PAGE			*Form Approved* OMB No. 0704-0188

Public reporting burden for this collection of information is estimated to average 1 hour per response, including the time for reviewing instructions, searching existing data sources, gathering and maintaining the data needed, and completing and reviewing the collection of information. Send comments regarding this burden estimate or any other aspect of this collection of information, including suggestions for reducing this burden, to Washington Headquarters Services, Directorate for Information Operations and Reports, 1215 Jefferson Davis Highway, Suite 1204, Arlington, VA 22202-4302, and to the Office of Management and Budget, Paperwork Reduction Project (0704-0188), Washington, DC 20503.

1. AGENCY USE ONLY (*Leave Blank*)	2. REPORT DATE 12/1/2007	3. REPORT TYPE AND DATES COVERED Final Technical 11/1/06 – 10/31/07	
4. TITLE AND SUBTITLE Distributed Propulsion: New Opportunities for an Old Concept			5. FUNDING NUMBERS Contract HR001-07-C-0005
6. AUTHORS Epstein, Alan H.			
7. PERFORMING ORGANIZATION NAME(S) AND ADDRESS(ES) Massachusetts Institute of Technology 77 Massachusetts Ave., 31-264 Cambridge, MA 02139			8. PERFORMING ORGANIZATION REPORT NUMBER
9. SPONSORING / MONITORING AGENCY NAME(S) AND ADDRESS(ES) Defense Advanced Research Projects Agency 3701 N. Fairfax Drive Arlington, VA 22203-1714			10. SPONSORING / MONITORING AGENCY REPORT NUMBER

11. SUPPLEMENTARY NOTES

The views and conclusions contained in this document are those of the authors and should not be interpreted as representing the official policies, either expressly or implied, of the Defense Advanced Research Projects Agency or the U.S. Government.

12a. DISTRIBUTION / AVAILABILITY STATEMENT Approved for public release, distribution unlimited	12b. DISTRIBUTION CODE

13. ABSTRACT (*Maximum 200 words*)

Distributed propulsion can be broadly defined as distributing the airflows and forces generated by the propulsion system about an aircraft in such a way as to improve the vehicle's aerodynamics, propulsive efficiency, structural efficiency, and aeroelasticity. The confluence of several synergistic factors with recent technical developments suggests distributed propulsion may now yield both new capabilities and new economics for military flight vehicles. Over a 12 month period, this study explored the potential for distributed propulsion combined with pneumatic aerodynamics and flow control to enable new capabilities and new economics for military air vehicles. Aircraft and gas turbine designs focused on an ESTOL application (100m takeoff run, for a nominally C-27 size aircraft). Study outputs include: a quantification of distributed propulsion benefits such as enabling new mission capabilities and improving performance, reliability, and cost; a conceptual design of a distributed propulsion air vehicle; a conceptual design of small engines optimized for distributed propulsion; and delineation of the technical barriers that must be overcome to realize distributed propulsion aircraft, and candidate plans for overcoming such barriers.

Propulsion systems, propulsive efficiency, flow control			15. NUMBER OF PAGES 12
			16. PRICE CODE
17. SECURITY CLASSIFICATION OF REPORT UNCLASSIFIED	18. SECURITY CLASSIFICATION OF THIS PAGE UNCLASSIFIED	19. SECURITY CLASSIFICATION OF ABSTRACT UNCLASSIFIED	20. LIMITATION OF ABSTRACT UL

NSN 7540-01-280-5500

Standard Form 298 (Rev. 2-89)
Prescribed by ANSI Std. Z39-1298-102

Gas Turbine Laboratory
Department of Aeronautics and Astronautics
Massachusetts Institute of Technology
Cambridge, MA 02139

Final Technical Report

on DARPA Contract #HR0011-07-C-0005

entitled

DISTRIBUTED PROPULSION: NEW OPPORTUNITIES FOR AN OLD
CONCEPT

submitted to

PRINICIPAL
INVESTIGATOR: Alan. H. Epstein (PI)
                     R.C. Maclaurin Professor of Aeronautics and Astronautics
                     Director, Gas Turbine Laboratory

December 2007

<u>Overall Program and Objectives</u>:

Distributed propulsion can be broadly defined as distributing the airflows and forces generated by the propulsion system about an aircraft in such a way as to improve the vehicle's aerodynamics, propulsive efficiency, structural efficiency, and aeroelasticity. The confluence of several synergistic factors with recent technical developments suggests distributed propulsion may now yield both new capabilities and new economics for military flight vehicles. Over a 12 month period, this study explored the potential for distributed propulsion combined with pneumatic aerodynamics and flow control to enable new capabilities and new economics for military air vehicles.   Aircraft and gas turbine designs were focused on ESTOL applications (100m takeoff run, for a nominally C-27 size aircraft). Study outputs include: a quantification of distributed propulsion benefits such as enabling new mission capabilities and improving performance, reliability, and cost; a conceptual design of a distributed propulsion air vehicle; a conceptual design of small engines optimized for distributed propulsion; and delineation of the technical barriers that must be overcome to realize distributed propulsion aircraft, and candidate plans for overcoming such barriers.

The final technical report is divided into three sections: the main body which contains of all the important technical findings; Appendix A, the final report from subcontractor Dr. Robert Engler of the Georgia Institute of Technology; and Appendix B, the MIT SM thesis by Nicholas Chan whose work were supported under this contract.

Distributed Propulsion
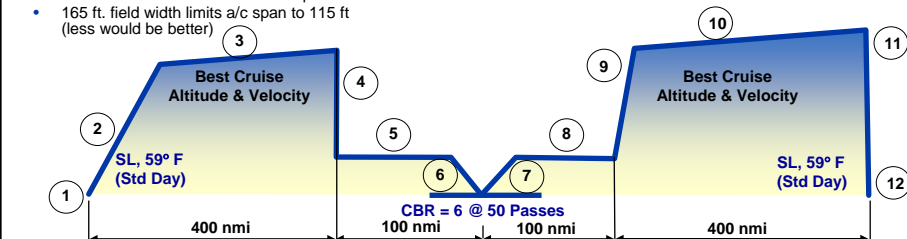
August 8, 2007 Review

Rich Ouellette

Flight Sciences, Advanced Design
Desk.714.896.1708
Cell.714.625.6502

Mission Guidelines Reflect Military CONOP

Boeing Technology | **Phantom Works**   **Air Vehicle Technology Enabled Concepts**

1. Takeoff prepared runway
   - 12,000 pounds payload
     → One HMMWV (12,000 lb) or 20 or more soldiers
   - Allowances: SLS, 5 min warm-up, taxi, takeoff
2. Climb & accelerate
3. Ingress cruise
   - 400 nm at best cruise Mach/Altitude (0.5M – 0.6M) pressurized to 9,000 ft
4. Decent (no distance of fuel credit)
5. Low altitude cruise
   - 100 nm, low altitude, best speed
6. Mid-Mission landing
   - Austere/soccer filed < 300ft ground roll
   - 40% thrust reverser effectiveness presumed
   - 165 ft. field width limits a/c span to 115 ft (less would be better)

7. Mid-Mission takeoff
   - 5,000 lb payload
   - < 300 ft austere field takeoff
     Balanced field length (over 50 ft obstacle) will be defined with all engines operating, 0.5g, 5k, 95°F
   - 5 min. maneuver & taxi takeoff allowances
8. Egress cruise
   - 100 nm, low altitude, best speed
9. Climb & accelerate
10. Egress cruise
    - 400 nm at best cruise Mach/Altitude (0.5M – 0.6M)
11. Decent (no distance of fuel credit)
12. Land on prepared field
    - 5% fuel reserve

page 2

Assumptions: Configuration

Passenger Capability
- Maximize
- 20 inch safety aisle in front, 14" side
- No considerations for litters

Cargo restraint:
- Longitudinal Requirement: 3g forward, 1.5g aft
- Lateral Requirement: 1.5g
- Vertical Requirement: 2g up, 4.5g down

Loadmaster

Nominal tie-down rings

Ramp toes/angle < 9 degrees

No rapid RORO or reconfiguration

No cockpit cargo bay (day/night) cameras

No cargo floor winch

No loaded ramp

No airdrop h/w

Assumptions : Aero/Propulsion

MIT/GTRI provides all high lift aero performance
- "Ideal" aerodynamic conditions presumed
- No provisions for 3D aero effects
  - Span wise flow, non-linear circulation, separations, boundary layer, hysteresis, etc.
  - Homogeneous flow conditions at exit plane

MIT provides all engine performance
- Bleed, horsepower extraction, recovery
- No provisions for engine operability
  - No FOD prevention
  - No turbulence or distortion
  - No inlet/exhaust separations/losses
  - No cross talk effects on surge margins
  - No boundary layer treatments/considerations
  - No limitations on throttle range of micro-turbines
  - No "non-linear" behaviors (secondary +/or tertiary circulation regions)
- No considerations for power takeoff, gearboxes, or AMAD
- No considerations for blade-out (shielding, fratricide, etc.)
- No considerations for fire bay extinguishers
- No provisions for noise

Analysis: Stability & Control (guidelines, no analyses done)

Longitudinal Static Stability
- Aircraft < 5% unstable
  - If unstable, time-double-amplitude < 1 second

Directional Static Stability
  - If unstable, time-double-amplitude < 1 second

Longitudinal Trim Over CG Range
- From V_{min}* to V_{mo}/M_{mo} , No consideration w/r to engine-out conditions in this case study

Lateral/Directional trim
- No consideration for critical engine(s) out over design cg or speed range

Maneuver Control Power:
- Angular accelerations per Boeing Best Practices
- Takeoff: Conventional takeoff rotation, minimum pitch angular acceleration > 3 deg/sec^2 with the most critical pitch control effector failed.
- Crosswind (typical): 35 knot direct crosswinds, side gusts < 10-knots.
  Takeoff/Landing: 25-knot direct crosswinds, side gusts < 10-knot side
  (no considerations for critical engine out in this study)

Assumptions : Mass Property

Qualitative Technology Readiness Levels shall be 6 by 2010

Advanced Design methods/philosophies will be used
- Proprietary databases or methods will not be detailed
- Vehicle level contingencies will be identified where applicable.

Operating Weight Empty cg will be within reasonable cg envelope

Loadable flat floor lengths

> 10% for the 2.25g maximum payload mission
> 16% for the 2.5g maximum payload mission
> 25% for the 3.0g maximum payload mission

OWE will include nominal considerations for tie down devices

Sized to 2.5g

Nominal consideration for high flotation landing gear as (CBR, sink rate)

NO Provisions for …
- Hi-Lo-Lo-Hi penetration (e.g. discrete gusts)
- Tactical Descent
- Load stabilizing

Assumptions: Field Conditions

DP study will use best practices
- Ignore FOD
- Nominal landing gear
- Determine balanced field length,
  but not be constrained by it.

**SOF soccer fields are
not typically like this**

**But more
like this**

Soccer Field Surface Conditions
CBR 4-10 (Moist to Soaked Soil)
CBR 5 (soft turf)
μ_{roll}　= 0.07
μ_{brake} = 0.25

Assumptions: Tactical Operation

Mid-Mission
- No considerations for engine failure
- Instantaneous braking and 40% net effective reverse thrust on dry grass

Austere Field
- Operations on surfaces CBR = 6 or better at 50 passes
  - Landing gear width compatible with 50 ft. wide road
  - Rough field (8" bump over 6 inches, 8" hole over 18 inches)
- No FOD protection or considerations
- APU to support austere ground operations

Maneuvering
- No considerations for reverse taxiing
- No considerations for 180 degree turn

Assumptions: Performance

Cruise Speed/Altitudes
- Best for maximum range
  - Pressurized to 9,000 ft.
- No considerations for maximum endurance (loiter speeds)

No Aerial Refueling

Atmosphere
- Hot/High & standard

Assault Rules
- No engine out/critical field length (Mil-C-005011B considerations)

Landing
- Distance from 50ft obstacle to stop (Mil-C-005011B)
- No dispersion allowance using flare-cue HUD

Assumptions: ILITIES

Survivability:
- Upper/Mid propulsion installation
- No considerations to meet Mil-Std Class B kill survivability
  - 23mm nor 30mm High Explosive Incendiary ammunition
- No provision for microwave/laser (IR) self defense system
- No other specific stealth devices or considerations
- No tactical descent

Susceptibility
- No considerations for signature control, defensive systems, nor performance/tactics

Vulnerability
- No specific considerations to insure recovery & continued flight after attack/damage

RM&S
- No specific considerations (doors, etc.) for accessibility features
- No consideration for mission capability rates
- No considerations for MMH/FH

Assumptions: Subsystems (not specifically addressed)

Environmental, Electrical, Hydraulic, Fuel Capabilities:
- Complete mission requirements
- Maintain cabin altitude of 9,000 ft. at maximum cruising altitude
- Sufficient avionics cooling capacity
- Nominal consideration to conduct airborne fuel dumping operations
- Not capable of single point or over-wing refueling operations

All-Weather Capability
- Nominal considerations for rain & ice protection/removal
- Operations in all weather conditions excluding thunderstorm related weather

Avionics and Sensors:
- Basic fraction: Major elements can be listed

Environmental System
- Standard ECS
- no provisions for NBC or filtered air

Assumptions: Miscellaneous

Oxygen
- Sufficient capability to meet military specification
- No individual outlets for HALO paratroop pre-breathing

Emergency Egress
- Meet military specifications

Passenger Capability
- Maximize number with seating on 24 inch centers

Litter Patients
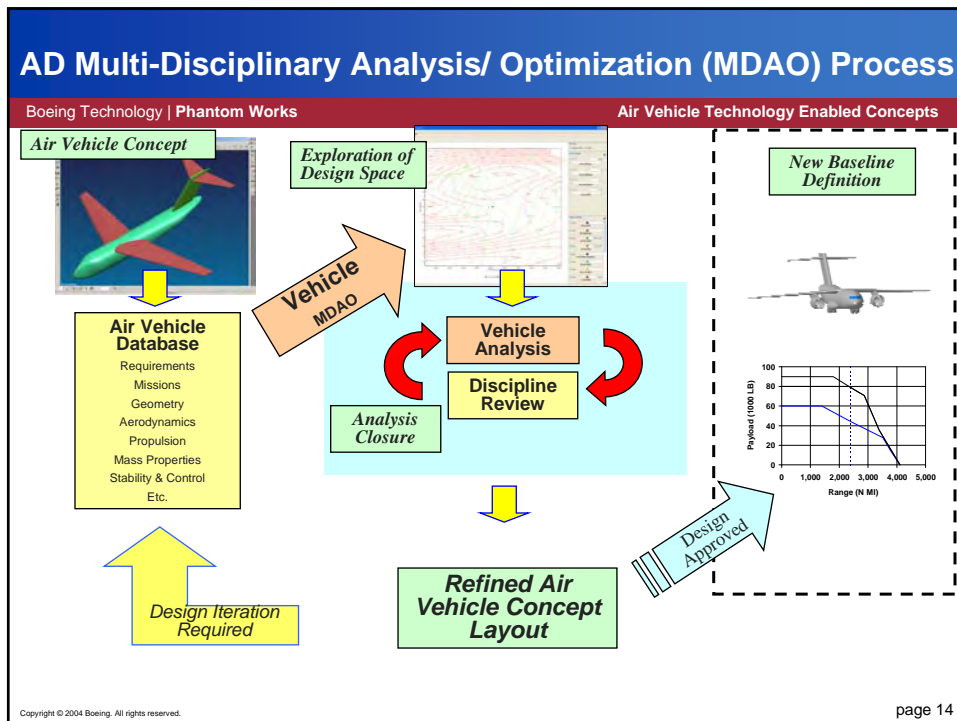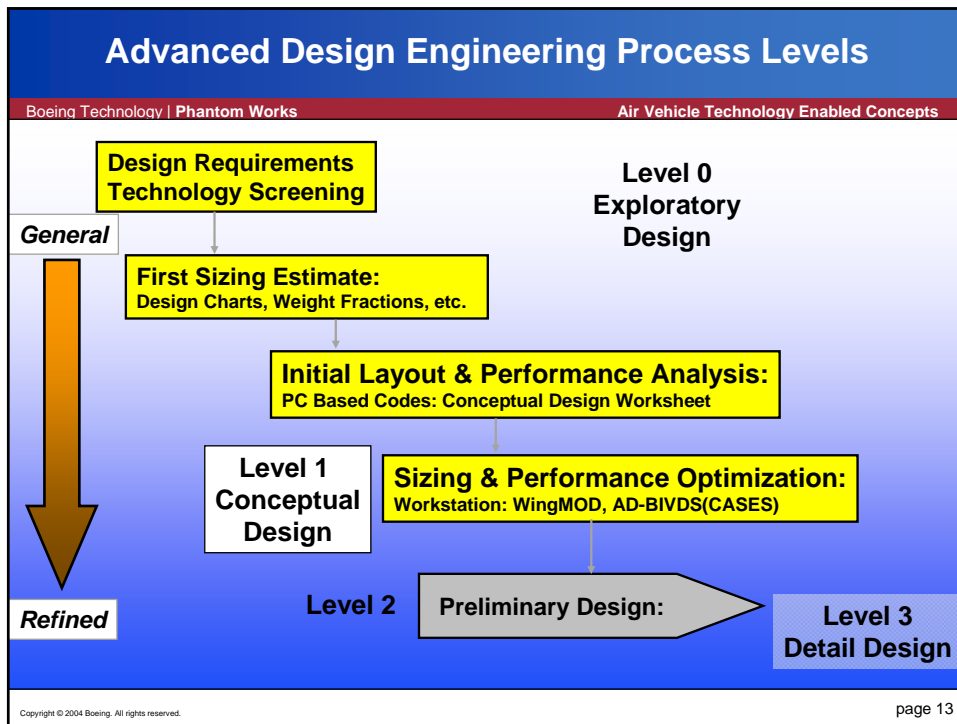- No considerations for litters

Other
- No consideration for ground refueling vendor to military vehicles/bladders
- No consideration to complete mission with single tire failure
- No consideration to meet stage 4 noise requirements
- No consideration to operate from ICAO airfields

Cost Goal:
- No consideration for average unit flyaway cost

Advanced Design Engineering Process Levels

Design Requirements Technology Screening

General

Level 0 Exploratory Design

First Sizing Estimate: Design Charts, Weight Fractions, etc.

Initial Layout & Performance Analysis: PC Based Codes: Conceptual Design Worksheet

Level 1 Conceptual Design

Sizing & Performance Optimization: Workstation: WingMOD, AD-BIVDS(CASES)

Refined

Level 2   **Preliminary Design:**   **Level 3 Detail Design**

AD Multi-Disciplinary Analysis/ Optimization (MDAO) Process

Air Vehicle Concept

Exploration of Design Space

New Baseline Definition

Vehicle MDAO

Air Vehicle Database
Requirements
Missions
Geometry
Aerodynamics
Propulsion
Mass Properties
Stability & Control
Etc.

Vehicle Analysis

Discipline Review

Analysis Closure

Design Approved

Payload (1000 LB)

Range (N MI)

Design Iteration Required

Refined Air Vehicle Concept Layout

Advanced Design Integrated Tool Suite
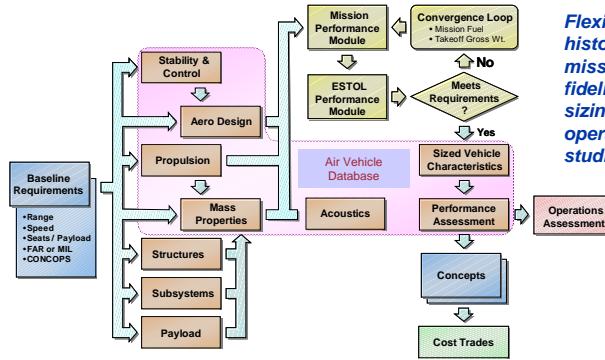
Flexible FAR and military time-history takeoff, flight path, and mission modeling allows higher fidelity evaluation of vehicle sizing, and off-design concept of operations (CONOPS) trade studies
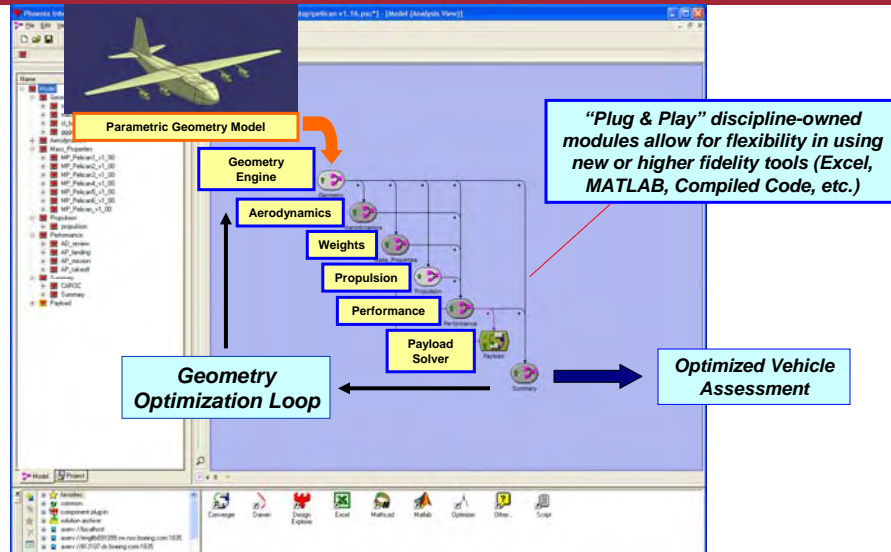
- *Discipline modules represent the best practices of the Boeing Company*
- *Multi-level design tools used extensively in military and commercial AD activities*
- *Common configuration database*
- *Additional modules can be added for analysis of complex vehicles*

Integrated multi-disciplinary analysis network for the rapid synthesis and assessment of new or derivative air vehicles at conceptual design level or higher

Conceptual Design MDAO (Level 1+) Supported with Higher Fidelity Configuration Models and Analysis Tools

"Plug & Play" discipline-owned modules allow for flexibility in using new or higher fidelity tools (Excel, MATLAB, Compiled Code, etc.)

Geometry Optimization Loop

Optimized Vehicle Assessment

Data Explorer: Geometry Parameter Influence on Design

Ability to display the influence of each variable upon another allows the design team to identify and address the most critical parameters
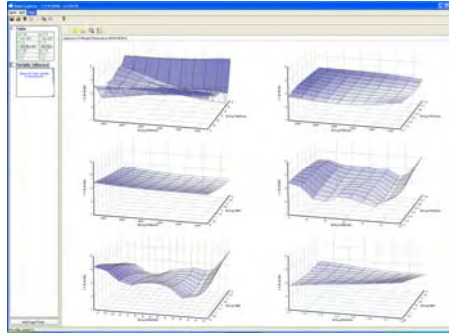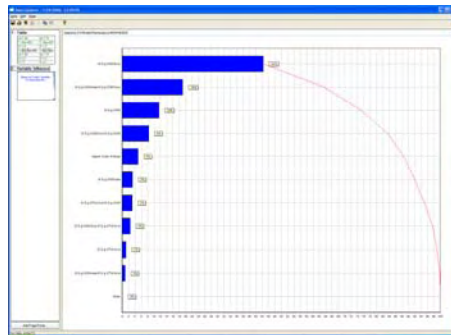
3-D response surfaces of parameters help to quickly illustrate the nature of relationships between them
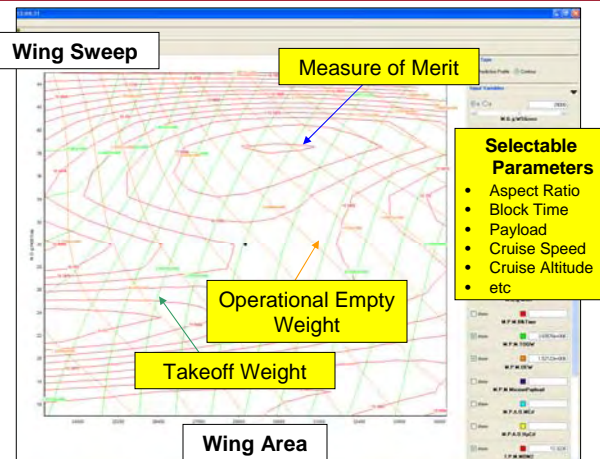

Data Explorer: The Design Space & Requirements Space

Wing Sweep

Measure of Merit

Selectable Parameters
- Aspect Ratio
- Block Time
- Payload
- Cruise Speed
- Cruise Altitude
- etc

Operational Empty Weight

Takeoff Weight

Wing Area

Easy to view trends across multiple dimensions

3-D Snapshots are manipulated by changing other inputs with slider bars.

Simple control of input / output graphical display

Engineering team now has unprecedented access to explore complex design spaces
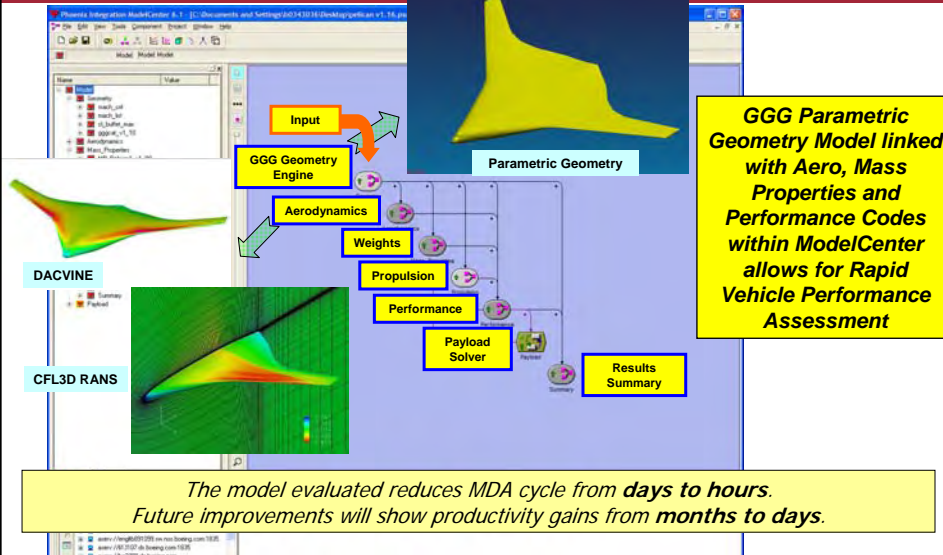
Integrating and Automating Tools and Processes Continues to Transform the FEOB

Input

GGG Geometry Engine

Parametric Geometry

Aerodynamics

Weights

Propulsion

Performance

Payload Solver

Results Summary

DACVINE

CFL3D RANS

GGG Parametric Geometry Model linked with Aero, Mass Properties and Performance Codes within ModelCenter allows for Rapid Vehicle Performance Assessment

*The model evaluated reduces MDA cycle from **days to hours**. Future improvements will show productivity gains from **months to days**.*

High-Lift Configuration Maturation

DP10 Performance

TP01 Fielding

RP02 LO/Austere

RP10 USMC

BWB Distributed propulsion Study

End-user needs
- RCS, IR, Acoustics
- Austere, FOD, hot gas
- 300' takeoff/landing, thrust reverse

Potential refinements
- Thin top/forward wing section
- Sharpen upper lip
- Raise aft/lower exhaust
- Consider "no cost" sweep
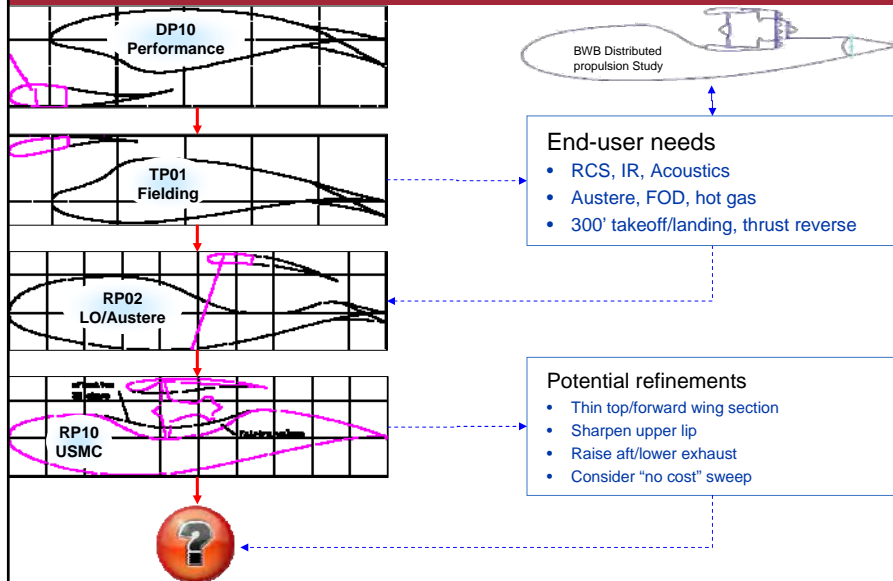
Initial DP10 Configuration

10' 9"

75 feet

115 feet
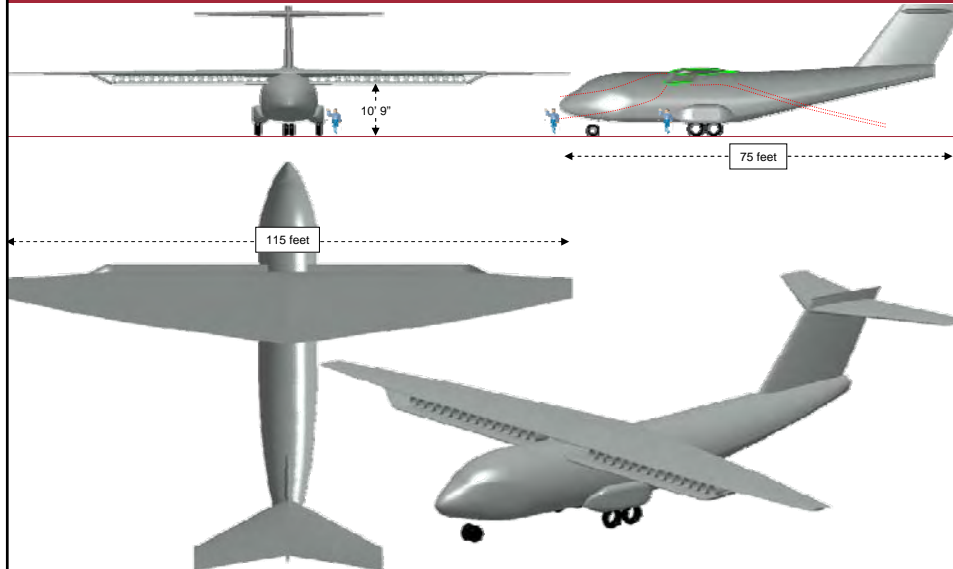
Parasol Variant Studied

RP06 configuration
• Potential means to reduce span

Wing span: 114' 11"
Fuse Length: 75' 4"
OA Length: 83' 9"

Baseline: Configuration

Wing span: 114' 11"
Fuse Length: 75' 4"
OA Length: 83' 9"

115 feet

10' 9"

75 feet
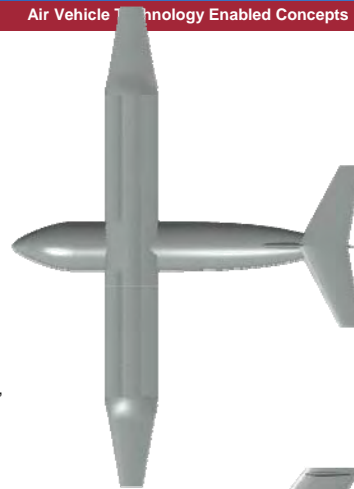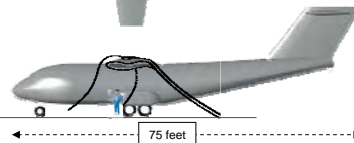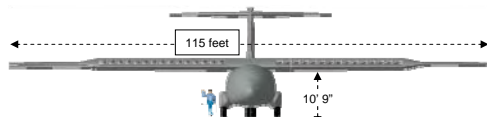
Baseline: Initial Design
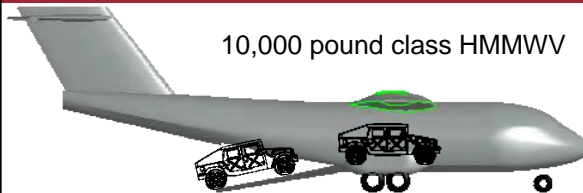
10,000 pound class HMMWV

or 33 troops (8,250lb.)

Curb Weight (Note 1)	6,780 lbs.	3,075 kg.
Payload (Notes 1&2)	3,520 lbs.	1,597 kg.
Gross Vehicle Weight (GVW)	10,300 lbs.	4,672 kg.
Gross Axle Weight Rating:		
Front	4,500 lbs.	2,041 kg.
Rear	6,500 lbs.	2,948 kg.
Length (Note 1)	190.5 in.	4.84 m.
Height (w/o weapons)	74 in.	1.88 m.
Min. Reducible Height	72 in.	1.83 m.
Reduced Shipping Cube	683 ft.³	19.3 m.³
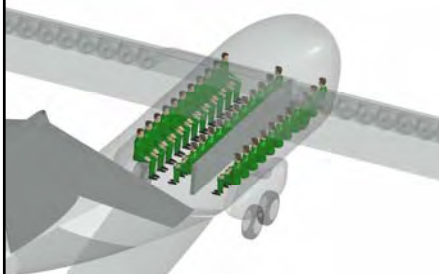
Comparison of Baseline to Other Transports

	C-212-300	CN-235	V-22 (STOL)	C-27J	BASELINE	C-130
TOGW	17,857 lb	36,376 lb	57,000 lb	70,107	85,600 lb	164,000 lb
Max Fuel	n/a	1,378 gal	1,448 gal	3,255 gal	1,350 gal	7,285 gal
Payload (pax)	4,500 lb (17)	13,227 lb (57)	10K (25)	22K lb (68)	10K lb (33)	41,790 lb (92)
Span	62' 4"	84' 8"	83.7'	94.2'	115'	132' 7"
Max. Cruise	200 kts	246 kts	250 kts	250 kts	> 300 kts	348 ktas
Take-off (50')	2,936'	2,475´	300' (est.)	1,800' (est.)	300' (est.)	4,700'
Landing (50')	2,837'	1,979´	600' (est.)	1,800' (est.)	500' (est.)	2,550'
Combat range	233 nm	700 nm	~650 nm	1,000 nm	1,000 nm	2,832 nm

page 25

CN-235 and C-212 Statistics

CN-235

Specs
- Span   84' 8"
- Length   70' 2"
- Pressurized Cabin
  - Length   31´ 8"
  - Cabin Height   6´ 3"
  - Cabin Width   8´ 11"
- Payload   13,227 lb. / 57 Troops

Performance
- Max. Cruise   246 ktas
- Take-off Dist.   2,475´ (SL/ISA MTOW@50')
- Landing Dist.   1,979´ (SL/ISA MTOW@50')
- STOL   n/a
- Combat range   700 nm (w/max p/l)
- Ext'd range   n/a
- Max fuel   2,700 nm (ferry)

Weights
- Max mil TOGW   36,376 lb
- Max Fuel   1,378 Gal

C-212-300

Specs
- Span   62' 4"
- Length   49' 9"
- Pressurized Cabin
  - Length   n/a
  - Cabin Height   n/a
  - Cabin Width   n/a
- Payload   18 Troops (4500 lb est.)

Performance
- Max. Cruise   200 ktas
- Take-off Dist.   2,936´ (SL/ISA MTOW@50')
- Landing Dist.   2,837´ (SL/ISA MTOW@50')
- STOL   n/a
- Combat range   233 nm (w/max p/l)
- Ext'd range   800 nm (w/4400 lb)
- Max fuel   1,100 nm (est.)

Weights
- Max mil TOGW   17,857 lb
- Max Fuel   n/a Gal

page 26

Configuration Concerns

Engine Size
- PW615 form factor doesn't fit in RP-06 envelope
- No upper wing skin continuity, biplane style structure may be required
- Accessory size significant for small engines
- Most of wing section not usable for fuel
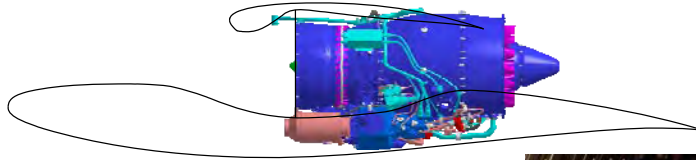
Acceleration / Deceleration Human Factors
- Large acceleration and deceleration may require passengers to face forward/aft with multi-point harnesses instead of sidewall seats with lap belts. This reduces aircraft flexibility substantially.

Configuration Concerns (continued)

No airdrop provisions

High flotation tire pressure (tire life and hard surface compatibility)

Fuel volume / tank arrangement (little volume in wing)

Survivability

LE / TE blowing ducts (high temperature ducts in fuel bay)

Conclusions

Substantially more wing area required
- Fit engine and accessories
- Fuel volume
- Adequate structure

DP aircraft carries 25% less payload, and weighs 2.5 times more than CN-235

Analysis: Aero Method (guidelines)

Low Speed
- Conceptual
  - Design charts
  - Flight derived increments
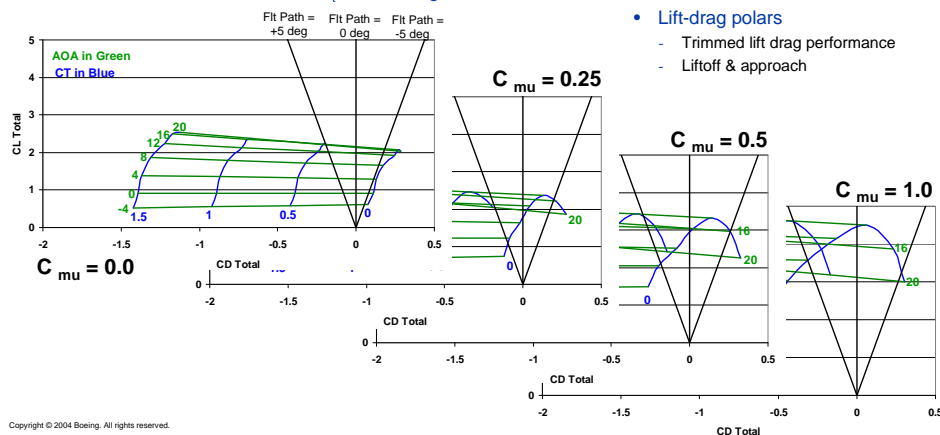 - In-House database
  - CASES direct input

High Speed Drag

$CD = CD_o + CD_i + CD_c + CD_t$

CD_o : Parasite Drag

CD_i : Induced Drag

CD_c : Compressibility Drag

CD_t : Trim Drag
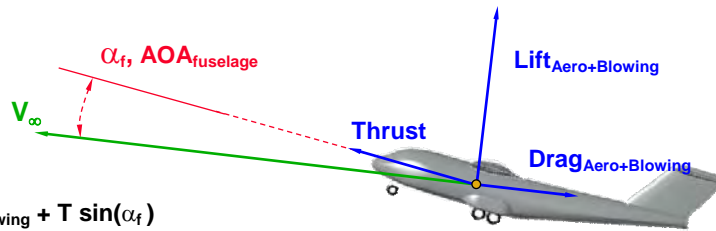
Define Level 1 parameters
- Takeoff & Landing geometry
- Critical engine inoperative
- Takeoff (VLO)
- Approach
- Power-on stall
- Lift-drag polars
  - Trimmed lift drag performance
  - Liftoff & approach

α_f, **AOA$_{fuselage}$**

V$_\infty$

Lift$_{Aero+Blowing}$

Thrust

Drag$_{Aero+Blowing}$

L $_{Total}$ = L $_{Aero + Blowing}$ + T sin(α_f)

Divide by q $_\infty$ S $_w$

C$_{L\ Total}$ = C$_{L\ Aero + Blowing}$ + C$_T$ sin (α_f)

D $_{Total}$ = D $_{Aero + Blowing}$ - T cos(α_f)

Divide by q $_\infty$ S $_w$

C$_{D\ Total}$ = C$_{D\ Aero + Blowing}$ - C$_T$ cos(α_f)

L $_{Total}$ & D $_{Total}$
Resolve Aerodynamic & Thrust Forces into
Lift & Drag Axis System (Stability Axes)

D $_{Total}$
Will be negative

For Lift - Drag Equilibrium In
Steady Flight with Wings Level :

$$L_{Total} - W\cos\gamma = 0$$

$$D_{Total} + W\sin\gamma = 0$$

$$\frac{L_{Total}}{q_\infty S_{REF}} = \frac{W}{S_{REF}}\frac{\cos\gamma}{q_\infty} = C_{L Total}$$

$$\frac{D_{Total}}{q_\infty S_{REF}} = \frac{-W}{S_{REF}}\frac{\sin\gamma}{q_\infty} = C_{D Total}$$

$$\boxed{\tan\gamma = -\frac{C_{D Total}}{C_{L Total}}}$$

$$q_\infty = \frac{W}{S_{REF}}\frac{\cos\gamma}{C_{L Total}} = \frac{1}{2}\rho_{SL}V_E^{\,2}$$

$$\boxed{V_E = \sqrt{2\frac{q_\infty}{\rho_{SL}}} = \sqrt{\frac{2}{\rho_{SL}}\frac{W}{S_{REF}}\frac{\cos\gamma}{C_{L Total}}}}$$

V_E = Equivalent Airspeed

L$_{Total}$

V$_\infty$

γ, +Flight Path

Local Horizon

D$_{Total}$

Wcos(γ)

Weight

Wsin(γ)
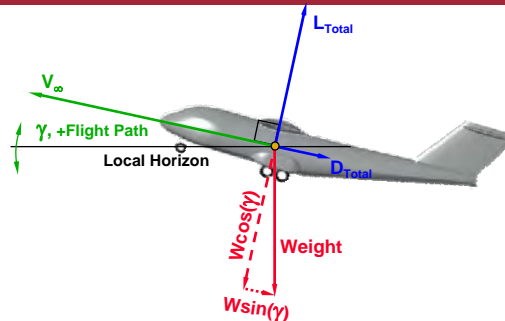
- Flight Path Direction Is Dependent Upon CD Total
  Direction at Positive Lift Values
- If cos γ ≈ 1, Trim Airspeed Driven By CL Total & W/S
- High C$_{LTotal}$ Decreases Trim Airspeed
- High Wing Loading Increases Trim Airspeed

DPA06 MIT High Speed Aerodynamic Efficiency

Sref = 1111.11 sq.ft.,   AR = 12.25,   sweep = 0.0 deg.,   t/c ave = 0.223

CL/CD TOTAL

ALL ENGINE
TRIMMED AT CG = 0.250

L/D=19.43, M=0.645, CL=0.8
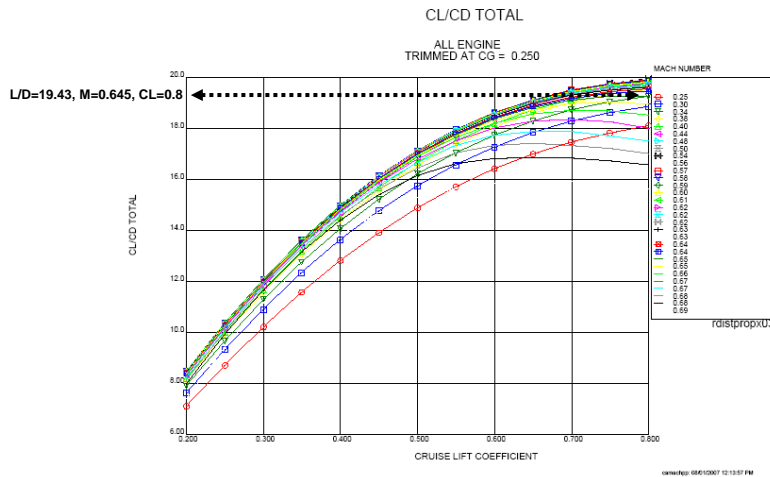
page 33

DPA06 High Speed Aerodynamic Efficiency Comparison

Cruise Efficiency Comparison

MIT and Boeing have comparable High Speed drag

MIT M=0.645
Boeing M=0.650
MIT M=0.60
Boeing M=0.60

12.53
12.40
11.88
11.53
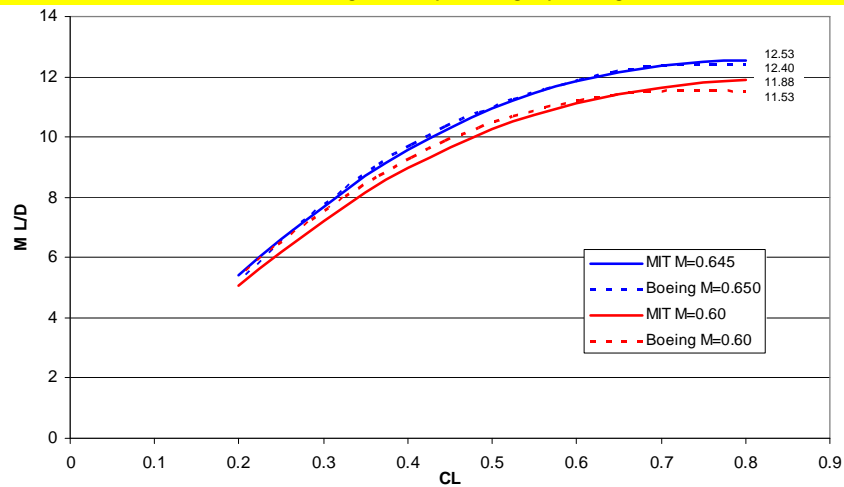
page 34

DPA06 High Speed Total Drag Buildup Comparison

MIT and Boeing have differences in drag buildup, however the total drag are comparable

Boeing Technology | **Phantom Works**   **Air Vehicle Technology Enabled Concepts**

DRAG BUILD-UP				
PROJECT NAME		rdistpropx03		rdistpropx08
		DPA06 MIT		DPA06 BOEING HS
SREF (FT**2)		1111.110		1111.110
FN (LBS)		15000.0		15000.0
AR		12.250		12.250
M-CRUISE		0.600		0.600
SWEEP (DEG)		0.000		0.000
T/C-AVE		0.2230		0.2230
AIRFOIL TYPE		SUPERCRIT. DTE		SUPERCRIT. DTE
S-HORIZ (FT**2)		313.000		313.000
S-VERT (FT**2)		165.870		165.870
F BUILD-UP (FT**2)				
BASE DRAG		0.0000		0.0000
FUSELAGE		5.9111		5.1700
WING		3.8889		11.0700
WINGLET		0.0000		0.0000
FLAP SUPPORT		0.0000		0.0000
HORIZONTAL		3.2000		1.9100
VERTICAL		2.6667		0.9100
N&P		0.0000		0.0000
CANOPY		0.0000		0.0321
GEAR PODS		0.0000		0.0000
ETC BEFORE SUB		0.8889		0.0000
EXCRESCENCE		0.0000 (0.0000)		1.3364 (0.0700)
INTERFERENCE		0.0000 (0.0000)		0.0000 (0.0000)
UPSWEEP		0.0000		2.2200
CONTROL GAPS		0.0000		0.0000
WING TWIST		0.0000		0.0000
STRAKES		0.0000		-0.6500
ETC AFTER SUB		0.0000		0.0000
FUSELAGE BUMP		0.0000		0.4900
FILLET		0.0000		0.0000
AIR CONDIT		0.0000		0.0000
-	-	-	-	-
F-TOTAL (FT**2)		16.5555		22.4885
E-VISC		0.9400		0.8340
CRUISE CD BUILD-UP				
M-CRUISE		0.6000		0.6000
CL-CRUISE		0.7500		0.7500
CD0		0.01490 (.390)		0.02024 (.520)
CDI		0.01555 (.407)		0.01753 (.450)
CDC		0.00771 (.202)		0.00117 (.030)
CDTRIM		0.00000 (.000)		0.00000 (.000)
-	-	-	-	-
CDTOT		0.03816		0.03894
L/D		19.6545 (0.0)		19.2628 (0.0)
ML/D		11.7927 (0.0)		11.5577 (0.0)

page 35

Comparison of Aircraft Aerodynamic Smoothness

Boeing Technology | **Phantom Works**   **Air Vehicle Technology Enabled Concepts**

Variation of Equivalent Flat Plate Drag
with Airplane Wetted Area

MIT accounting does not reflect total parasite drag in Profile drag total listed
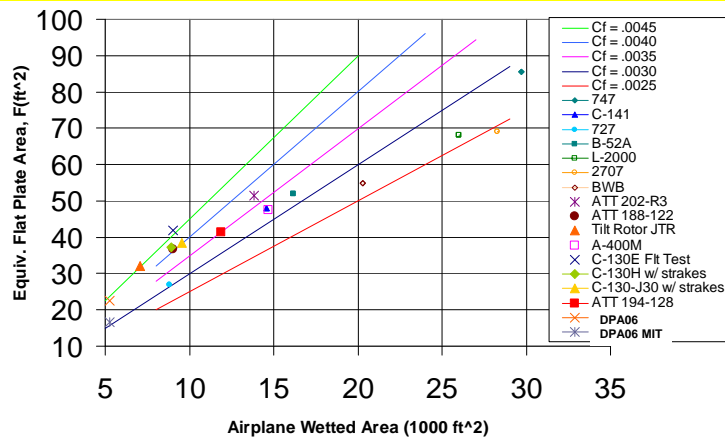
page 36

DPA06 Low Speed Powered Lift Curves, C_T = 0.0752

$C_T = C_J + C_{\mu \text{ blowing}}$: **GTRI**

$C_T = C_J$: **MIT**

$C_{\mu} = C_J = C_T$: **Boeing**

LOW SPEED LIFT CURVE

TAKEOFF TRIM CG= 0.250
FREE AIR
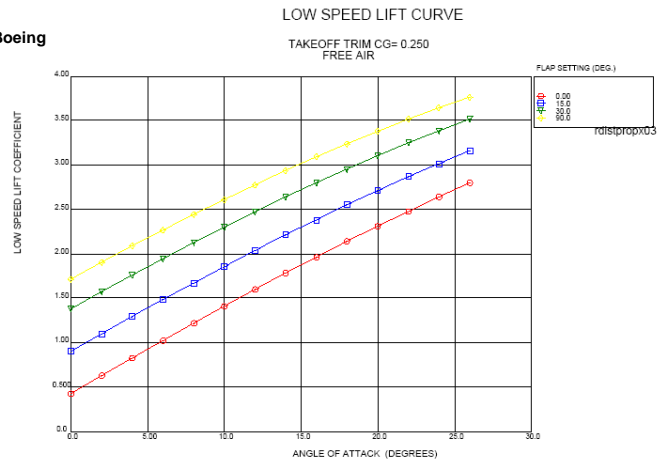
Extrapolated 90 degree data (landing flap)

DPA06 Low Speed Powered Lift Curves, C_T = 2.2070

$C_T = C_J + C_{\mu \text{ blowing}}$: **GTRI**

$C_T = C_J$: **MIT**

$C_{\mu} = C_J = C_T$: **Boeing**

LOW SPEED LIFT CURVE

TAKEOFF TRIM CG= 0.250
FREE AIR

$C_{\mu \text{ blowing}} = 0.3$

GRTI data at 90 degrees merged to MIT Takeoff data
GRTI data includes trailing edge blowing

DPA06 Low Speed Powered Lift Curves, C_T = 4.3388

Air Vehicle Technology Enabled Concepts

$C_T = C_J + C_{\mu \text{ blowing}}$: GTRI

$C_T = C_J$: MIT

$C_\mu = C_J = C_T$: Boeing

LOW SPEED LIFT CURVE

TAKEOFF TRIM CG= 0.250
FREE AIR

GRTI data at 90 degrees merged to MIT Takeoff data
GRTI data includes trailing edge blowing

page 39

DPA06 Low Speed Parabolic Drag Polars, C_T = 0.0752

Air Vehicle Technology Enabled Concepts

$C_T = C_J + C_{\mu \text{ blowing}}$: GTRI

$C_T = C_J$: MIT

$C_\mu = C_J = C_T$: Boeing

LOW SPEED POLAR

TAKEOFF TRIM CG= 0.250
FREE AIR

Extrapolated 90 degree data

page 40

DPA06 Low Speed Parabolic Drag Polars

FREE AIR DRAG POLAR
$C_T = 2.2070$

- ◆— MIT FLAPS= 0.0
- ■— MIT FLAPS=15.0
- ▲— MIT FLAPS=30.0
- —— GTRI $C_{\mu\ blowing}$=0.0 flaps=90.0
- —— GTRI $C_{\mu\ blowing}$=0.1 flaps=90.0
- —— GTRI $C_{\mu\ blowing}$=0.2 flaps=90.0
- —— GTRI $C_{\mu\ blowing}$=0.3 flaps=90.0
- —— GTRI $C_{\mu\ blowing}$=0.4 flaps=90.0

CL^2 (vertical axis: 0.0, 20.0, 40.0, 60.0, 80.0, 100.0, 120.0)

CD (horizontal axis: -2.00, -1.00, 0.00, 1.00, 2.00, 3.00, 4.00)
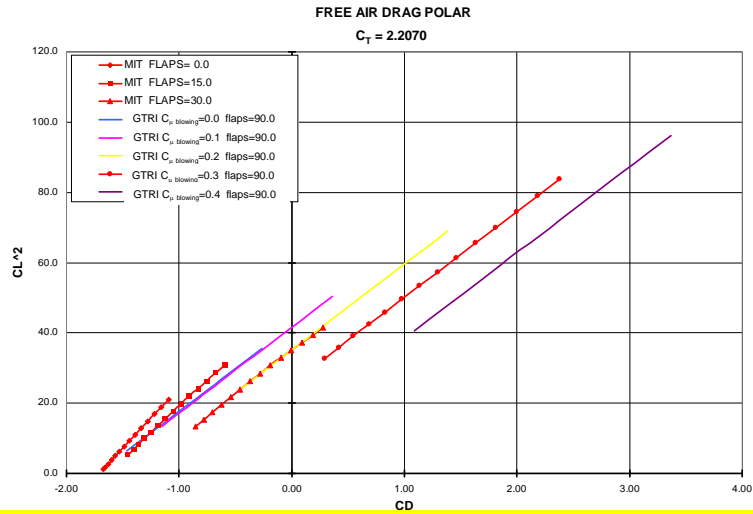
GRTI data at 90 degrees merged to MIT Takeoff data
GRTI data includes trailing edge blowing, $C_{\mu\ blowing}$=0.3 used in Performance

　　　　　　　　　　page 41

DPA06 Low Speed Parabolic Drag Polars, $C_T = 2.2070$

$C_T\ =\ C_J + C_{\mu\ blowing}\ :\ GTRI$

$C_T = C_J\ :\ MIT$

$C_\mu = C_J = C_T\ :\ Boeing$

LOW SPEED POLAR

TAKEOFF TRIM CG= 0.250
FREE AIR

FLAP SETTING (DEG.)
- 0.00
- 15.0
- 30.0
- 90.0

rdistpropx03

CL (SQUARED) (vertical axis: 0.0, 10.0, 20.0, 30.0, 40.0, 50.0, 60.0, 70.0, 80.0, 90.0)

$C_{\mu\ blowing}$ = 0.3

DRAG COEFFICIENT -CD0(.014900) (horizontal axis: -2.00, -1.50, -1.00, -0.500, 0.0, 0.500, 1.00, 1.50, 2.00, 2.50)
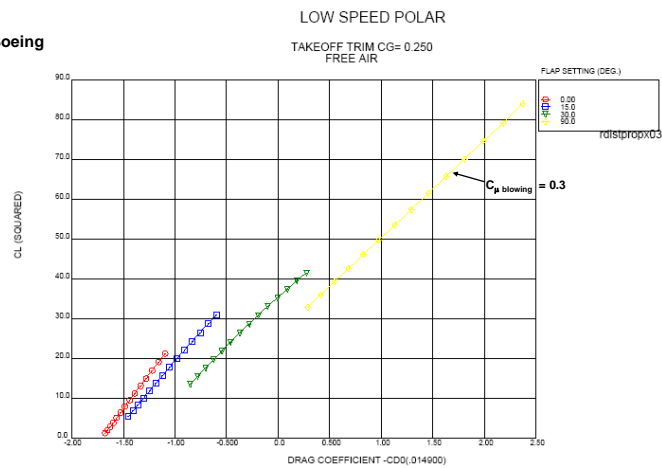
GRTI data at 90 degrees merged to MIT Takeoff data
GRTI data includes trailing edge blowing

　　　　　　　　　　page 42

DPA06 Low Speed Parabolic Drag Polars

FREE AIR DRAG POLAR
$C_T = 4.3388$

CL^2 (y-axis): 0.0, 20.0, 40.0, 60.0, 80.0, 100.0, 120.0, 140.0, 160.0

CD (x-axis): -5.00, -4.00, -3.00, -2.00, -1.00, 0.00, 1.00, 2.00, 3.00, 4.00, 5.00

Legend:
- MIT FLAPS= 0.0
- MIT FLAPS=15.0
- MIT FLAPS=30.0
- GTRI $C_{\mu\ blowing}$=0.0 flaps=90.0
- GTRI $C_{\mu\ blowing}$=0.1 flaps=90.0
- GTRI $C_{\mu\ blowing}$=0.2 flaps=90.0
- GTRI $C_{\mu\ blowing}$=0.3 flaps=90.0
- GTRI $C_{\mu\ blowing}$=0.4 flaps=90.0
- GTRI $C_{\mu\ blowing}$=0.5 flaps=90.0
- GTRI $C_{\mu\ blowing}$=0.6 flaps=90.0
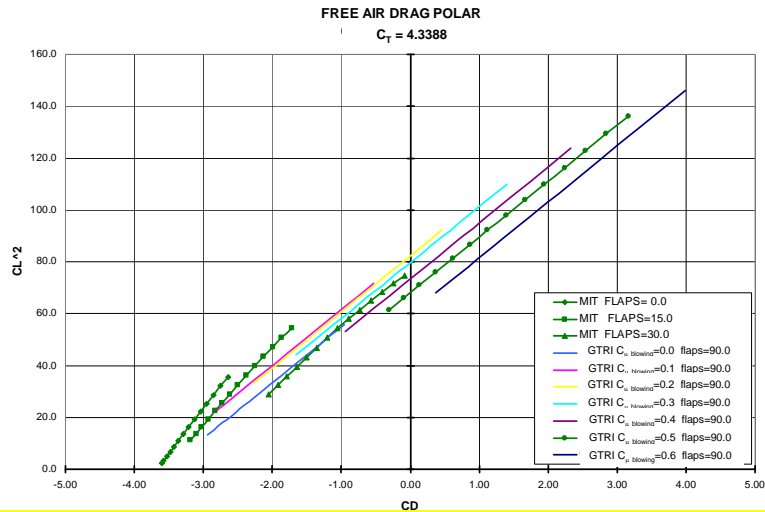
GRTI data at 90 degrees merged to MIT Takeoff data
GRTI data includes trailing edge blowing, $C_{\mu\ blowing}$=0.5 used in Performance

---

DPA06 Low Speed Parabolic Drag Polars, $C_T = 4.3388$

$C_T = C_J + C_{\mu\ blowing}$: GTRI

$C_T = C_J$: MIT

$C_\mu = C_J = C_T$: Boeing

LOW SPEED POLAR

TAKEOFF TRIM CG= 0.250
FREE AIR

FLAP SETTING (DEG.)
- 0.00
- 15.0
- 30.0
- 90.0

rdlstpropx03

$C_{\mu\ blowing}$ = 0.5

CL (SQUARED) (y-axis): 0.0, 20.0, 40.0, 60.0, 80.0, 100.0, 120.0, 140.0

DRAG COEFFICIENT -CD0(.014900) (x-axis): -4.00, -3.00, -2.00, -1.00, 0.0, 1.00, 2.00, 3.00, 4.00
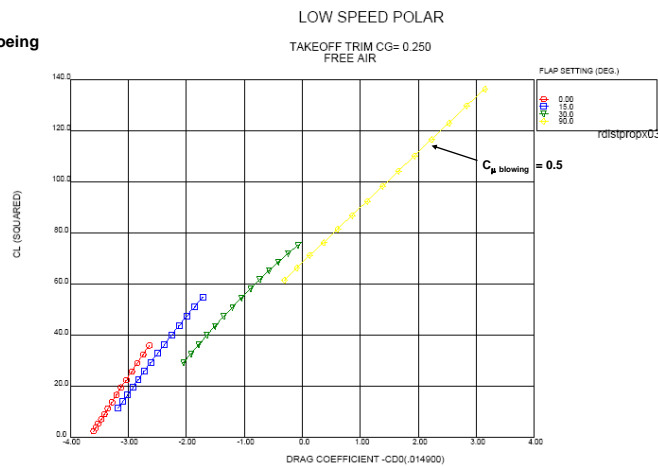
GRTI data at 90 degrees merged to MIT Takeoff data
GRTI data includes trailing edge blowing

DPA06 Low Speed Powered Lift Curves Comparison

Extrapolated 90 degree data

Boeing Technology | **Phantom Works**   **Air Vehicle Technology Enabled Concepts**

FREE AIR LIFT CURVE
$C_T = 0.0752$
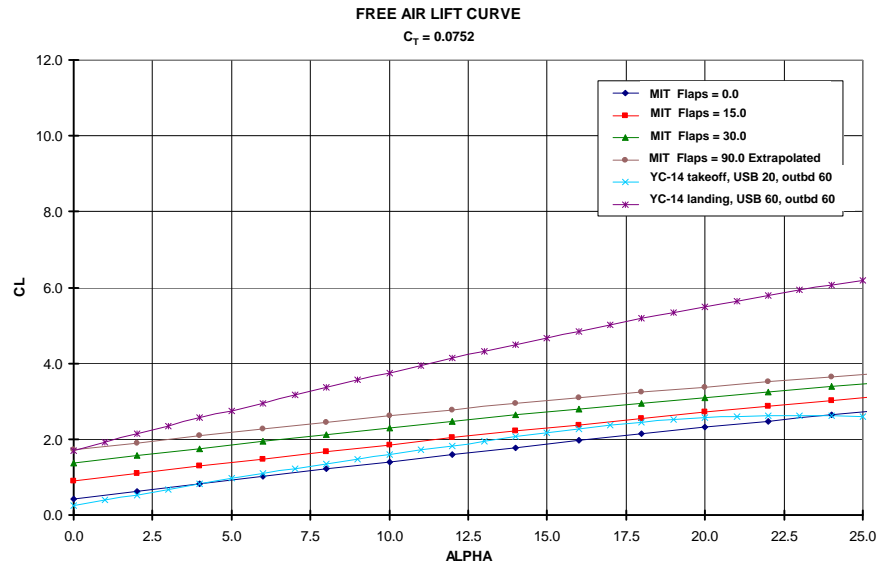
page 45

DPA06 Low Speed Powered Lift Curves Comparison

Boeing Technology | **Phantom Works**   **Air Vehicle Technology Enabled Concepts**

FREE AIR LIFT CURVE
$C_T = 2.2070$

GTRI landing flaps 90.0   w/ $C_{\mu\ blowing} = 0.30$

$\Delta CL \sim 1.7$

$\Delta CL \sim 1.0$

page 46

DPA06 Low Speed Powered Lift Curves Comparison

Conclusion

- Good comparison between MIT and Boeing PD high speed drag

- Aero Propulsion Design and Integration assumes 2 dimensional wing flow
- Approach and Landing includes blowing for high C_T and flap deflections
- GRTI approach and landing data merged to MIT takeoff data
- Released powered data are better than YC-14 takeoff and landing data

MIT Aero installation

Aircraft loft reflected "generic" engine installation

- MIT Aero installation did not match engine dimensional guidance (PW615)
- Loft engine was considered entirely "rubber"
- No considerations for gearbox(s) or AMAD(s)
- No considerations for Thrust Mounts, Hook-ups and R&R Access

---
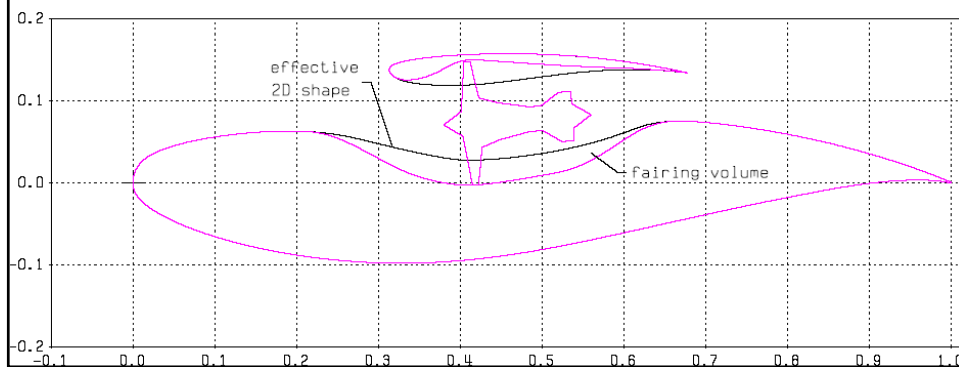
PW615F MAJOR DIMENSIONS

Propulsion Details, Observations & Next Steps

Installation Effects

- Assumed ideal recovery and discharge coefficients
  - Similar installations would result in 2 to 4% loss in recovery and 2 to 3% loss in Cfg
- Assumed no bleed and horsepower extraction
  - Similar sized vehicles would expect 1 to 2 lb/sec bleed flows and 75 to 150 hpx from each wing (per side of aircraft) for conventional take-off and landing
  - Current DP powered lift config will require medium or high pressure bleed supply for LE and TE blowing system, typically beyond comparable APU capabilities
- Assumed ideal operability characteristics
  - Similar installations experience higher distortion levels and reduced engine operability at take-off and landing AOAs
  - Embedded installation also sensitive to BLI arrangement for lower pressure ratio fans

---

Propulsion Details, Observations & Next Steps

Engine Cycle data

- Initial check of baseline MIT cycle (VLJ2) revealed unexpected parameter unit differences (minor) to few key parameters
  - Fuel flow & Ram drag
- Review of Mid and Far term cycle data underway (VLJ4 & VLJ3)
  - Based on submittal timeline, performance eval may include factors for thrust and fuel flow
  - Some concerns regarding Core Size (*a bit sporty*)

Parameter	Baseline (VLJ2)	Mid Term (VLJ4)	Far Term (VLJ3)
Rated Fn (Lbfs)	1647	1860	1982
BPR	2.56	7.8	12.7
OPR	18	27	36
T4 max (R)	2280	2800	3500
Core Size	1.4	0.53	0.27
Sfc (Lbs/hr/Lbf)	0.49	0.34	0.31

Risks - Propulsion

Engine Cycle
- Technology projections for Mid and Far Term engine cycles present challenges
  - Counter to idea of mass produced, non-complex units with simplified controls
  - Minimum Core Size for Operability, even for centrifugal compressor (less than 0.6 pps)

Installation
- Embedded installation and low pressure ratio fans
  - Distortion and surge margin
  - Stall/Surge propagation, engine to engine with "*daisy-chain*" installation

---

Introduction

Extremely coarse exploratory type analysis
- No S&C analysis
- No aircraft balance & loadability analysis
- No field flotation analyses performed
- Backing-up an incline not analyzed

Boeing proprietary methods used

Parametric methods used except for wing

Complex wing and propulsion design pose weight risk
- Require analyses with greater detail

Weight Summary

Sizing Assumptions:

- 12,000 lb Payload @ 2.5 g
- Representative Operational Items
- Mission Fuel

	Distributed Propulsion
Structure	28,396
Propulsion	13,840
Systems	9,376
Weight Empty	**51,612**
Op Items	3,658
Operating Weight Empty	**55,270**
Payload	12,000
Fuel	18,309
MTOW	**85,579**

Wing Sizing

Sizing Assumptions:

- Lower wing primary structure
- Upper wing aero fairing
- Connecting vertical shear webs - also separate engines
- Upper wing & propulsion installation purely parasitic
        Neither beneficial nor detrimental
- Front spar at 20% chord, rear spar at 60%, equivalent 7% t/c
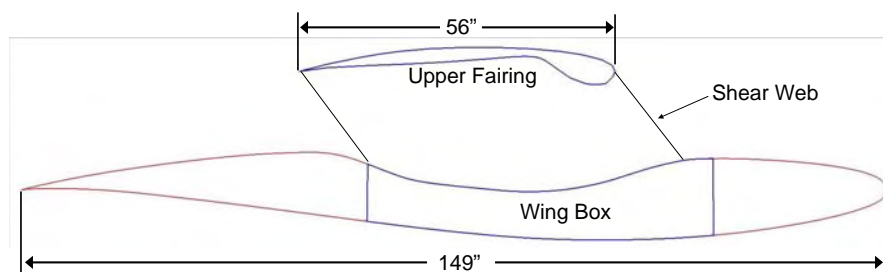
56"

Upper Fairing

Shear Web

Wing Box

149"

Wing Weight

Weight Bases:

- Station analysis-based bending material
- Assume advanced materials
- Parametric methods used for all remaining

- Upper wing weight includes vertical shear webs

Wing	12,270
Bending Material	4,915
Shear Web	719
Ribs & Bulkheads	675
Leading Edge	1,013
Trailing Edge	2,920
Upper Wing	2,028

Structure Summary

Weight Bases:

- Tail weight assumes advanced materials

- Body 5.97psia cabin differential pressure
- Floor includes cargo/payload restraint capability

- Nacelles assume aero cowling around each engine
- Nacelle weight includes cowling and mounting provisions

Structure		28,396
Wing	12,270	
Tail	2,681	
Body	8,452	
Landing Gear	3,634	
Engine or Nacelle	1,359	

Propulsion

Weight Bases:
- 30 Engines, 10 have gearboxes (similar to PW615C)

- Exhaust weight includes thrust reversers
- Thrust reversers based on judgment

- No aerial refueling
- Discrete fuel feed tank for each engine
- No catastrophic engine failure provisions

Propulsion		13,840
Engines	8,500	
Exhaust	3,600	
Fuel	1,140	
Engine Systems	600	

Subsystems

Weight Bases:
- Subsystems assumed standard

- No TE or LE flow control systems
- Anti-Icing is critical - assume no ice is allowed to form.

- No NBC provisions

Systems		9,376
Flight Controls	1,387	
APU	359	
Instruments	170	
Hydraulics & Pneumatics	883	
Electrical	2,062	
Avionics	1,077	
Furnishings & Equip	1,580	
Air Conditioning	494	
Anti-Icing	724	
Load & Handling	641	

Structure		28,396
Wing		12,270
Bending Material	4,915	
Shear Web	719	
Ribs & Bulkheads	675	
Leading Edge	1,013	
Trailing Edge	2,920	
Upper Wing	2,028	
Tail		2,681
Body		8,452
Landing Gear		3,634
Engine or Nacelle		1,359
Air Induction		
Propulsion		13,840
Engines	8,500	
Exhaust	3,600	
Fuel	1,140	
Engine Systems	600	
Systems		9,376
Flight Controls	1,387	
APU	359	
Instruments	170	
Hydraulics & Pneumatics	883	
Electrical	2,062	
Avionics	1,077	
Furnishings & Equip	1,580	
Air Conditioning	494	
Anti-Icing	724	
Load & Handling	641	
Weight Empty		**51,612**
Op Items		3,658
Operating Weight Empty		**55,270**
Payload		12,000
Fuel		18,309
MTOW		**85,579**

Mission Guidelines Reflect Military CONOP

1. Takeoff prepared runway
   - 12,000 pounds payload
     → One HMMWV (12,000 lb) or 20 or more soldiers
   - Allowances: SLS, 5 min warm-up, taxi, takeoff
2. Climb & accelerate
3. Ingress cruise
   - 400 nm at best cruise Mach/Altitude (0.5M – 0.6M) pressurized to 9,000 ft
4. Decent (no distance of fuel credit)
5. Low altitude cruise
   - 100 nm, low altitude, best speed
6. Mid-Mission landing
   - Austere/soccer filed < 300ft ground roll
   - 40% thrust reverser effectiveness presumed
   - 165 ft. field width limits a/c span to 115 ft (less would be better)

7. Mid-Mission takeoff
   - 5,000 lb payload
   - < 300 ft austere field takeoff
     Balanced field length (over 50 ft obstacle) will be defined with all engines operating, 0.5g, 5k, 95°F
   - 5 min. maneuver & taxi takeoff allowances
8. Egress cruise
   - 100 nm, low altitude, best speed
9. Climb & accelerate
10. Egress cruise
    - 400 nm at best cruise Mach/Altitude (0.5M – 0.6M)
11. Decent (no distance of fuel credit)
12. Land on prepared field
    - 5% fuel reserve

Best Cruise Altitude & Velocity

SL, 59° F (Std Day)

CBR = 6 @ 50 Passes

400 nmi   100 nmi   100 nmi   400 nmi

Distributed Propulsion Reference Mission Summary

TOGW	84,364
OEW	55,270
Payload	12,000
Block Fuel	16,239
Reserve Fuel	855
Block Distance	1,000
Total Distance	1,000
Initial Cruise Mach	0.652
Initial Cruise L/D	16.97
Initial Cruise SFC	0.816
T/W	0.56
W/S (psf)	75.9

M 0.65 @ 35K
L/D: 17.0
SFC: 0.82

M 0.4 @ 200ft
L/D: 11.8
SFC: 1.1

M 0.65 @ 35K
L/D: 16.4
SFC: 0.84

Drop 7,000lbs of payload

5% Reserves

TOGW = 84K

Landing Wt. = 69K   Takeoff Wt. = 76K

Landing = 60K

400 nmi   200 nmi   400 nmi

500 nmi Radius
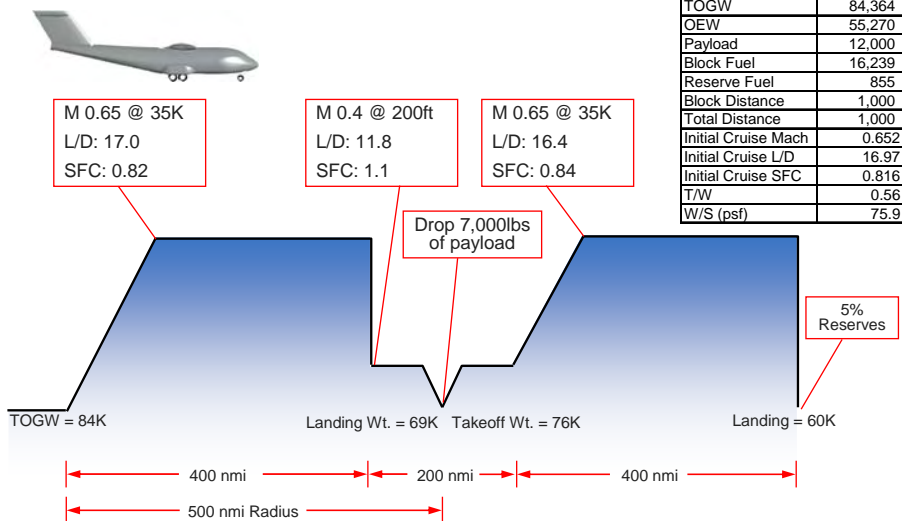
Distributed Propulsion Reference Takeoff Performance

- **No distance for engine spool-up**
- **Best flap deflection angle for shortest groundroll**
- **No climb gradient requirement**
- **Obstacle requirements not critical**
- **10% Liftoff speed margin for tailstrike**

Mid-mission Landing Weight (69,100 lb.), 5000' MSL 95°F

V_R
7.2 sec
342 ft
52 kts

V_{LO}
10.1 sec
625 ft
64 kts

V_{obs}
15.4 sec
1229 ft
68.9 kts

All Engine

50 Ft

Distance to Liftoff

625 ft
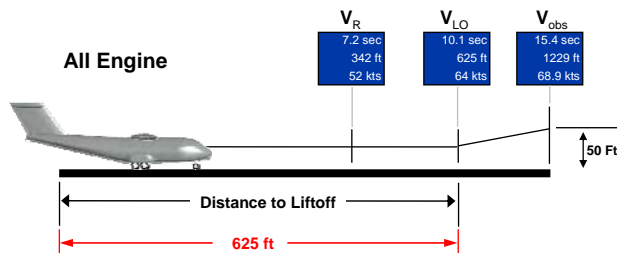
Distributed Propulsion Reference Landing Performance

- **Power-on stall speed (V$_{sp}$) as reference speed** $V_{APP} = 1.2(V_{sp})$
- **Assume no flare precision touchdown** $V_c = V_{APP}$
- **Instantaneous device actuation (spoilers and thrust reversers)**
- **Thrust reverser is 40% available forward thrust**
- **Assume no flare precision touchdown**
- **Braking coefficient = 0.25**

> **Mid-mission Landing Weight (76,100 lb.), 5000' MSL 95°F**
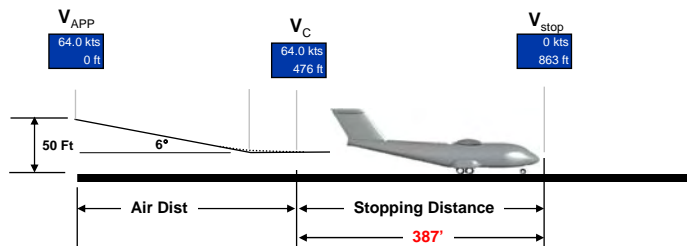
V$_{APP}$

64.0 kts
0 ft

V$_C$

64.0 kts
476 ft

V$_{stop}$

0 kts
863 ft

50 Ft   6°

Air Dist   **Stopping Distance**

387'

Mid-Mission Liftoff Distance vs. T/W and W/S

- **T/W and W/S are in terms of mid-mission landing weight**
- **Thrust is in terms of reference thrust (SL STATIC)**
- **5000' MSL, 95°F**
- **Takeoff and Landing Distances are groundroll only**

REFERENCE
T/W = 0.75
W/S = 68.5

Distance to Liftoff (ft.)

300' Landing
250' Landing
T/W = 0.6
T/W = 0.725
T/W = 0.85
T/W = 0.975
T/W = 1.1
Cu liftoff = 4
Cu liftoff = 5
Cu liftoff = 6
Cu liftoff = 7
Cu liftoff = 4.34
W/S = 60
W/S = 55
W/S = 50
W/S = 45
W/S = 40
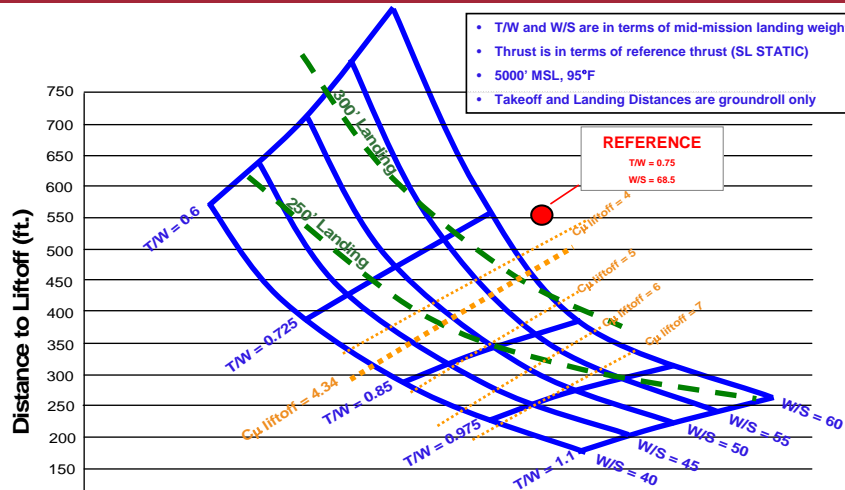
Mid-Mission Takeoff and Landing Distance vs. Weight

- **5000' MSL, 95°F**
- **Takeoff and Landing Distances are groundroll only**
- **Rolling Coeff has small effect on takeoff roll (~1%)**
- **Optimum flap deflection for min. ground roll on takeoff**
- **Landing deceleration delay time adds 104 ft of distance per second**

REFERENCE

Takeoff and Landing Distance (ft.)

Mid-Mission Takeoff Rol, 5000' MSL 95°F
Mid-Mission Takeoff Roll, STD, SL
Mid-Mission Landing Roll, brake mu 0.25
Mid-Mission Landing Roll, brake mu 0.25, STD, SL
Mid-Mission Landing Roll, brake mu 0.35
Mid-Mission Landing Roll, brake mu 0.45

Mid-Mission Weight (lb.)

| T/W = 0.86 | T/W = 0.79 | T/W = 0.73 | T/W = 0.69 | T/W = 0.63 | T/W = 0.59 |
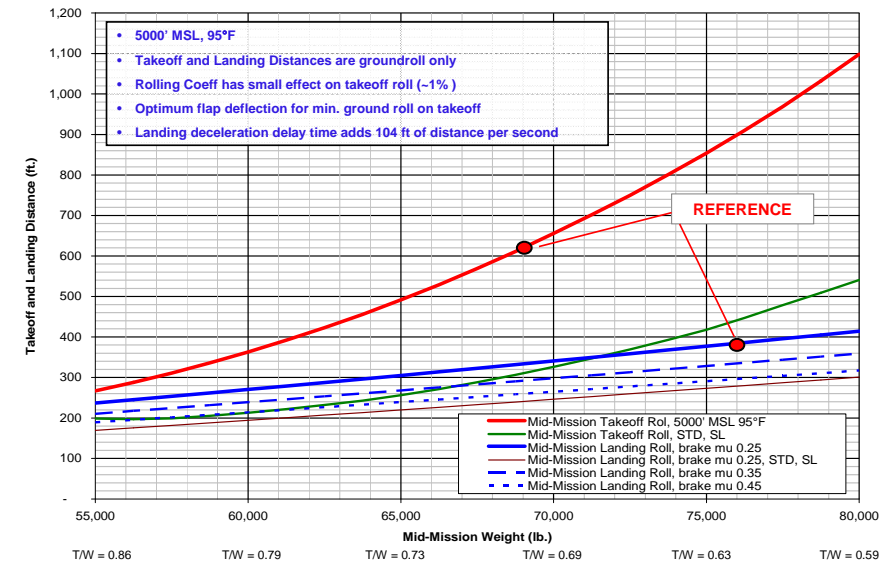
Mid-Mission Takeoff Distance vs. Weight

- **5000' MSL, 95°F**
- **Takeoff Distance is groundroll only**
- **Optimum flap deflection for min. ground roll**
- **Fixed Reference Thrust**

REFERENCE

Takeoff (ft.)

Lift-off Cmu

Mid-Mission Takeoff Roll
Mid-Mission Liftoff Cmu

Mid-Mission Weight (lb.)

| T/W = 0.86 | T/W = 0.79 | T/W = 0.73 | T/W = 0.69 | T/W = 0.63 | T/W = 0.59 |
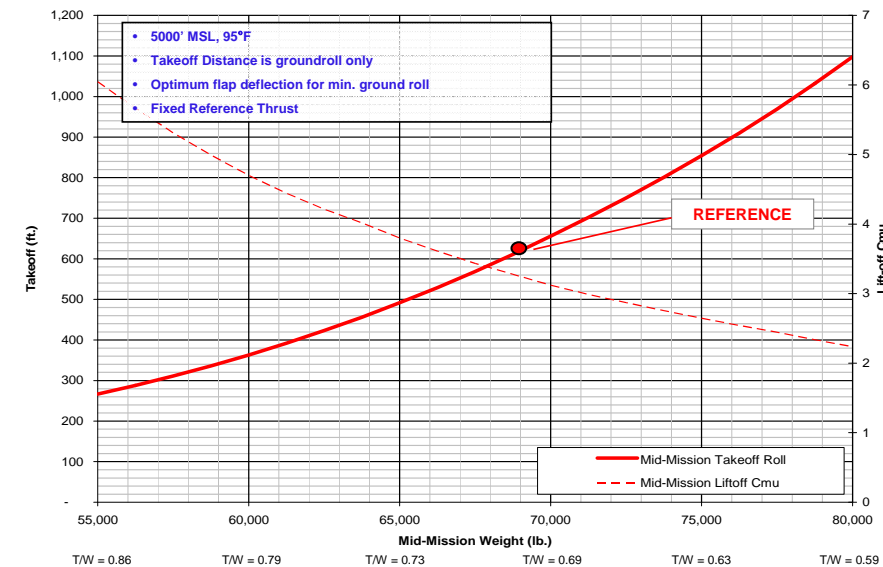
Landing Weight and %Thrust Reversing vs. Ground Roll
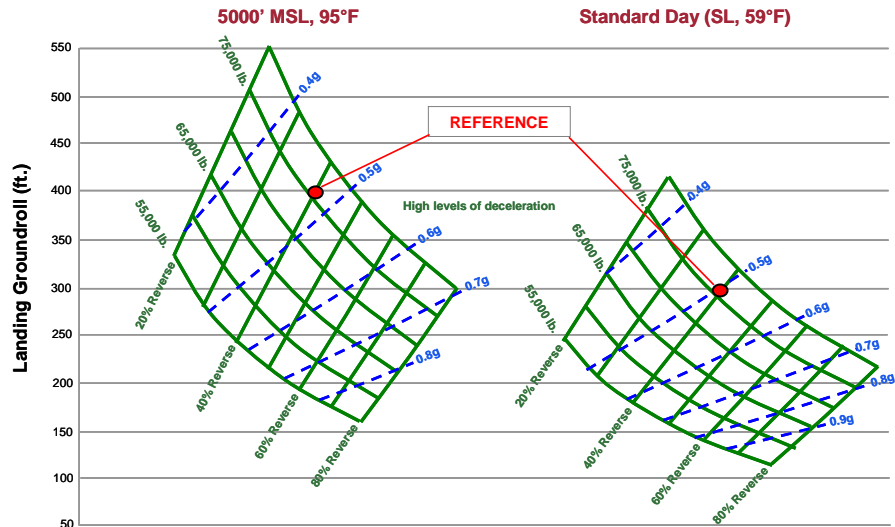
Ways to Make it Work…

Decrease Mid-mission weight

- Shutoff some engines in cruise (16% sfc decrease by shutting down half the engines)
- Decrease mission radius
- Work at decreasing OEW (especially DP wing weight)
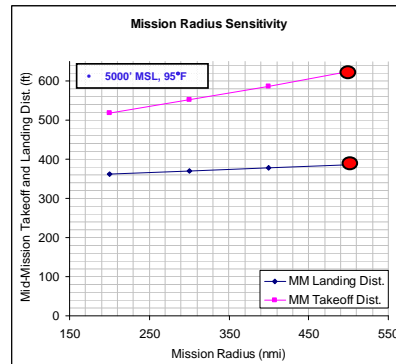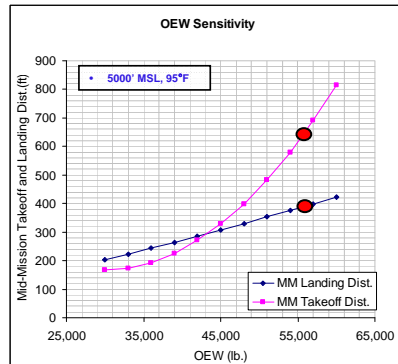
Ways to Make it Work…

Increase thrust available

- Consider standard day, sea level for 300 ft field lengths
- Little benefit from increasing the span of DP system since it is a significant portion of the empty weight.
- Far-term engine could provide sufficient thrust (~20% more) with current vehicle size.
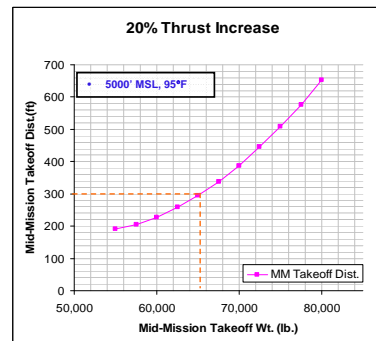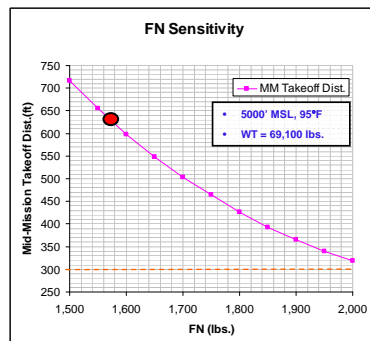
page 71

Ways to Make it Work…

Decrease liftoff speed

- Reduce tailstrike margins
- Increase empennage upsweep angle

~ 20% decrease in groundroll
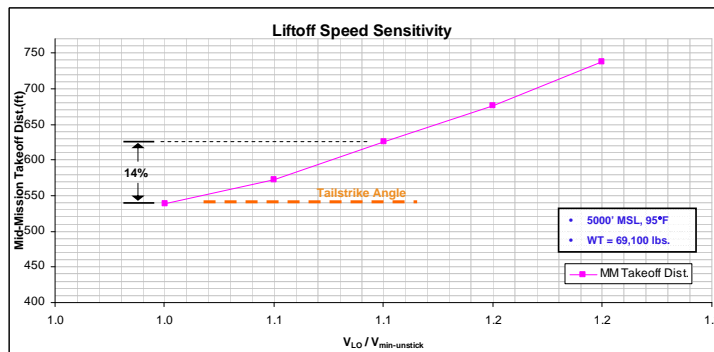
page 72

Mid-Mission Liftoff Distance vs. T/W and W/S

- **T/W and W/S are in terms of mid-mission weights**
- **5000' MSL, 95°F**
- **Takeoff and Landing Distances are groundroll only** ●

Distance to Liftoff (ft.)

750, 700, 650, 600, 550, 500, 450, 400, 350, 300, 250, 200, 150, 100, 50, 0

300' Landing, 250' Landing

T/W = 0.6, T/W = 0.725, T/W = 0.85, T/W = 0.975, T/W = 1.1

Cµ liftoff = 4, Cµ liftoff = 5, Cµ liftoff = 6, Cµ liftoff = 7, Cµ liftoff = 4.34

W/S = 60, W/S = 55, W/S = 50, W/S = 45, W/S = 40
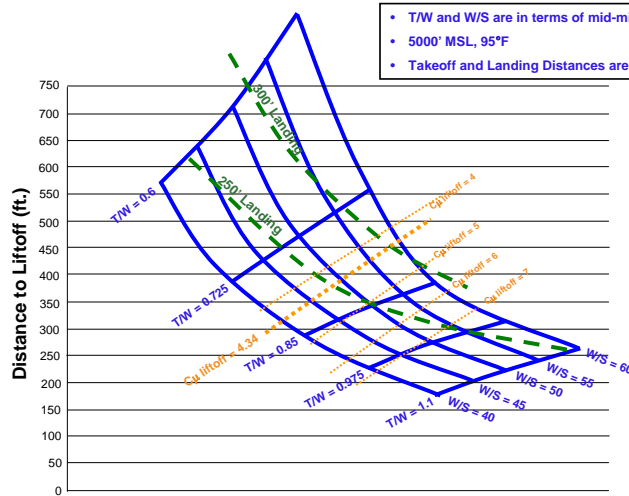
Approach Calculations

$$\sin(\gamma) = \frac{T-D}{W}$$

$\xrightarrow{\text{Propulsion Integrated into blown aero data}}$

$$\sin(\gamma) = \frac{-D}{W}$$

$$V_{APP} = 1.2(V_{stall})$$

$$V_{APP} = 1.2(V_{sp})$$
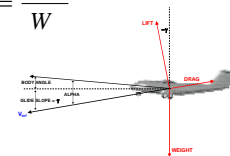
MIL STD 3013 states power-off stall speed must be used, but that the procuring agency can specify alternate design criteria. Power-on stall speed is a function of Cmu, which determines the lift and drag and ultimately the glide slope. Using the power-on stall speed as the reference for approach speed ultimately leads to stall speed being a function of glide slope, so trends involving glide slope could be non-intuitive. Further, the power-on CLmax is a function of Cmu, which is based on a q. As such, solving for the power-on stall speed (Vsp) is an iterative process. For this study, we will use the power-on stall speed as the approach speed reference.

$\xrightarrow{\gamma_{desired}\ V_{APP}}$

$$C_L = \frac{W\cos\gamma}{qS}$$

$\xrightarrow{C_{\mu}\_lookup}$

$$\sin(\gamma) = \frac{-D}{W}$$

Solve Cmu for Drag
to satisfy glide slope

Performance Analysis Tools

ModelCenter Integration

Spreadsheets

Legacy Database Aero/Performance Codes
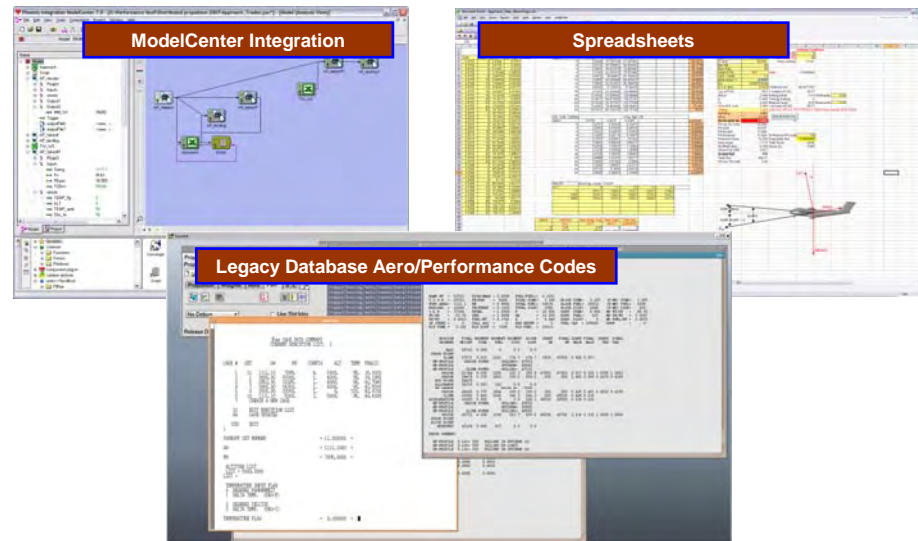
Risks

Non-ideal, 3D high lift
- Span wise flow, non-linear circulation, separations/hysteresis, non-homogeneous flow etc.
- Cross winds/guts, more detailed S&C

Extremely high accelerations/deceleration
- Limited thrust reversing, limits landing potential
- No dispersions, flares, cross winds, time lags

Turbofan
- Availability, Life Cycle Costs (particularly O&S)
- Operability
  → Recovery, bleed +/or horsepower extraction for LE/TE blowing +/or electrical power management, power takeoff +/or remote gearbox/number, AMAD, FOD, blade-out shielding, fratricide, turbulence, boundary layer control, cross talk, surge margins & throttle range, engine out

Numerous "not considered" items

DP aircraft carries 25% less payload, and weighs 2.5 times more than CN-235

Add design considerations

- 4 months: Add model fidelity to reflect aspects "ignored"
  (e.g., turbulence, boundary layer, fratricide, etc.)

Additional DP iterations

- 6 months: Additional thrust needed for reverse, to accomplish short landing.
  Span is limited by field. Add engines to body? Add tandem wing?

Commoditized engine cost feasibility

- 8 months: Compare cost of a DP vehicle to one with conventional systems.

R/C flight demo

- 12 months: COTS electric fans, small engine/generator or Li-ion batteries
  - NextGen fabricates model
  - Possible NGRC or NARC CRADA

Developed DP conceptual design

- Objective: Enable new capabilities for military transport aircraft

Assessed Mission Requirements

- Developed mission flight and ground operation requirements
- Derived design and performance "Most Important Requirements"

Developed baseline configuration

- This was based on earlier "spreadsheet" level calculations

Revised configuration

- Evaluated basic design trades (quantitatively & qualitatively)

Iterated & implemented MIT/GTRI Aerodynamics

- Performed trades (DP10 -> RP06)

Assessed Mass Properties

- Estimated basic structural arrangement and weight

Integrated MIT propulsion provided

Managed program cost/schedule and deliverables

Appendix A

GTRI Final Report
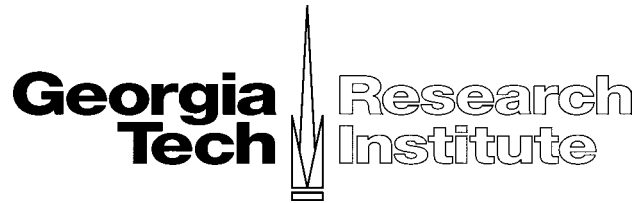
Georgia Tech | Research Institute

Pneumatic Aerodynamic/Propulsive Concepts for Distributed Propulsion, Phase I

QUARTERLY PROGRESS REPORT NO. 4
August 1 to October 31, 2007
Final Report, November 1. 2006 to October 31, 2007

CONTRACT NO. 5710002091,
HR0011-07-C-0005

GTRI Project No. D-5251

Prepared for:

Dr. Alan H. Epstein,
R. C. Maclaurin Professor of Aeronautics and Astronautics
Director, Gas Turbine Laboratory
Massachusetts Institute of Technology
Room 31-265
Cambridge, MA 02139-4307

Prepared by:

Robert J. Englar, Principal Research Engineer
Aerospace, Transportation and Advanced Systems Laboratory
Georgia Tech Research Institute
Georgia Institute of Technology
Atlanta, GA 30332-0844

October 30, 2007

Pneumatic Aerodynamic/Propulsive Concepts for Distributed Propulsion, Phase I

Quarterly Progress Report No. 4: August 1 to October 31, 2007
Final Report, November 1, 2006 to October 31, 2007

Principal Investigator: Robert J. Englar, Principal Research Engineer
Georgia Tech Research Institute
Aerospace, Transportation & Advanced Systems
Laboratory

CCRF, Code 0844
Atlanta, GA 30332-0844
(770) 528-3222, Office
(770) 528-7077, Fax
(770) 528-7586, Wind Tunnel
bob.englar@gtri.gatech.edu

Program Objective: As requested by MIT/DARPA, Georgia Tech Research Institute (GTRI) Principal Research Engineer Robert J. Englar will team with Massachusetts Institute of Technology (MIT) and Boeing Technology Phantom Works (Boeing) in the planning and development of Distributed Propulsion (DP) concepts of interest to DARPA, with special emphasis by GTRI on pneumatic technology integrated with aerodynamic, propulsive, and control systems.

Approach: Robert J. Englar of GTRI will employ 39+ years experience in Circulation Control (CC) aerodynamics and airfoil/wing/aircraft development to assist MIT/DARPA in pneumatic technology identification, characterization, and development for Distributed Propulsion concepts. The partnership of MIT, GTRI, and Boeing will explore the potential for Distributed Propulsion combined with pneumatic aerodynamics/propulsion, powered lift, and flow control to enable new capabilities for military air vehicles. This study will includeboth aircraft and gas turbine engine designs as well as propulsion integration considerations, including pneumatic powered-lift and control system integration.

  As per the original MIT/DARPA Request for Proposal, the team will perform the following (with specific GTRI areas of involvement noted):

1. Explore the potential benefits that distributed propulsion may bring to military missions such as ESTOL or others as selected in concert with DARPA (**GTRI involvement**).

2. Execute a conceptual design of the selected distributed propulsion air vehicle. This will include configuration, control, performance and weight estimates (**GTRI involvement**).

3. Execute a conceptual design of small engines optimized for distributed propulsion. This will include engine configuration, performance and weight estimates.

4. Quantify how distributed propulsion can enable new mission capabilities, improve performance, improve reliability, and reduce cost (**GTRI involvement**).

5. Delineate the technical barriers that must be overcome to make distributed propulsion aircraft a reality (**GTRI involvement**).

Specifically in this effort, Mr. Englar/GTRI **will provide engineering and technical services** to perform certain portions of the above tasks for MIT/DARPA in the anticipated 12-month-duration DP program. It is assumed here that efforts relating to aerodynamics/propulsion integration, powered lift, and control which involve pneumatic technology will be led by GTRI, that the propulsion-related technology effort will be led by MIT, and that the aircraft design tasks will be led by Boeing.

DARPA Contract Start Date: November 1, 2006 (Ph. I)   **Duration:** 12 months

Current Progress:

During the current Quarter 4 effort, GTRI has continued to participate with the Distributed Propulsion (DP) team in Tasks 1, 2, 4, and 5 above, primarily in the further conceptual development of a preliminary aircraft design for an Extreme Short Takeoff and Landing (ESTOL) aircraft capable of 300-ft takeoff and landing field lengths with certain specified payload, plus steep climb outs and steep approach glide slopes. In the first and second quarter efforts, the DP team had formulated an upper surface blowing (USB) type of powered-lift configuration, with either a mechanical flap, or a pneumatic (blown) flap or Circulation Control (CC) flap downstream of the engines to deflect thrust and augment lift (such as in Figure 1). During the third quarter, MIT continued development of the takeoff and climb configuration of this powered-lift aircraft, concentrating on a mechanical flap entraining engine thrust to yield high lift for short takeoff and high thrust recovery for climbout. GTRI concentrated on the approach/landing configurations using pneumatic aerodynamics. This fourth quarter report (the final report) is primarily a summary of that STOL approach analysis by GTRI.

GTRI argued in Refs. 1 and 2 that powered-lift configurations of this type could produce a problem for Extreme STOL landings down steep glide slopes, where the required powered-lift thrust and aircraft weight component along the glide slope must be offset by high jet turning and high aerodynamic drag in order to provide an equilibrium approach with very low approach speeds and short stopping distances. GTRI provided data (Refs. 3, 4, 5, and 6) for an Upper Surface Blowing (USB) arrangement of a number of small engines (multiplicity of engines being the DP goal) combined with CC blowing on a small highly-deflected flap to achieve very high lift and drag. As a means to offset powered-lift required thrust on approach, GTRI proposed the incorporation of the dual-radius CC pneumatic flap shown in Fig. 1 because thrust could be turned pneumatically to as much as 90°-165° deflection; this can provide flow-field entrainment and very high lift and high drag. Refs. 5, 6, 7, and 8 presented powered-lift "drag polars" based on existing experimental data for pneumatic aircraft of this type. Two typical powered-lift drag

4

polars are presented in Figures 2 and 3 below. Resulting lift curves for typical thrust and blowing coefficients are shown in Figures 4 and 5. In these data, thrust and drag are combined into a horizontal force coefficient along the flight path, C_X, which when combined with the non-dimensional aircraft weight along the glide slope ($C_W \sin \gamma$) must equal 0.0 for equilibrium.
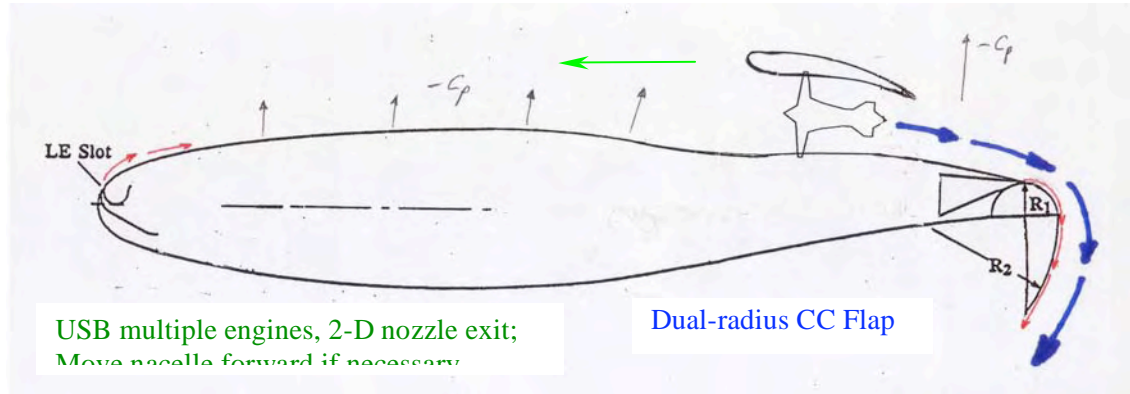
Figure 1 - Preliminary USB/CC Pneumatic Design
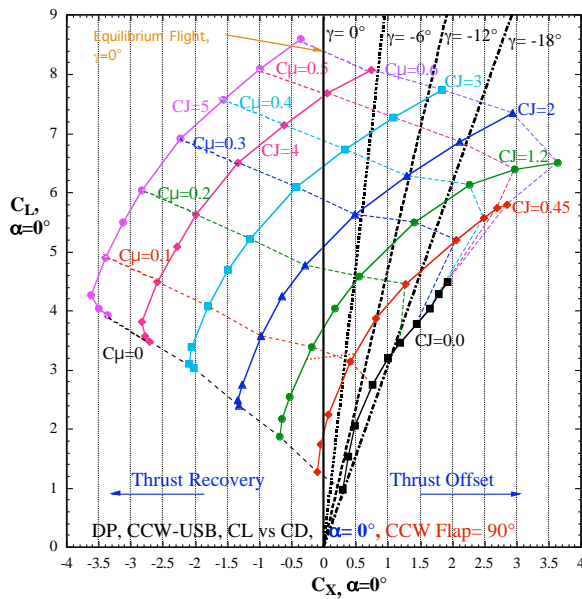
Fig. 2- Pneumatic Powered-lift drag polar on Approach, $\alpha = 0°$
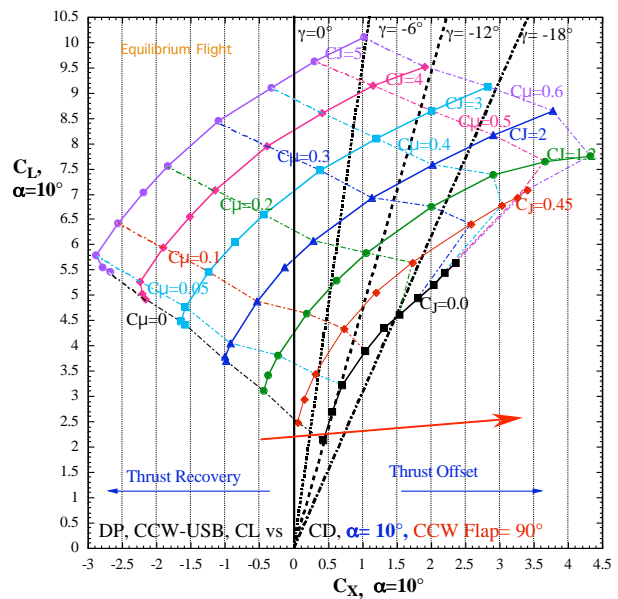
Fig. 3- Pneumatic Powered-lift drag polar on Approach, $\alpha = 10°$
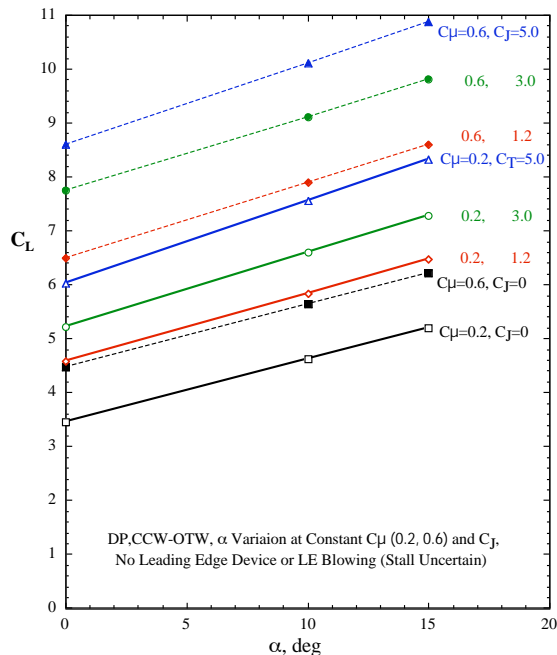
Fig. 4- Pneumatic Powered-lift Lift Curves, Variation with α, μ
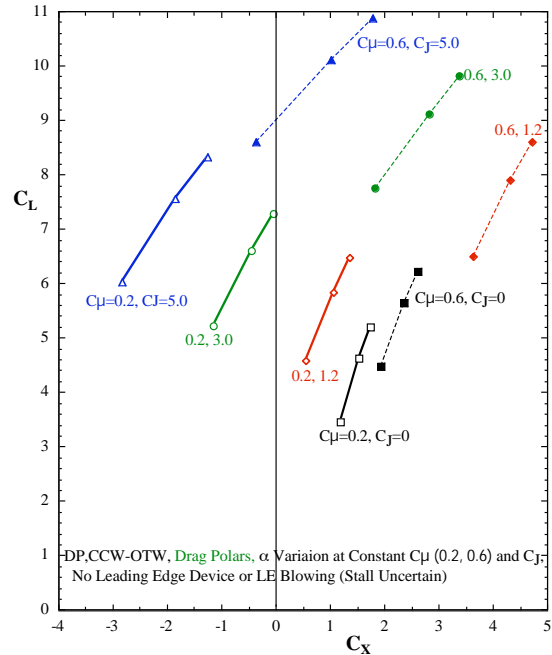
Fig. 5- Pneumatic Powered-lift Drag Polar Variation with α, μ

Up through this final quarter, GTRI has continued the development of a data base supporting this pneumatic powered-lift system which could provide even greater lift coefficient than for takeoff while also converting the input engine thrust needed to yield that lift into an increased drag component and thus allow equilibrium flight down steep glide slopes. These data are included in the revised PowerPoint presentation (Attachment A to this current report), which includes the GTRI data presentation at the August 3, 2007 DP Team's Review Meeting.

As a continuing effort, the CCW/USB STOL approach and landing analysis presented in Ref. 6 has been updated by use of a GTRI computerized iterative routine (Refs. 9 and 10) to yield equilibrium approach conditions. Updated results were presented by Englar at the DP Team Meeting with the DARPA/MIT sponsors held August 3, 2007 at the Boeing Huntington Beach, CA, facility, and updated in Attachment A, which includes changes and updates requested during that meeting. Typical data are presented here in this final report as a summary of the potential of pneumatic powered-lift configurations. Figures 6 and 7 present equilibrium lift and drag (including thrust) coefficient values iterated along various glides slopes. Unlike conventional high lift devices, the available equilibrium values vary with aircraft weight, thrust and blowing, with higher values required for lower speeds. Typical resulting equilibrium approach velocities are shown in Figure 8.
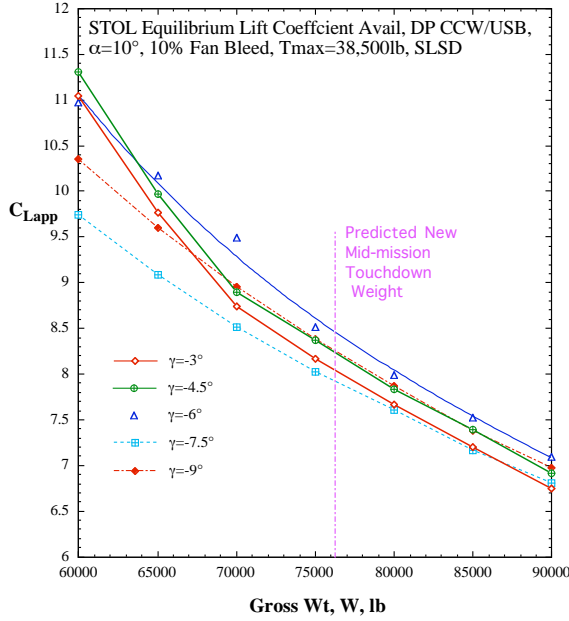
Fig. 6- Equilibrium Approach Iterated C_L Available with α =10°
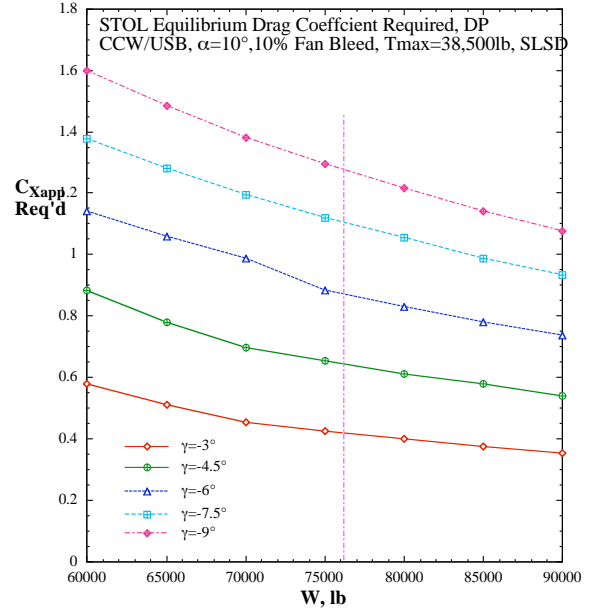
Fig. 7- Equilibrium Approach Iterated C_X Available with α =10°
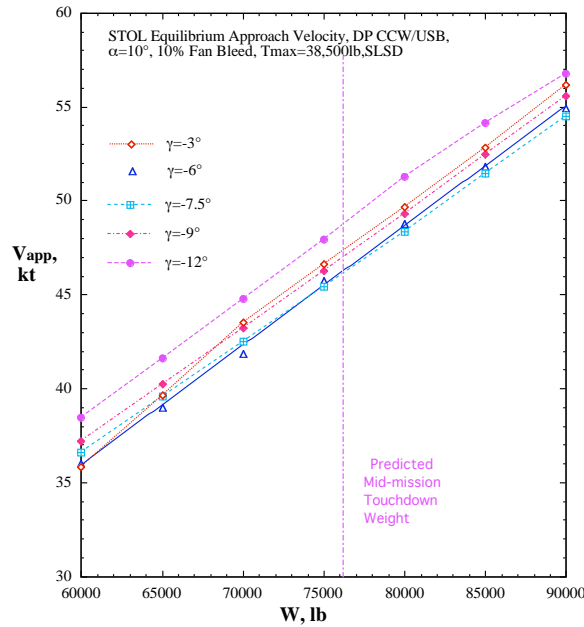
Fig 8- Equilibrium Approach Velocities, α=10°

Included in the data shown are landing ground roll after touchdown at the end of the STOL glide path (Fig. 9 below), and total landing distances along a constant glide slope over a 50-ft obstacle (Fig. 10 below). In the ground roll calculations, ground friction coefficient of μ_g=0.025 and braking coefficient of μ_{brake}=0.25 were used at Boeing suggestion, as was a thrust reverser effectiveness of 40% thrust reversal, applied immediately upon touchdown. Calculations were run for a range of glide slopes from γ= 0° to –12°. An input thrust limitation of 38,500 lb total and bleed limit for the blowing of 10% of total thrust (mVj = 0.10 x T_{total}) were

applied, and then CC bleed and engine thrust were adjusted until equilibrium was achieved for each approach condition being calculated. A predicted typical touchdown weight of 76,100 lbs was used, although this may not be the final touchdown weight after further design analyses. Fig. 8 above shows corresponding equilibrium approach velocities. For the typical mid-course touchdown/landing weight around 76,100 lb., approach velocities V_{app} of 45 -> 50 knots are predicted for sea-level standard day, depending on glide slope. Ground rolls using thrust reversal were shown in Fig. 9, where the goal of approximately 300 ft is seen to be possible. Fig. 10 shows total landing distance covered (air plus ground distance) if flying in equilibrium along a constant glide slope over a 50-ft obstacle with no flare at touchdown. Much larger distances than in Fig. 9 result due to the addition of air distance over the obstacle, with the steeper glide slopes yielding the shorter distance ($\gamma=0°$ is not relevant with respect to the 50-ft obstacle clearance). The importance of glide slope as a major factor in total STOL landing distance is obvious. Rate of sink limits have not yet been applied, and it is uncertain if the 50-ft obstacle clearance is a DARPA requirement for STOL approach. Please see the revised Ref. 11 (Attachment A) for further details.
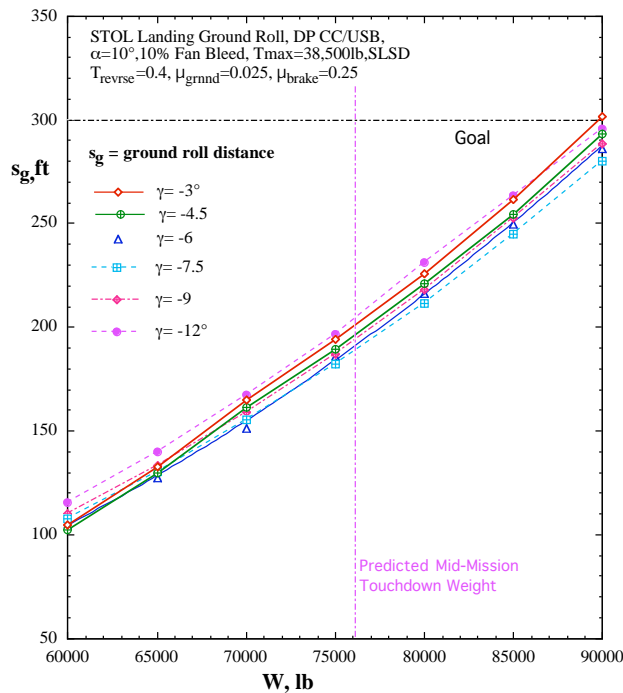
Fig. 9- STOL Ground Rolls after Touchdown, $\alpha=10°$
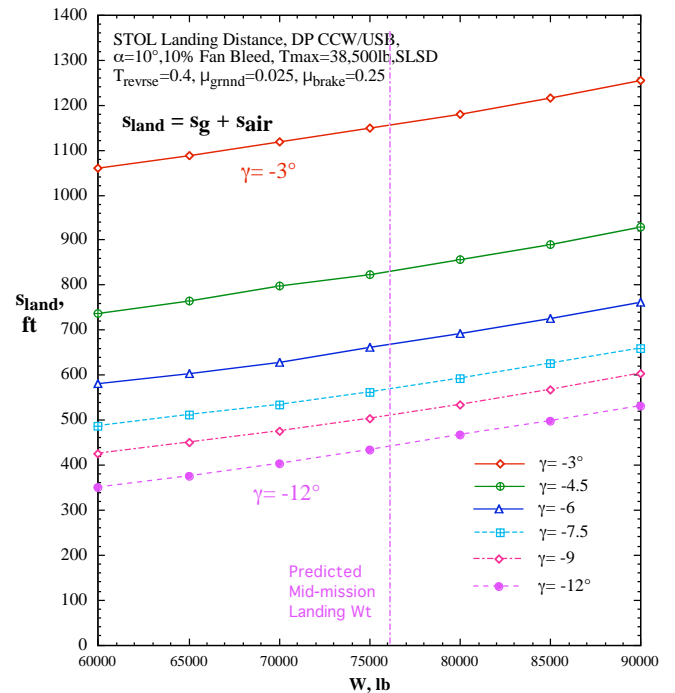
Fig. 10- Equilibrium Landing Distances $\alpha=10°$

Issues and Challenges: Whereas the STOL equilibrium landing performance shown above and in Ref. 11 predicts that the proposed CCW/USB powered-lift configuration should be able to meet the 300-ft landing ground roll goal, there are a number of issues yet to be resolved. Along those lines, GTRI has further concentrated during Quarters 3 and 4 on design/performance/operation of the approach/landing configuration, including required blowing mass flows and pressures. The Boeing DP powered-lift configuration design is heavily dependent on the input aerodynamic characteristics, but it needs to be understood that both the takeoff and landing aerodynamic/propulsive data inputs to these designs were based either on

analytical predictive tools or experimental data bases of similar but not exactly the same configurations. **It is thus recommended that prior to any further larger-scale designs of related vehicles, a much more reliable experimental data set based on the Fig. 1 concept be first acquired.**

Conclusions: The following conclusions were drawn by GTRI based on it's involvement up through Quarter 4 in the Distributed Propulsion Team's analyses of the above described powered-lift aircraft concept:

1. Based on the limiting assumptions made during these preliminary analyses, the desired STOL landing ground rolls of 300 feet or less appear to be possible due to very high lift and very high drag being achievable as needed on approach due to the pneumatic powered-lift configuration. Variations in multiple-engine characteristics and available powered-lift can improve this further.

2. Powered-lift aerodynamic characteristics achieved purely by analytical prediction for takeoff analyses or from empirically-modified powered-lift wind-tunnel model data leave some questions as to how close a Distributed Propulsion configuration with a 2-D nozzle (like the one shown in Figure 1) will match that preliminary data.

3. Parametric variations in such parameters as engine-nozzle–to-pneumatic flap relationships; pneumatic flap systems; engine/conventional flap systems; engine exhaust height and aspect ratio; pneumatic slot height and aspect ratio; wing leading-edge devices; and many other geometric issues have not yet been conducted, and are clearly needed to allow accurate characterization of these powered- lift configurations.

4. A conclusion of the August 3 DP Team Review meeting was that a larger-scale powered-lift 3-D model should be designed, fabricated, and tested in a large tunnel to provide the aerodynamic/propulsive data base for the DP ESTOL aircraft. **GTRI proposes here that prior to that large-scale test, smaller-scale testing (such as seen in Figure 11) should be conducted to provide the above parametric analyses (engine nozzle details, flap type for takeoff and landing, blowing geometries, control capabilities, pneumatic and engine parameter variation, etc.) prior to fabrication of a very expensive large-scale powered-lift model containing multiple real engines.** This large model will lack much of the parametric evaluation capabilities mainly because of the cost of complex multiple elements and variable geometries at large size undergoing expensive testing. GTRI stands ready and would be pleased to assist by conducting many of the parametric variations on smaller models and tests to guide the large model design during a follow-on effort to this current DARPA program.
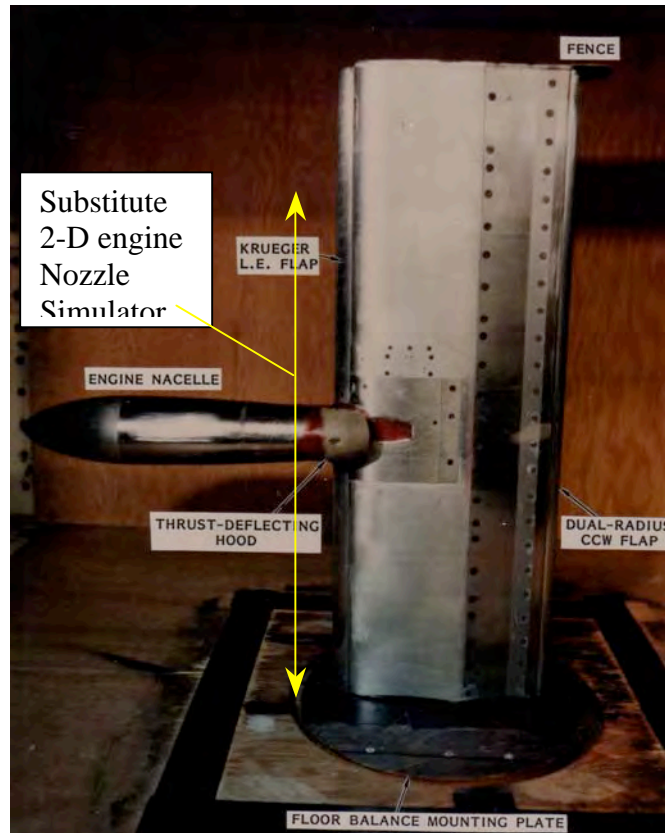
Fig 11- Smaller-scale Powered-lift Parametric Testing at GTRI
[Semi-span model with separate engine and pneumatic air sources]

Budget Information (end of September, 2007): Funds allocated and expended at the end of this Quarter 4 effort are shown below. The actual subcontract for GTRI participation in this program went into effect in early December, 2006, but the DARPA/MIT start date was November 1, 2006. The GTRI one-year effort is now complete.

The following summary financial data are supplied for Quarter 3:

Funds Allocated by MIT Subcontract	$87.5K
Costs Expended to Date (through 10/31/2007)	$89.3K

Key Deliverables and Milestone Status: As discussed above, progress is presented in this Quarter 4 and Final Progress Report, which is the only deliverable due at this time. It covers the time frame for work at GTRI from August 1 through October 31, 2007.

References:

1. Englar, Robert J., "Upper Engine versus Lower Engine Powered-lift Configurations, the STOL Takeoff and Landing Conflict," DARPA Distributed Propulsion Study, Working Paper G-2, Englar, January 10, 2007.

2. Englar, Robert J., "Supporting Data for Upper Surface Engine Powered-lift Configurations, and Related Technical Issues," DARPA Distributed Propulsion Study, Working Paper G-3, Englar, January 25, 2007.

3. Englar, Robert J., "Aerodynamic/Propulsive Data for Pneumatic Upper Surface Engine Powered-lift Configurations on STOL Approach," DARPA Distributed Propulsion Study, Working Paper G-4A, Englar, February 5, 2007.

4. Englar, Robert J., "Aerodynamic/Propulsive Data for Pneumatic Upper Surface Engine Powered-lift Configurations on STOL Approach, Data Supplement," DARPA Distributed Propulsion Study, Working Paper G-4B, Englar, February 8, 2007.

5. Englar, Robert J., "Pneumatic High Lift for Super STOL Approach: The Importance of Lift Augmentation and Drag" presented at DARPA/MIT Distributed Propulsion Review Meeting at MIT, Cambridge, MA, February 15, 2007.

6. Englar, R. J. "Pneumatic Aerodynamic/Propulsive Concepts for Distributed Propulsion, Phase I," GTRI Quarterly Progress Report 1, Nov. 1, 2006 to January 31, 2007", Feb. 14, 2007.

7. Englar, Robert J., "Pneumatic High Lift for Super STOL Approach: The Importance of Lift Augmentation and Drag, **Revision B**" presented at DARPA/MIT Distributed Propulsion Review Meeting at MIT, Cambridge, MA, **February 20**, 2007.

8. Englar, R. J., "Pneumatic Aerodynamic/Propulsive Concepts for Distributed Propulsion, Phase I," Quarterly Progress Report No. 2, Feb. 1 to April 30, 2007, May 7, 2007.

9. Harris, M. H., J. H. Nichols Jr., R. J. Englar, and G. G. Huson, "Development of the Circulation Control Wing/Upper Surface Blowing Powered-Lift System for STOL Aircraft," Paper No. ICAS-82-6.5.1, Proceedings of the ICAS/AIAA Aircraft Systems and Technology Conference, Seattle (22-27 August 1982).

10. Englar, Robert J., Marilyn J. Smith, Sean M. Kelley and Richard C. Rover III, "Development of Circulation Control Technology for Application to Advanced Subsonic Transport Aircraft, Part II: Transport Application", *AIAA Journal of Aircraft,* Vol. 31, No. 5, pp. 1169-1177, Sept-Oct 1994.

11. Englar, R. J., "Pneumatic High Lift for Super STOL Approach: High Lift and High Drag Development," Briefing presented at the DARPA/MIT Distributed Propulsion Review Meeting, at Boeing HB, August 3, 2007; Revision A, August 7, 2007.

Appendix B

Sponsored MIT Thesis

Scaling Considerations for Small Aircraft Engines

by

Nicholas Y.S. Chan

Submitted to the Department of Aeronautics and Astronautics
in partial fulfillment of the requirements for the degree of

Master of Science in Aeronautics and Astronautics

at the

MASSACHUSETTS INSTITUTE OF TECHNOLOGY

June 2008

Author . . . .
Department of Aeronautics and Astronautics
June 2008

Certified by . . . .
Alan Epstein
R. C. MacLaurin Professor of Aeronautics and Astronautics
Thesis Supervisor

Accepted by . . . .
Prof. David L. Darmofal
Associate Department Head
Chair, Committee on Graduate Students
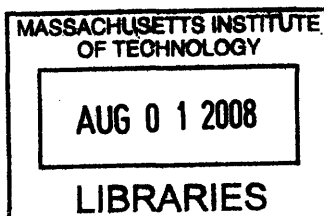
Scaling Considerations for Small Aircraft Engines

by

Nicholas Y.S. Chan

Submitted to the Department of Aeronautics and Astronautics
on June 2008, in partial fulfillment of the
requirements for the degree of
Master of Science in Aeronautics and Astronautics

Abstract

Small aircraft engines traditionally have poorer performance compared to larger engines, which until recently, has been a factor that outweighed the aerodynamic benefits of commoditized and distributed propulsion. Improvements in the performance of small engines have, however, prompted another look at this old concept.

This thesis examines aspects of aircraft engines that may have application to commodity thrust or distributed propulsion applications. Trends of engine performance with size and time are investigated. These trends are further extended to justify parameter choices for conceptual engines of the current, mid-term (10 years) and far-term (20 years). Uninstalled and installed performances are evaluated for these engines, and parametric studies are performed to determine the most influential and limiting factors.

It is found that scaling down of engines is detrimental to SFC and fuel burn, mainly due to the Reynolds number effect. The more scaling done, the more prominent the effect. It is determined that new technology such as higher TIT, OPR and turbomachinery η_{poly}'s for small aircraft engines enable the operation of larger bypass ratios, which is the most influential parameter to SFC and fuel burn. The increase of bypass ratio up to a value of 8 is found to be effective for such improvement. SFC decrease from the current to mid-term model is found to be ~20% and ~9% from mid-term to far-term. Range and endurance improvements are found to be ~30% and ~10% respectively for the mission examined. Finally, the mid-term engine model has performance comparable to that of a current, larger state-of-the-art engine, thus suggesting that improvement in small gas turbine technology in the next 10 years will make the application of commodity thrust or distributed propulsion an attractive option for future aircraft.

Thesis Supervisor: Alan Epstein
Title: R. C. MacLaurin Professor of Aeronautics and Astronautics

Acknowledgments

I would first like to thank my advisor Prof. Epstein for his continued support through difficult times. I would also like to thank Prof. Drela and Prof. Greitzer for their guidance while Prof. Epstein was away.

Over the last two years, the GTL has provided a friendly environment for me to work, thus I am indebted to everyone in the lab, particularly Lori and Holly for keeping everything running so smoothly. I also appreciate Dr. Tan's constant curiosity in what each student is doing; it kept me motivated.

I feel very privileged to have spent six years at MIT, which have been some of my best years, but more significantly, I made lifelong friends. I would especially like to thank Ben, Tri and Tudor for making these last few years so unbelievable. Most important to me, however, has been the support of my family: Stephen, Marjorie and Doug.

Contents

List of Figures

List of Tables

Nomenclature

ESTOL	Extremely Short Takeoff and Landing	
SFC	Specific Fuel Consumption	$\frac{lb}{lb-h}$
$\frac{T}{W}$	Thrust to Weight Ratio	
m_f	Fuel Mass Flow	$\frac{lb}{s}$
η_{th}	Thermal Efficiency	
u_0	Flight Velocity	$\frac{ft}{s}$
ISP	Specific Impulse	s
$\frac{L}{D}$	Lift to Drag Ratio	
W_g	Takeoff Gross Weight	lb
W_f	Weight of Fuel Burned	lb
η_{prop}	Propulsive Efficiency	
BPR	Bypass Ratio	
SLS	Sea Level Static	
TIT	Turbine Inlet Temperature	$^\circ R$
g	Gravitational Acceleration	$\frac{ft}{s}$
ρ_{avg}	Average Engine Density	
m_{dot}	Total Mass Flow	$\frac{lb}{s}$
V_8	Mixed-out Exhaust Velocity	$\frac{ft}{s}$
V_2	Inlet Velocity	$\frac{ft}{s}$
ρ_{air}	Air Density	$\frac{lb}{ft^3}$
OPR	Overall Pressure Ratio	
δ	Boundary Layer Height	
η_{poly}	Polytropic Efficiency	
Re	Reynolds Number	
Re_c	Reynolds Number Based on Chord	
c	Chord	
ν	Kinematic Viscosity	
FPR	Fan Pressure Ratio	
θ_t	TIT-atmospheric temperature ratio	
M_0	Flight Mach Number	
m_{dot}	Total Mass Flow	$\frac{lb}{s}$
u_e	Mixed out Exhaust Velocity	$\frac{ft}{s}$

FAA	Federal Aviation Administration	
FAR	Federal Aviation Regulations	
C_L	Coefficient of Lift	
$\frac{W}{S}$	Normalized Wing Loading	
S	Wing Surface Area	ft^2
b	Wingspan	ft
c_{avg}	Average Wing Chord	ft
c_{eng}	Average Wing Chord at Engines	ft
b_{eng}	Span Covered by Engines	ft
p_0	Static Pressure	psf
T_0	Static Temperature	$°R$
a	Speed of Sound	$\frac{ft}{s}$
μ	Viscosity	$\frac{lb}{ft-s}$
VLJ	Very Light Jet	
VLJ1	Current Term Engine	
VLJ2	Mid-term Engine	
VLJ3	Far-term Engine	
EE	Existing Small Engine	
EGT	Exhaust Gas Temperature	$°R$
W_2	Inlet Weight Flow	$\frac{lb}{s}$
TO	Takeoff	
OPR	Overall Pressure Ratio	
HPC	High Pressure Compressor	
LPC	Low Pressure Compressor	
HPT	High Pressure Turbine	
LPT	Low Pressure Turbine	
π_{HPC}	HPC Pressure Ratio	
π_{LPC}	LPC Pressure Ratio	
π_{comb}	Combustor Pressure Ratio	
E	Energy Level	BTU
h	Altitude	ft
T_{ex}	Excess Thrust	lb
T_{net}	Net Thrust	lb
D	Aircraft Drag	lb
C_D	Coefficient of Drag	
q_∞	Dynamic Pressure	$\frac{lb}{ft-s^2}$
ΔE_{ex}	Change in 'Excess Energy'	BTU
Δt	Time Step	s
$\frac{dh}{dt}$	Rate of Change of Altitude	$\frac{ft}{t}$
γ	Flight Angle	
α	Angle of Attack	
$\alpha_{L=0}$	Zero-lift Angle of Attack	
V_0	Flight Velocity	$\frac{ft}{s}$
$\frac{dV}{dt}$	Acceleration (of Aircraft)	$\frac{ft}{s^2}$

Chapter 1

Introduction

1.1 Context and Background

Historically, it is considered that for aircraft, the bigger the better [2]. The same applies for aircraft engines and until recently, the conventional transport aircraft has favored twin-engine configurations [22]. It is possible however, to distribute the airflows and forces generated by the propulsive systems to improve the flight vehicle's aerodynamics, propulsive efficiency [36, 18], structural efficiency and/or aeroelasticity. Such a concept can be more broadly defined as distributed propulsion. It is implemented via an array of many small engines, rather than a few larger ones. However, smaller engines have poorer performance compared to their larger counterparts [6]. As such, it is traditionally viewed that this observation, along with the complexity, weight and possible impracticality of installation outweigh the gains associated with distributed propulsion.

Other than aerodynamic benefits, distributed propulsion enables propulsion-enhanced concepts, circulation control and viscous flow control. Circulation control works by increasing the velocity of the airflow over the leading edge and trailing edge of a wing via blowing [28]. In the context of distributed propulsion, this can be achieved through the exhaust of the propulsive systems if the engines are embedded in the wing (such an example is studied by Ko et al. [18]). These concepts allow for the blowing and/or suction of airflow over aerodynamics surfaces to enable boundary layer control, high lift augmentation and reduced drag [28, 29]. Further, there has been significant improvement in performance of

small engines [3], largely due to advancement of materials and manufacturing techniques [26, 6], in recent years. These factors, along with possible cost benefits through economies of scale, have prompted a re-evaluation of small aircraft engines in the application of commodity and distributed thrust.

1.2 Objectives and Outline

An integral part of such a distributed propulsion aircraft is the propulsive system, which is the focus of this study. This propulsive system is conceptualized as an array of many small engines (rated at between 1,000 and 10,000lbs). As scaling down of engines affects its performance non-linearly, it is deemed important to detail trends of how engine performance varies with respect to size. The improvement of small engines with time is also examined to determine how attractive distributed propulsion is now, and will be in the future.

Chapter 2 details and justifies these trends, of how engines performance varies with size, and how that has developed over time. More specifically, the chapter evaluates the relationships between SFC, thrust-weight ratio and, to a lesser extent, fuel burn with size and time. Loss effects and weight trimming tradeoffs from engine scaling are analyzed. Economic, reliability, noise and emission implications of distributed propulsion are also discussed.

The focus of chapter 3 is to determine how developing technology in small aircraft engines affects the application of commoditized thrust and distributed propulsion. Trends from chapter 2 are used in chapter 3 to develop conceptual engines for a distributed propulsion aircraft for the current, mid-term and far-term. Mid-term and far-term loosely represent 10 and 20 years from now. The trends from chapter 2 help justify the parameter choices (such as overall pressure ratio) for the mid-term and far-term engines. The uninstalled and installed performance of these model engines are examined to determine the viability of an ESTOL distributed propulsion aircraft today, and in the future. Further, parametric studies are performed to single out the most influential and limiting factors on performance. Finally, a mission for each installed engine model is analyzed to compare their performance, and hence compare the performance of today's conceptualized ESTOL

distributed propulsion aircraft with that of 10 years and 20 years away.

Chapter 2

Trends of Aircraft Engine Performance

The beginning of this chapter will focus on two important trends for distributed propulsion, aircraft engine performance as functions of time and size. The latter section will discuss the remaining trends and also factors invisible to the data points such as the economics of commodity thrust. Engine data used in this section are predominantly obtained from Jane's Aero-engines [1].

2.1 Key Trends for Distributed Propulsion

2.1.1 Performance, Size and Time

The purpose of this research is to evaluate propulsive systems in the application of commoditized or distributed propulsion. If distributed propulsion is applied to a Boeing 747 that initially operates four turbofan engines rated at 50,000lb each, the resulting 200,000lb of static thrust could hypothetically be divided into 10, 20 or any other number of engines. While the conceptual design for these smaller engines could be a scale down of the original engine, the performance of simply scaled down engines would be worse due to a variety of factors that are discussed in this chapter.

The first trend assessed is the relationship between engine performance and size, the second between performance and technology available at the time of development. Historically, gains in aircraft performance through distributed propulsion were outweighed by

its complexity and the poor performance of small aircraft engines [6]. Improvement in performance through time has prompted a revisit of the concept. By reviewing trends of performance (and other parameters) versus time, one could project a conceptual engine's performance and evaluate its value for distributed propulsion. Examples are examined in chapter 3.

Before these trends can be developed, engine performance, time and size need to be quantified. Performance can be broadly defined to include thrust to weight ratio, fuel consumption, operability, emissions and noise. The focus of this analysis will be on thrust to weight ratio and fuel consumption, which are measured by $\frac{T}{W}$ itself and thrust specific fuel consumption (SFC) respectively. SFC is defined by equation 2.1, and is inversely proportional to thermal efficiency. In this equation, m_f is the fuel mass flow, T is the net thrust, and η_{th} is the thermal efficiency.

$$SFC = \frac{m_f}{T} \sim O(\frac{1}{\eta_{th}}) \tag{2.1}$$

Thermal efficiency can be conceptually viewed as the fraction of thermal energy converted into mechanical work. This work is then converted into propulsive work on the aircraft. The efficiency in which the mechanical work is converted into propulsive work is called the propulsive efficiency (η_{prop}). The multiplication of η_{th} and η_{prop} is essentially the overall efficiency ($\eta_{overall}$, equation 2.2). Several other efficiencies can be defined (such as the transmission efficiency), but η_{th} and η_{prop} are particularly important in the efficiency discussion of aircraft engines [5]. The focus of studying SFC is on addressing η_{th}, which is the cycle efficiency. Data for η_{prop} is lacking since it also depends on the operating aircraft flight conditions. As a result, η_{prop} is not studied as a trend but discussed briefly in this chapter.

$$\eta_{overall} = \eta_{th} * \eta_{prop} \tag{2.2}$$

The most important output for transport aircraft is fuel burn. Its relationship with engine and aircraft parameters is demonstrated in the classic Brequet Range Equation (2.3) [5, p.5] where u_0 is the flight velocity, ISP is the specific impulse, which is inversely proportional to

SFC (equation 2.4), $\frac{L}{D}$ is the lift-drag ratio, W_g is the takeoff gross weight and W_f is weight of fuel burned. g in equation 2.4 is earth's gravitational acceleration.

$$Range = ISP * u_0 * \frac{L}{D} * ln\frac{W_g}{W_g - W_f} \qquad (2.3)$$

$$ISP = \frac{1}{SFC * g} \qquad (2.4)$$

For a given range, a commercial aircraft's likely mission is to minimize cost per passenger. $\frac{L}{D}$ and u_0 are predominantly governed by the airframe design. The engine contributes to the equation in the form of cycle efficiency (ISP) and engine weight (part of W_g). In this chapter, SFC is used instead of ISP, and engine weight is non-dimensionalized in the form of $\frac{T}{W}$.

When the relationships between fuel burn, size and time are studied, it can be seen that other factors, including weight and SFC, affect it, as shown by the range equation. However, trend analysis in this chapter is limited to two dimensions, which limits the validity of conclusions drawn in this chapter with regards to fuel burn. A breakdown of fuel burn into its simpler parts could yield insight into how it may be affected by technology. This breakdown can be separated into weight, SFC and propulsive efficiency (η_{prop}).

Other parameter choices for this trends analysis are time and size. These are respectively quantified by year of certification and the engine's rated thrust at sea level static (SLS) conditions. The quantities more frequently associated with size are volume and mass. Volume varies greatly with the bypass ratio (BPR), which would provide a false sense of size. For example, two engines with different BPR's operating with the same technology (such as the same turbine inlet temperature (TIT)) may produce the same thrust, but because they operate at different BPR's, they would be sized differently and hence their volumes would be different. As a result, comparison of these engines by volume would not be fair. Mass, directly related to volume, also varies with BPR and technology. The higher the BPR, the larger the fan and hence the more casing required to contain blades. With technology, lighter and more performance-effective material may become available, affecting the density and volume, and subsequently mass of the engines. Thrust is also dependent on BPR

21

but its effects are mitigated by observing the trends for different ranges of BPR's separately.

Before presenting the trends, it is important to note that they offer insight, but are not necessarily quantitatively accurate. Factors for this include the mission for which the engine is designed for, the multi-dimensional dependence of parameters, etc. These factors are discussed in the chapter.

2.1.2 Performance vs. Size

$\frac{T}{W}$ vs. size

In order to analyze $\frac{T}{W}$ with varying size, some meaningful relationship between the two must be developed. One approach is to assume that as size of an engine increases, the length (l) increase is proportional to the fan radius (r) increase. This is a reasonable assumption, considering that engines in general have similar shapes. With this assumption, that l and r are of the same order, it can be deduced that weight increases with the cube of r (equation 2.5). Thrust on the other hand, increases with the square of the r (equation 2.6). Combining these relations leads to what is known as the cube-square law, where weight increases by a factor of $\frac{3}{2}$ faster than thrust with increasing diameter. Theoretically, this law shows that as thrust of the engine increases, $\frac{T}{W}$ should vary by $O(\frac{1}{\sqrt{T}})$ (equation 2.7). Note that in equation 2.5, g is gravitational acceleration, ρ_{avg} is the average density of the engine (irrelevant but included for completeness) and in equation 2.6, m_{dot} is the total mass flow, V_8 is the mixed out exhaust velocity, V_2 is the fan inlet velocity and ρ_{air} is the density of air.

$$W = g * Volume * Density = g\pi r^2 l \rho_{avg} \sim O(r^3) \tag{2.5}$$

$$T = m_{dot} * (V_8 - V_2) = \rho_{air}V_2\pi r^2(V_8 - V_2) \sim O(r^2) \tag{2.6}$$

$$\frac{T}{W} \sim O(\frac{r^2}{r^3}) \sim O(\frac{1}{r}) \sim O(\frac{1}{\sqrt{T}}) \tag{2.7}$$

Figure 2-1 compares this theoretical trend to engine data. While the cube-square law
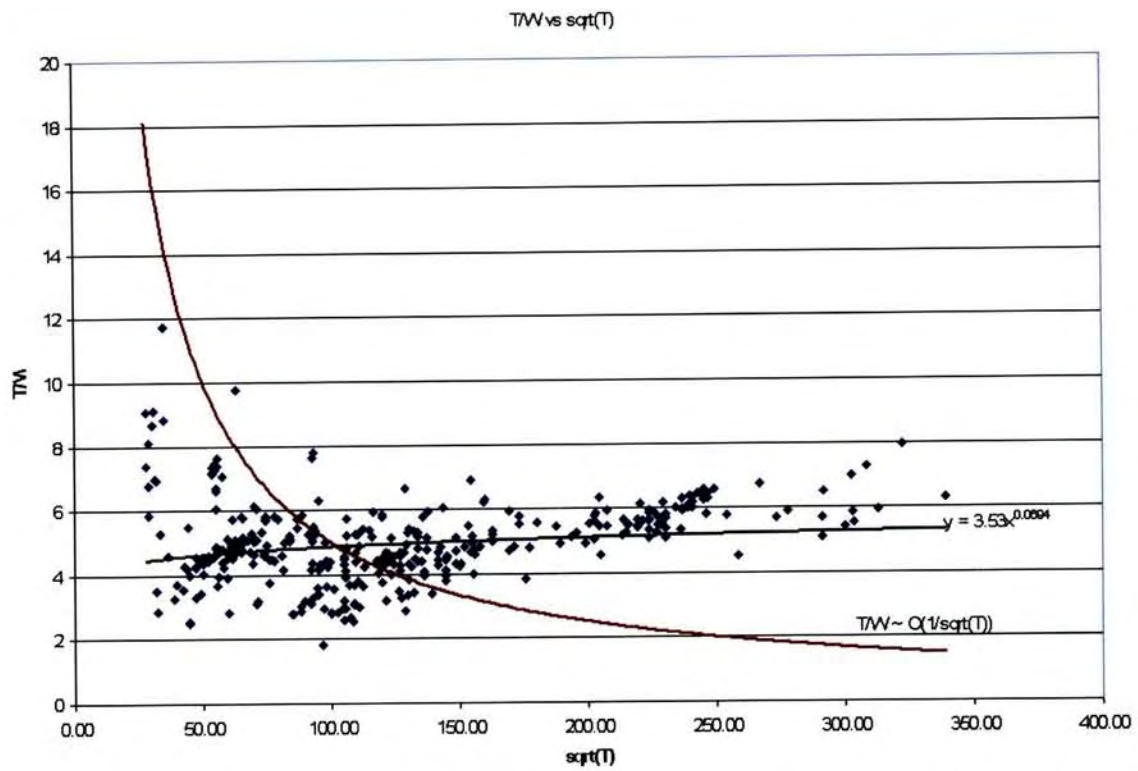
Figure 2-1: $\frac{T}{W}$ vs. $\sqrt{T}$: Brown line indicates how $\frac{T}{W}$ should theoretically vary with $\sqrt{T}$, black line indicates power-based trendline for actual data

predicts that $\frac{T}{W}$ should be decreasing with increasing engine size (i.e. $\sqrt{T}$), the figure shows that the actual $\frac{T}{W}$ is increasing slightly. This difference can be attributed largely to the fact that accessory weights do not scale linearly with size [6, p.18]. Furthermore, the relatively thicker casing (to contain the blades)[6, p.25] and larger combustor [6, p.21] also contribute to this difference between actual and theoretical trend.

It has been conjectured that the cube-square law may be more accurately characterized as a $\frac{5}{4}$ law [6, 16]. However, the observations from figure 2-1 suggest that even this characterization does not describe the data. In addition, the reference to the $\frac{5}{4}$ law may be outdated since the cited paper [16] was presented in 1955.

A further explanation is that the mission requirements drive the weight of larger engines to be proportionately less. Larger engines were, and are developed for applications that justify higher development costs compared to smaller engines [6, 11]. Therefore, more resources may have been put into design, expensive materials, and complex manufacturing techniques such as hollow blades that may not have been an option for small engines due to cost. The weight of the small engine and thrust density may therefore lag behind its larger counterpart.

SFC vs. Size

The SFC is examined at cruise conditions since fuel efficiency matters most at this flight condition. The data demonstrates that larger engines with higher thrust ratings have lower cruise SFC compared to smaller engines as shown in figure 2-2. Several factors contribute to this higher efficiency (lower SFC). A reason for why larger engines have higher overall pressure ratios (OPR) and lower SFC's is that they are designed for such demands even at the tradeoff expense of increased weight and cost [6, p.16] [11]. In addition, this accumulation of data represents engines intended for many different applications from different era. A more careful evaluation of the data needs to be done before definitive statements can be made.

SFC vs. Cruise Thrust
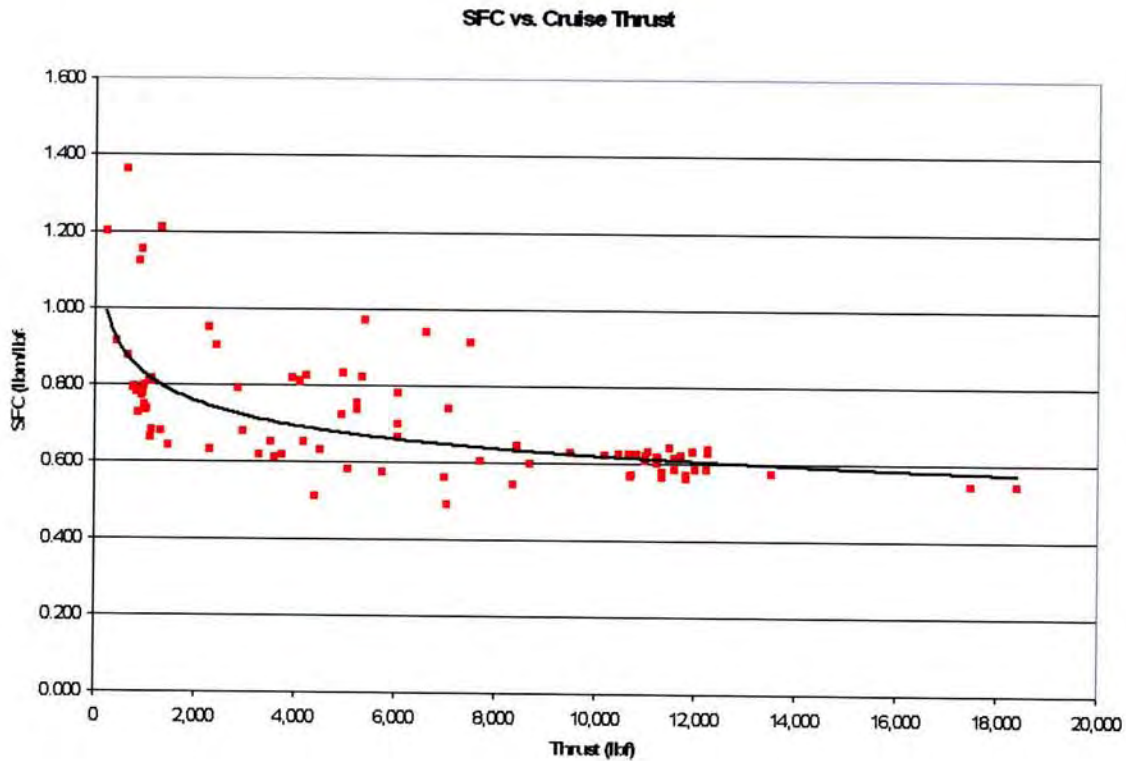
Figure 2-2: Cruise SFC vs. SLS Thrust [1]

Turbomachinery's Scaling Effects on SFC

Smaller engines have larger tip clearances relative to their blade and vane lengths, and as a result induce higher pressure losses in the flow percentagewise [4, 6]. Similarly, the boundary layers developed are larger in scale for the smaller engines, meaning viscous losses are proportionally higher. The Reynolds number effect further contributes to viscous losses. With shorter chord blades, the Reynolds number of the flow is lower. These lower Reynolds numbers result in higher drag coefficients [14]. Further, smaller engines suffer loss in turbomachinery efficiency due to reduced Reynolds numbers from increasing altitude [6, P.18] [12, 14]. Lower Reynolds numbers with laminar flow can also result in tip clearance losses as high as twice that of high Reynolds number flows [15].

Figure 2-3 depicts the OPR as a function of SLS thrust. It can be seen that OPR increases with increasing size. A major reason for the lower OPR of small engines is the development cost associated with high OPR's. Whereas for large engines, higher OPR's are selected to achieve a lower SFC, which is worth the tradeoff of higher cost and possibly

25
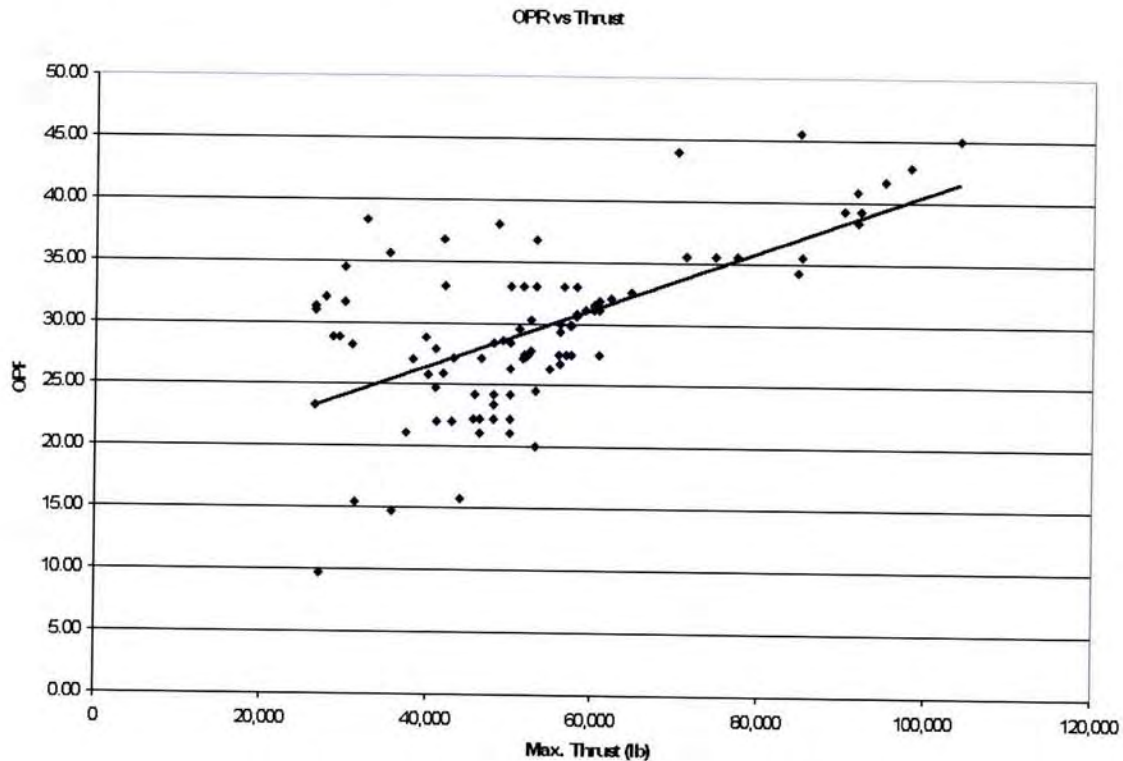
Figure 2-3: Overall Pressure Ratio vs. SLS Thrust

weight [11]. The Reynolds number effect and boundary layers further contribute to this OPR differential between large and small engines by inducing greater pressure loss. As a result of different design motivation, a better comparison between large and small engines would be pressure rise per compressor stage.

Smaller engines have the disadvantage of limited capability for effective cooling due to manufacturing, material and cost constraints [6, p.23]. Its ability to achieve higher turbine inlet temperatures (TIT's) is affected as a result. The predominant laminar boundary layer of smaller engines due to the Reynolds number effect also plays a role in limiting the maximum achievable TIT. A higher TIT allows for higher thermal efficiency though for a given BPR, propulsive efficiency suffers due to the greater exhaust velocity. While there is this tradeoff, a more powerful core enables the use of larger fans, which in turn improves propulsive efficiency [5, p.69].

A Study of Reynolds Number Effect on Polytropic Efficiency

To quantify the Reynolds number (Re) effect on polytropic efficiency (η_{poly}) and SFC, a study is performed based on the empirical model expressed in equation 2.8 [4, 7, 8]. In this equation, η_{poly} is the polytropic efficiency of the compressor, k is a constant, Re_c is the Reynold number based on chord at the midspan of the compressor, and n is a parameter dependent on the engine and blade geometry. Typical values for n are between 0.1 and 0.3 [4]; a value of 0.2 is used in this study.

$$1 - \eta_{poly} = kRe_c^{-n} \tag{2.8}$$

For this model, it is assumed that the Reynolds number losses are independent of Mach number. Concerns regarding the correlation of flow Mach number and Reynolds number are discussed in [7]. The reference engine used in this study is the CFM56-7B22, for which a cycle model is developed using GasTurb [25]. The design point is at top-of-climb such that the OPR, maximum climb thrust and corrected airflow are matched (data obtained from [1, 9]). It is assumed that the η_{poly}'s of the compressors are 0.89, η_{poly}'s of the turbines are 0.90 and the Re_c is $1*10^6$, which are believed to be representative values for state-of-the-art engines of this size. With these assumptions, the constant k is determined.

$$Re_c = \frac{uc}{v} \tag{2.9}$$

Reynolds number based on chord is defined in equation 2.9. In this equation, u is the incident flow velocity, c is the chord and v is the kinematic viscosity. It is assumed that u and v remain constant with the scaling of the engine. Since it is also assumed that the compressor tip velocity remains constant during scaling, the mid-span velocity of the blade, and hence u, also stay the same. With v and u constant, Re_c is thus linearly correlated to chord, which means that scaling down of the engine affects Re_c linearly. The resulting compressor η_{poly}'s are shown in figure 2-4.

Since scaling up is not considered, the point of highest efficiency is associated with the CFM56 model. The graph shows that the compressor η_{poly} decreases faster when at lower Reynold numbers. In other words, the smaller the engine becomes, the more the

Reynolds Number Effect on Compressor Polytropic Efficiency
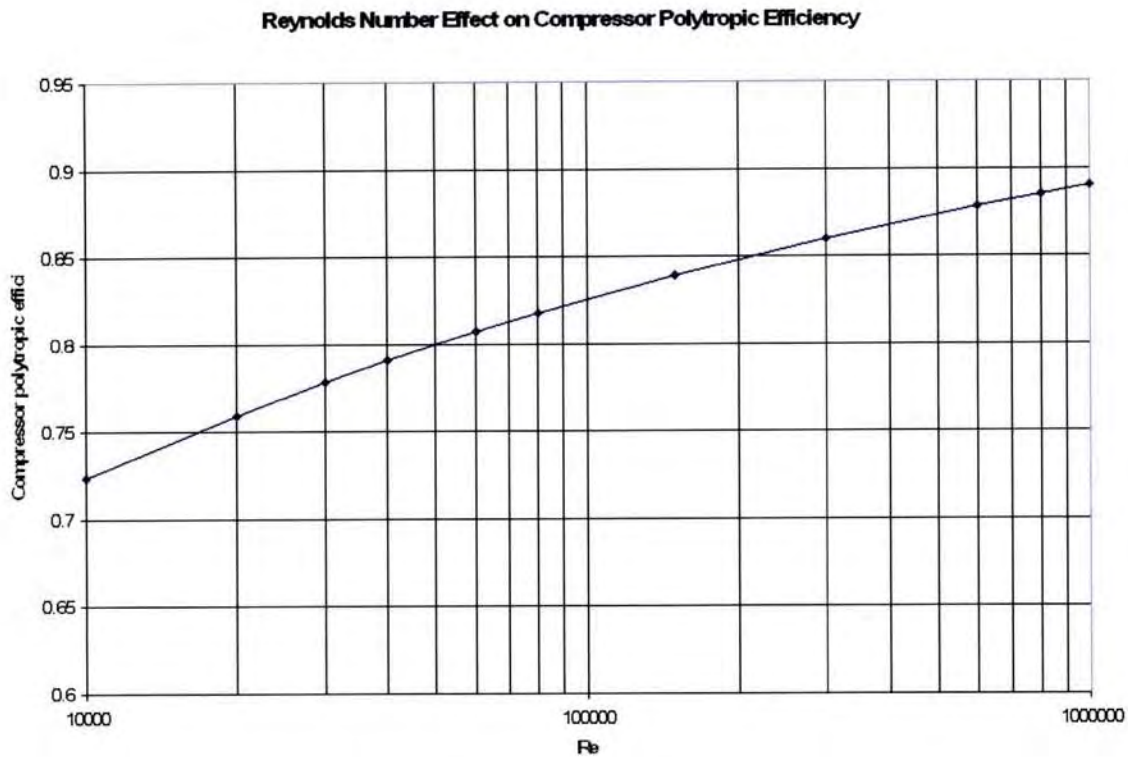
Figure 2-4: Reynolds number effect on compressor polytropic efficiency

compressor efficiencies suffer from scaling down.

The effects of Reynolds number on turbomachinery efficiency is taken one step further by examining the cycle in which these turbomachineries operate. These efficiencies are adapted into the engine cycle model to reflect Reynolds number effects from scaling down the CFM56. Note that thus far, the efficiencies estimated are for compressors. For simplicity, the turbines are assumed to follow the same trend as the compressors but with 1.5% higher polytropic efficiencies. Each of these scaled down models have fan pressure ratios (FPR) optimized for cruise. The result of this analysis is shown in figure 2-5, which is a plot of SFC versus Reynolds number. As in the case of η_{poly}, the SFC degradation due to the Reynolds number effect is greatest at low Reynolds numbers. This indicates that losses in very small engines are dominated by the Reynolds number effects.

So far, the study has been limited to the conceptual scaling of the CFM56. In the application of commoditized and distributed propulsion, this concept can be further developed by implementing the scaled models into a baseline aircraft, such as the Boeing 737. This

28
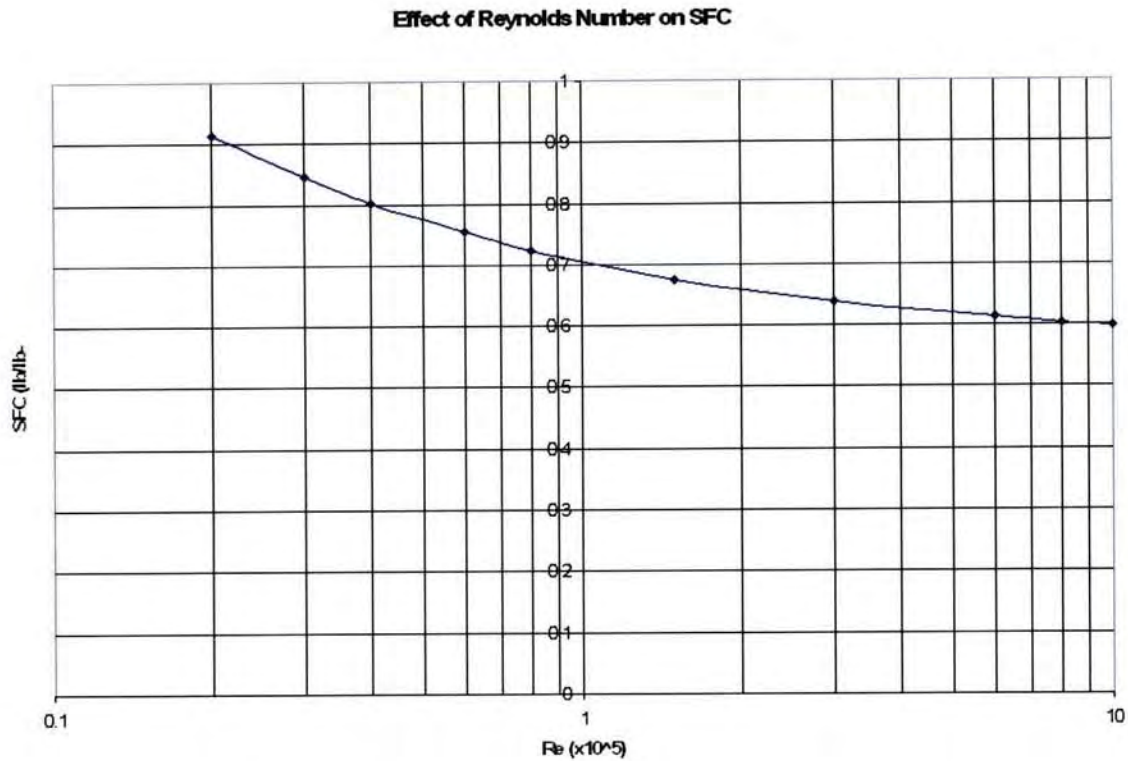
Figure 2-5: Reynolds number effect on cruise SFC of CFM56 model

case is examined to evaluate the installed performance of scaled engines via parameters such as fuel burn and range. The Breguet Range equation (2.3) is used for this analysis.

$\frac{L}{D}$ and u_0 are constant for each configuration so the insight gained from this study is how engine weight and cycle efficiency trade off. The weight of the CFM56 is 5216lb and its length is 98.7in. In theory, weight should scale with length cubically, but components such as accessories, casing and blades do not scaling accordingly [6]. For simplicity, the $\frac{5}{4}$ law [6, 16] is adopted for relating weight to thrust when scaling. This is a rough estimate, especially since earlier in the chapter, data presented raised questions regarding the validity of this $\frac{5}{4}$ observation. Recall that the lack of $\frac{T}{W}$ gain in smaller engines is partly due to the cost of development [6]. If a transport aircraft, such as one similar to the Boeing 737, is designed using distributed propulsion, there may be added incentive and funds to develop this lower $\frac{T}{W}$ potential of smaller engines. In light of this, it is believed that the $\frac{5}{4}$ observation is a realistic goal for the future (if distributed propulsion were to become a priority), and hence adopted for this study.

29

Table 2.1: Baseline Aircraft Parameters: Adaptation of a Boeing 737-600 [10]

Aircraft Empty Weight with Payload (lb)	88500
Range (nmi)	3000
Cruise Speed (M)	0.785
Cruise Altitude (ft)	35,000ft

The lower thrust from scaling is represented by the decrease in mass flow through the inlet, which simply varies with the square of the engine length (equation 2.10). This mass flow is an input to the cycle model, which returns the thrust at cruise for a given scaled-down model. The $\frac{5}{4}$ observation is then used to estimate the weight of the engines from scaling down.

$$m_{dot} = \rho_{air} V_2 \pi r_{fan}^2 \sim O(l^2)$$ (2.10)

By knowing the thrust that each engine produces at takeoff, the number of engines needed to power the baseline aircraft can be determined. This number is determined by matching the total takeoff thrust to that of two CFM56 engines (45,400lb). This method is a rough estimate, since it assumes that the takeoff thrust required for all configurations are the same, which is not the case when considering that each engine has a different $\frac{T}{W}$. However, a more thorough estimate would require more assumptions, such as ones for the aircraft takeoff parameters, which would in turn introduce more errors.

The takeoff thrust is calculated in the engine models with the same turbine inlet temperature (TIT). This value is derived from the CFM56 baseline model such that the maximum takeoff thrust of 22,700lb is achieved.

These scaled engine models are implemented in a baseline aircraft, which is the 737-600. This aircraft is selected as it operates the CFM56-7B22 engine. The aircraft parameters are depicted in table 2.1. The $\frac{L}{D}$ is calibrated such that the CFM56 baseline configuration completes the cruise mission with the initial fuel load specified for the 737 (~46400lb) [10]. This $\frac{L}{D}$ is 10.3, which seems a slightly low estimation. The $\frac{L}{D}$ of the airplane at cruise should be more like 15~17. However, this $\frac{L}{D}$ is applied for all configurations, and has no effect on the results for comparing the scaled engine models since it is an aircraft parameter

30

Fuel Weight Required vs. Number of Engines
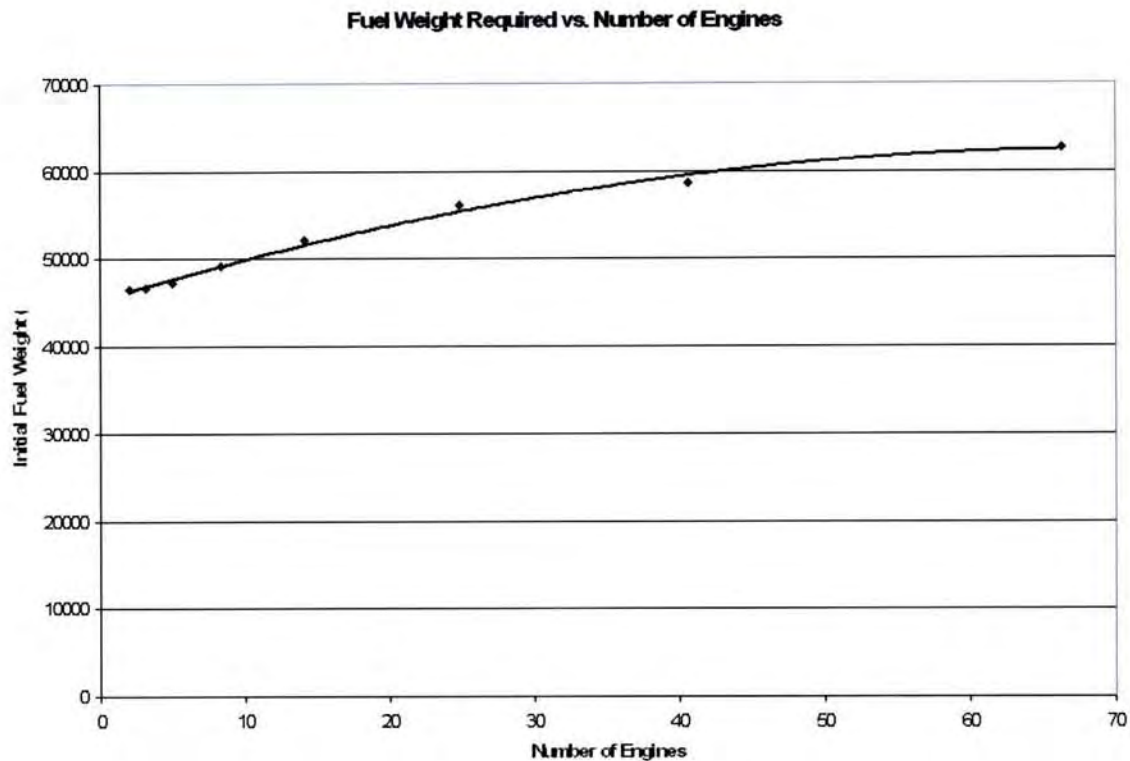
Figure 2-6: Initial Fuel Weight vs. Number of Engines

and not an engine one.

Figure 2-6 shows the initial fuel weight as a function of the number of engines. This initial fuel weight is computed using the range equation (2.3) to satisfy the range of the baseline aircraft (3000nmi). It can be seen that the fuel weight required increases when scaling down the engines, thus indicating that the Reynolds number effect on the cycle efficiency dominates that of the lower weight. As the number of engines increases, this worse fuel burn tapers, not because the Reynolds number effect becomes less dominant, but because the number of engines increases disproportionately. Simply stated, doubling the number of engines when there are only 2 results in 4 engines, but doubling 50 engines results in an absolute increase of 50 engines, thus stretching the x-axis of the graph disproportionately.

Figure 2-7 depicts a plot of the takeoff gross weight against the number of engines. The first data point, with 2 engines, is that of the CFM56 model. It can be seen that the first two iterations, which require 3 and 5 engines, result in a lower takeoff gross weight. This

31
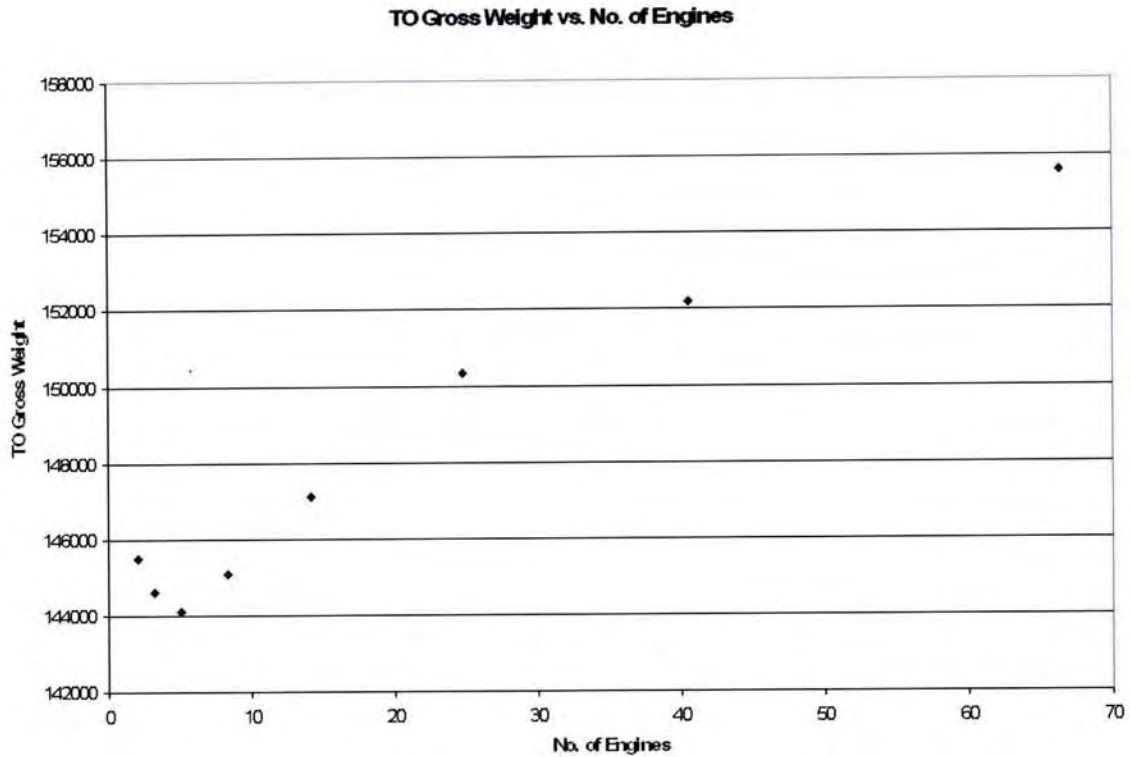
Figure 2-7: Aircraft Takeoff Gross Weight vs. Number of Engines

reduced weight indicates that the trimmed weight of the engines from scaling is greater than the fuel weight increase due to the Reynolds number effect. The goal for scaling however, is ultimately to lower the fuel burn since this is a commercial transport category aircraft. As a result, the lower takeoff gross weight achieved is null in this case, but it does indicate that depending on the mission, lower fuel burn can be achieved through $\frac{T}{W}$ gains from scaling.

To demonstrate that for shorter missions, lower fuel burn can be achieved through scaling, a mission for the same baseline aircraft is performed for a target range of 1000nmi. The empty weight of the aircraft is kept for consistency, i.e. such that the takeoff thrust required is similar. Further, it is assumed that 500lbs of engine weight trimmed corresponds to approximately 1% in SFC for a CFM56 class engine flying such a range. The same analysis is thus performed for this "corrected SFC" approach as a check for the Reynolds scaling approach. The results for both approaches are shown in figure 2-8. Blue represents the original model and pink represents the "corrected SFC" model. It can be seen that both approaches follow the same trend, but diverge as the number of engines increases. The
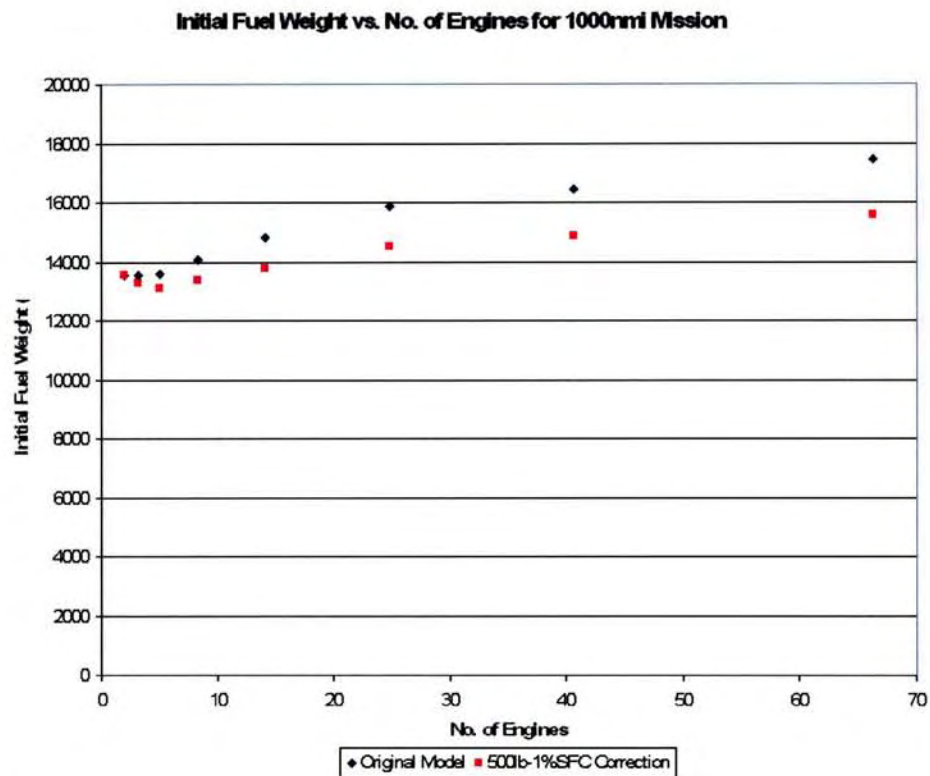
Figure 2-8: 1000nmi mission: Reynolds effect analysis and check of Reynolds scaling approach. Pink represents the "500lb to 1% SFC" model, blue is the original Reynolds scaling model applied to the Breguet range equation.

maximum difference (not necessarily uncertainty, since both approaches are estimates) is ~ 10%, which is reasonable considering the high level nature of both models.

Referring to the original model, there is a slight decrease in initial fuel required by increasing the number of engines (up to 5 engines). This indicates that for the shorter range mission of 1,000nmi, the $\frac{T}{W}$ improvement effect from scaling initially dominates (though marginally) that of the Reynolds number effect. For significant scaling down, however, it is clear that the Reynolds number effect negatively impacts the cycle efficiency too much for $\frac{T}{W}$ to compensate. If the empty weight of the aircraft is lower, or if missions are even shorter, the beneficial effects of $\frac{T}{W}$ from scaling would likely be more prominent.

Comparison of $\frac{3}{2}$ Scaling with $\frac{5}{4}$ Scaling

An examination of $\frac{3}{2}$ (cube-square) scaling demonstrates the extent to which scaling down may improve fuel efficiency of an aircraft. Again, such improvement is achieved through the benefits of increased $\frac{T}{W}$ outweighing those of the Reynolds number effect. Figure 2-9 depicts a comparison of cube-square scaling and $\frac{5}{4}$ scaling for the Boeing 737-class, 3,000nmi mission. It can be seen that with cube-square scaling, the fuel efficiency improves initially with scaling down of the engine. This beneficial $\frac{T}{W}$ effect of scaling, however, is outweighed by the Reynolds number effect beyond 10 engines. For the given mission, it can be determined that scaling down of the CFM56 can improve overall aircraft fuel efficiency if $\frac{3}{2}$ scaling is achieved.

An alternative view of $\frac{T}{W}$ effects from scaling down is its implication on SFC. In this case, 1% lowered SFC is assumed to be the benefit of every 500lbs engine weight saved from scaling down. Implications of this are similar to that of analysis already performed: it is essentially the extent to which SFC deficit due to the Reynolds number effect is balanced or superseded by the $\frac{T}{W}$ gains from scaling down. Comparison of this method with the original model are performed and demonstrated in figure 2-8, which was discussed earlier in this section.

Recall from figure 2-1, data showed that $\frac{T}{W}$ does not follow the cube-square law. The argument for this is that low weight and high efficiency is not a high priority for today's small aircraft engines. Rather, it is often low cost that is the driver. For larger engines,

Fuel Burn Comparison of 3/2 vs. 5/4 Scaling
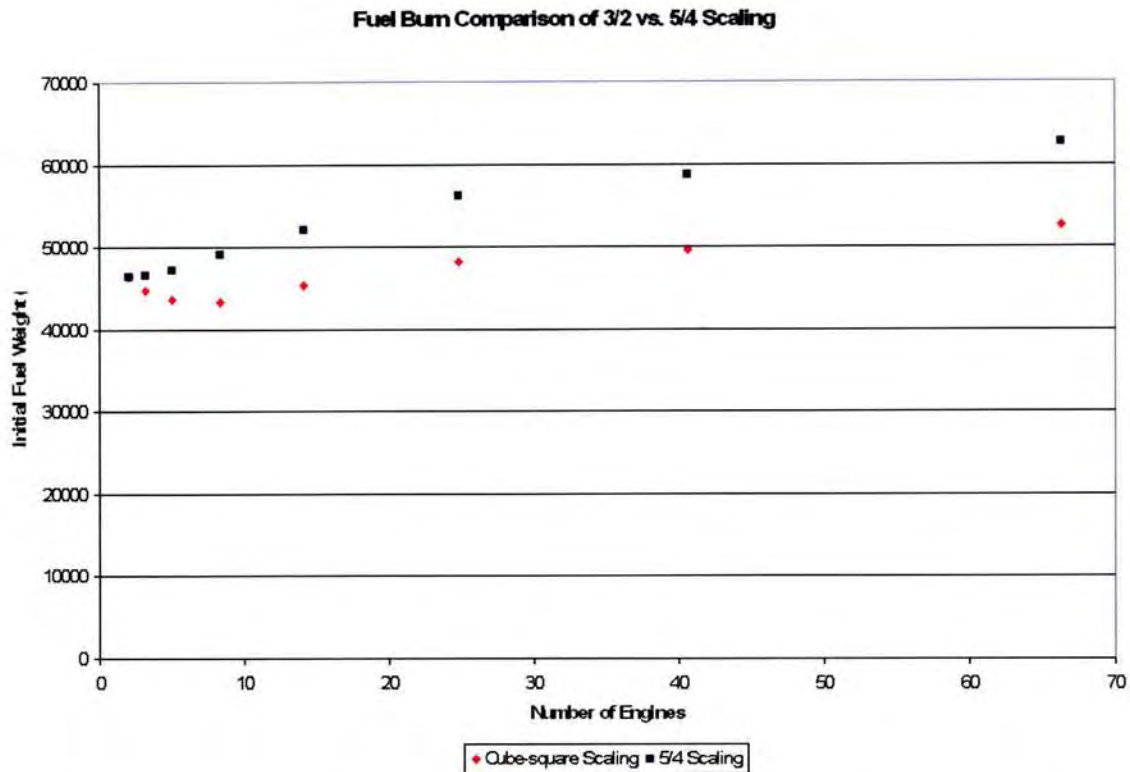
Figure 2-9: A comparison of $\frac{3}{2}$ scaling and $\frac{5}{4}$ scaling: Initial fuel weight versus number of engines for a Boeing 737 class, 3,000nmi mission.

this priority exists, since the associated aircraft and missions demand this low weight and high performance. The first-order estimation performed in this study demonstrates that there is opportunity for improvement in fuel efficiency with the application of scaled down engines. As a result, the missions that currently operate larger engines may have a competitive alternative by using small engines with the application of commoditized and distributed propulsion. With incentive in place, the cube-square law may be realized.

A factor unaccounted for in this analysis is that the Federal Aviation Regulations (FAR) requires aircraft with 4 or more engines to produce less thrust for takeoff than 2 engine aircraft; thus there would be weight savings that would ultimately lead to higher fuel efficiency. Further, the Reynolds number effect estimated in this study is empirically based on turbomachinery that currently exist. With technology improvements, it is likely that this effect will be less prominent in the future.

SFC vs. SLS Thrust (BPR<4)

$y = -2.40E-06x + 8.18E-01$
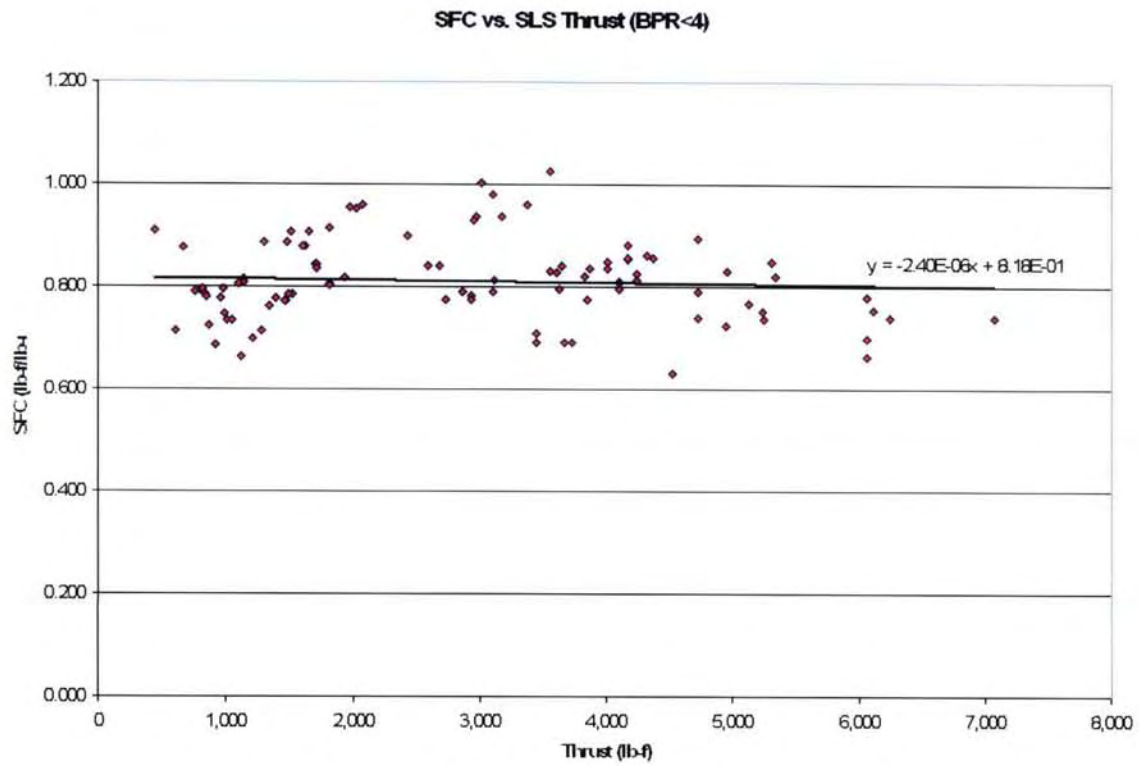
Figure 2-10: Cruise SFC vs. SLS Thrust for BPR < 4

Table 2.2: Cruise SFC variation with Thrust for different BPR's

BPR	SFC vs. Thrust slope
< 4	$-2.4 * 10^{-6}$
4 − 6	$-4.9 * 10^{-6}$
> 6	$-8.3 * 10^{-6}$
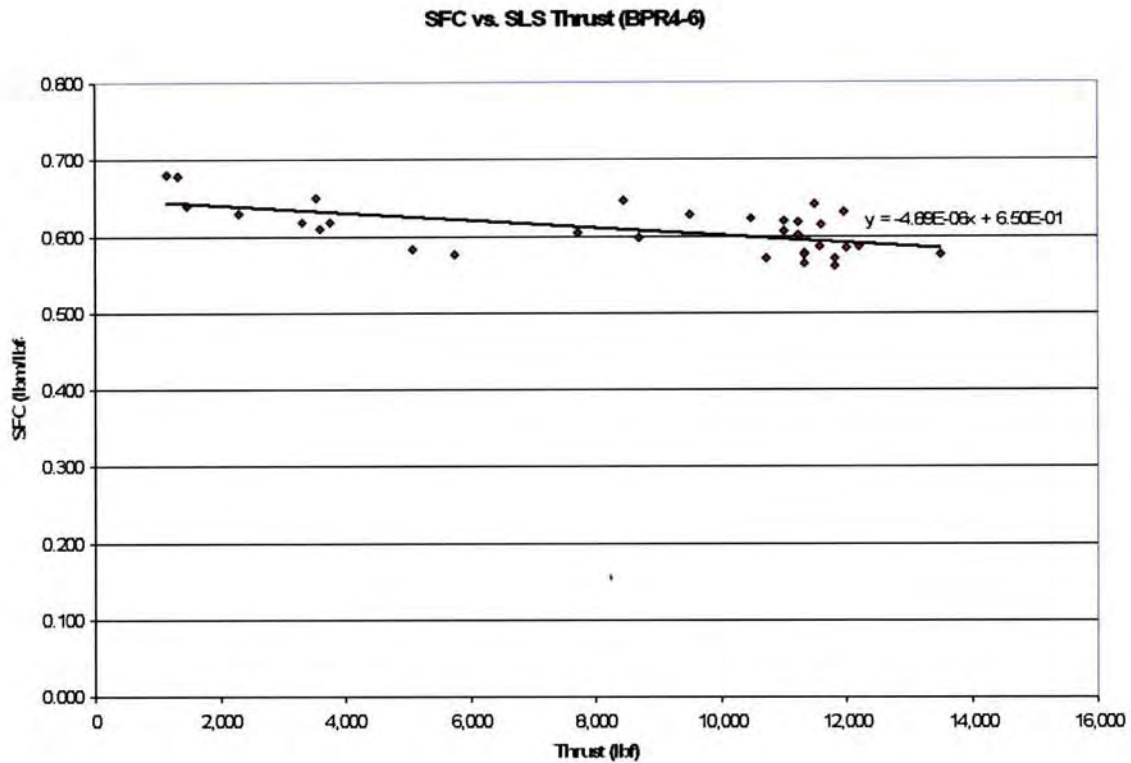
Figure 2-11: Cruise SFC vs. SLS Thrust for BPR of 4-6

Bypass Ratio's Effect on SFC

The SFC versus SLS thrust can be broken down into ranges of BPR. Figures 2-10, 2-11, and 2-12 depict the cruise SFC versus SLS thrust for BPR's below 4, between 4 and 6, and over 6 respectively. Like before, cruise SFC is examined because of the importance of efficiency at cruise (compared to takeoff). SLS thrust is used instead of cruise thrust since it is the reference for sizing the engine throughout this chapter.

The slopes of these graphs represent the rate of change of cruise SFC with size (table 2.2). The decrease in SFC with increasing thrust is doubled from a sub-4 BPR to a midrange BPR of 4-6, and then a further factor of 1.6 for higher BPR's, thus indicating that having larger engines is more beneficial for higher BPR's. It has to be noted however, that the comparisons are of engines that vary in design dates and uses.

Due to the uncertainty associated with the data, the theoretical effects of BPR is examined in figure 2-13 [5, p.50]. The curves depicted in the figure assume ideal BPR, which is considerably different than ones chosen for real engines. Nonetheless, trends can be drawn

37
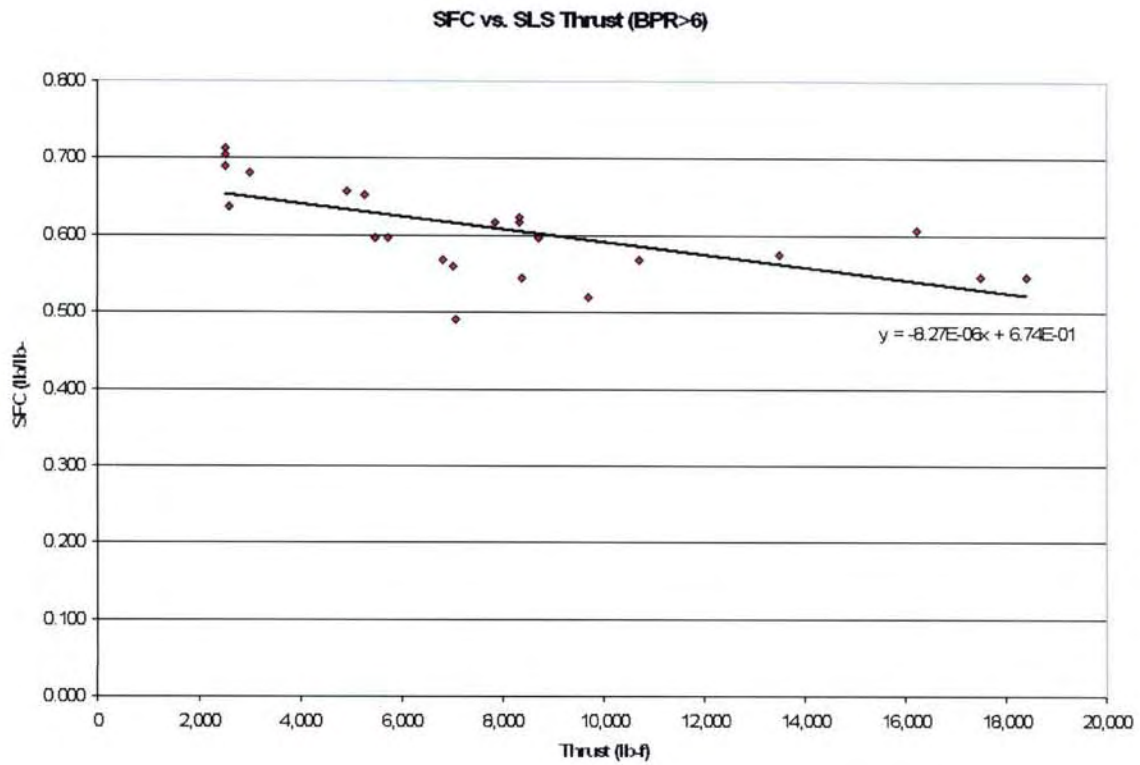
Figure 2-12: Cruise SFC vs. SLS Thrust for BPR > 6
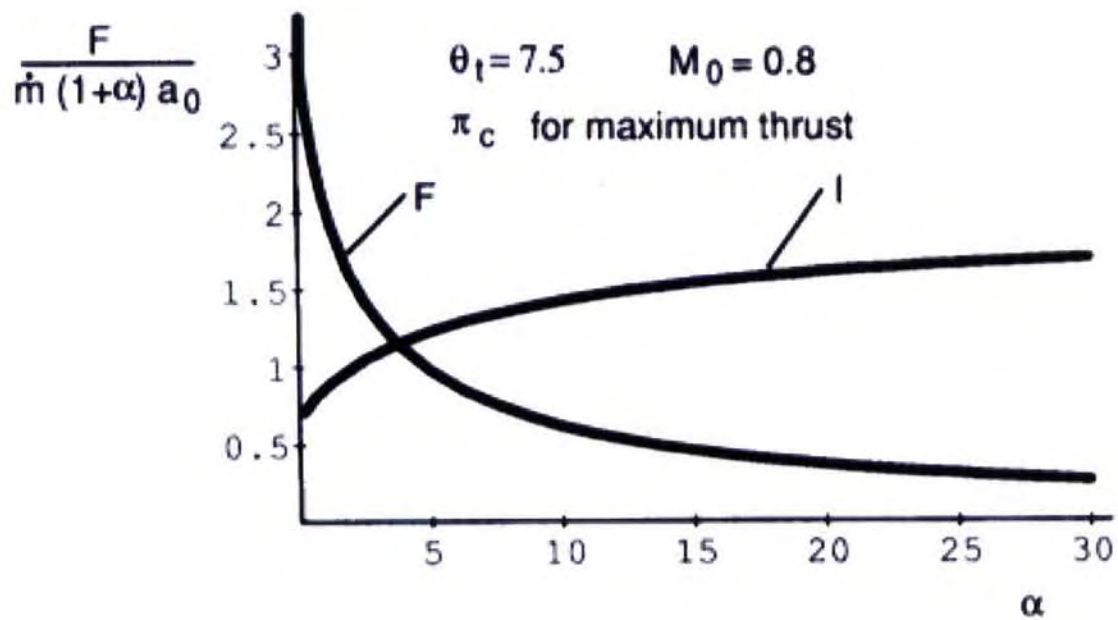
Figure 2-13: Effect of BPR on specific impulse and thrust per unit mass flow at flight conditions of $\theta_t = 7.5$ and $M_0 = 0.8$, [5, p.50]

Cruise SFC vs Year
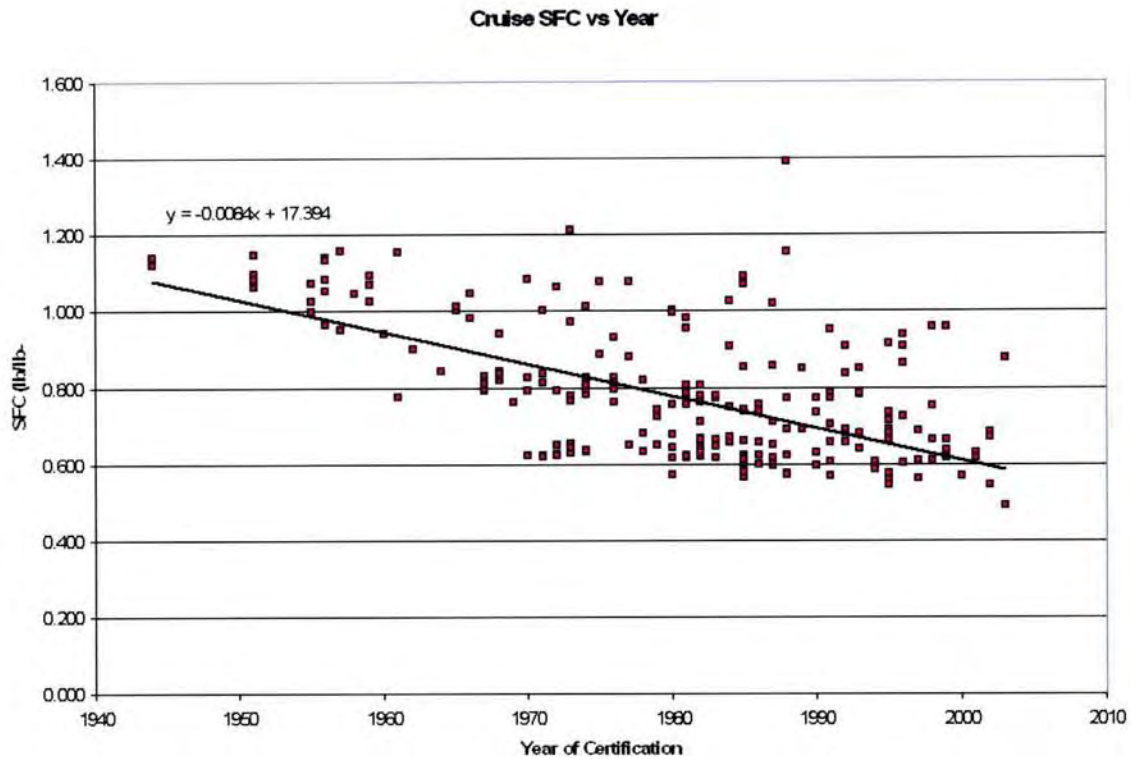
Figure 2-14: SFC vs. Year of Certification for all engines

from such a case to demonstrate its theoretical effects. With a fixed Mach number of 0.8 and TIT-atmospheric temperature ratio (θ_t) of 7.5, the effect of BPR on specific impulse (ISP) and thrust per unit mass flow is plotted. ISP is inversely proportional to SFC, so an increase of ISP can be viewed as an equivalent decrease of SFC. With higher BPR's, it can be seen that ISP increases but with a diminishing gradient, indicating that efficiency gains from increasing BPR is most significant in the lower BPR range. Further, the thrust per unit mass decreases dramatically with increasing BPR in a tapered manner. This decrease in thrust per unit mass implies that a proportional increase in total SLS thrust would require a much bigger engine for higher BPR's. In other words, thrust increase from scaling an engine is not linear, but depends on BPR. The extra gain in size leads to gains in performance through size effects, which can account for much of the steeper SFC vs. thrust slopes of larger BPR's in table 2.2.

39

Cruise SFC vs. Year (<15000lb Thrust)
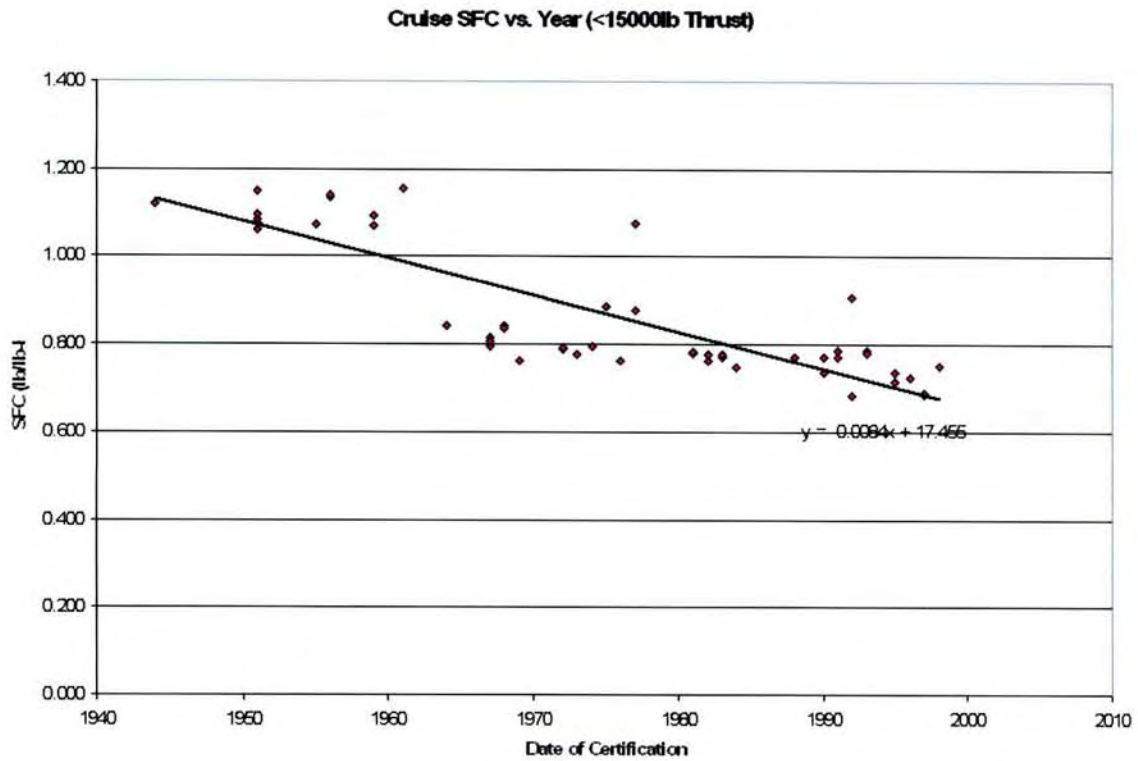
Figure 2-15: SFC vs. Year of Certification for engines with SLS thrust under 15000lb

Table 2.3: Cruise SFC vs. Year slopes segmented by thrust rating

Thrust	SFC vs. Year slope	Relative improvement compared to average
All	$-8.4 * 10^{-3}$	–
< 15000lb	$-9.2 * 10^{-3}$	+9.5%
> 15000lb	$-7.6 * 10^{-3}$	-9.5%
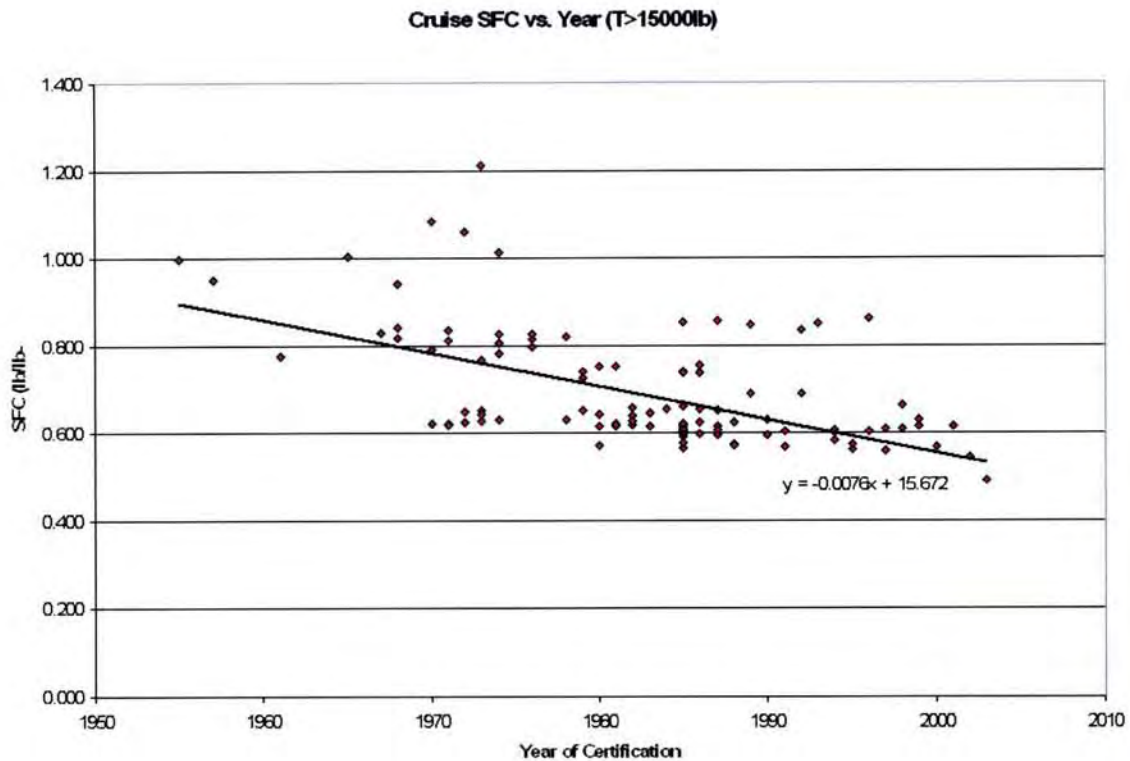
Figure 2-16: SFC vs. Year of Certification for engines with SLS thrust over 15000lb

2.1.3   Performance vs. Time

SFC vs. Time

As expected, smaller engines have poorer cycle efficiency, but it is important to realize how much worse and how that has changed over time. Figure 2-14 demonstrates the overall improvement of SFC with time. For engines of a very similar class, SFC has improved by about 1.5% per year over the last 20 years. Of interest to the distributed propulsion configuration are the smaller engines. By segmenting the data, improvement of engines with SLS thrust of less than 15000lb can be compared with those with more than 15000lb. Figures 2-15 and 2-16 represent these SFC timelines respectively. The slopes of these graphs demonstrate the rate at which SFC decreases over time. Table 2.3 depicts this improvement rate against the average (all engines). While the table indicates that smaller (sub-15000lb thrust) engines are improving faster, the uncertainty is too high to reach this conclusion. The results do demonstrate that the SFC improvement with time is at least similar for en-

41
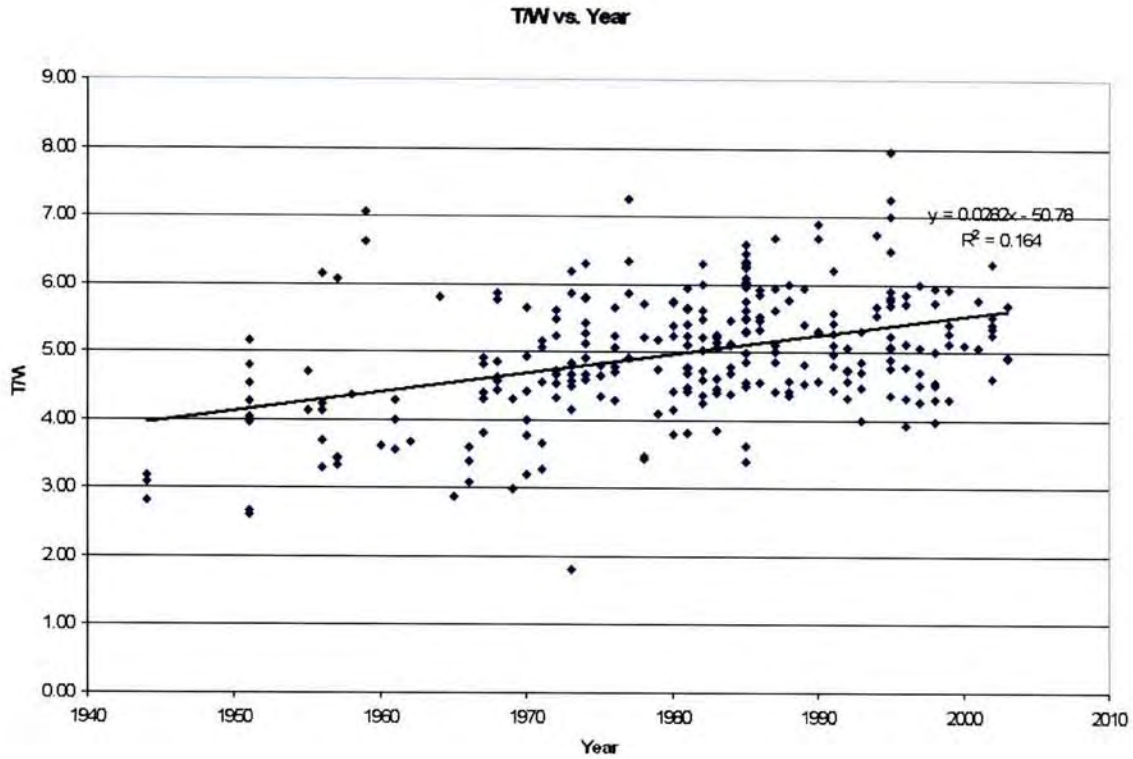
Figure 2-17: $\frac{T}{W}$ vs. Year of Certification for all engines

gines of different sizes.

Another consideration with time is that more powerful cores are being produced. This is due to improvement in manufacturing techniques, material and other design advances such as cooling technology [3]. For smaller engines, a higher BPR can now be operated since the smaller, but more energy-dense cores can generate the power to drive the larger fan. Referring back to figure 2-13, the largest gains in ISP from increasing BPR are at small BPR's, especially up to about 8. Gains taper off significantly thereafter. Currently, the upper bound of BPR for engines under 15000lb SLS thrust is 6.2, and for engines under 4000lb the cap is 4.0 [1]. Thus there is room for improvement for SFC by increasing the operating BPR. For example, if an old core that powered a fan with BPR of 4.0 is adapted with new technology and is now able to power a fan with BPR of 8.0, the SFC improvement is approximately 40% all else being equal. However, all else is not equal such as the decrease of thrust density from increasing BPR; such tradeoffs are discussed in the next chapter.

42

$\frac{T}{W}$ vs. Time

Figure 2-17 shows that the trend for $\frac{T}{W}$ is improving with time. This improvement can be segmented into the thrust aspect and the weight aspect. The thrust improvement is due to the same reasons as the improvement in SFC. The decrease in weight of newer engines can be attributed in part to improved engine efficiency, however the more significant factor is likely to be the advancement of materials technology that allowed for lighter blades/vanes and casing. There is no indication that smaller engines are improving at a different rate compared to larger engines.

Propulsive Efficiency

η_{prop} can be defined by equation (2.11) [5, p.3] where m_{dot} is the inlet mass flow and exhaust mass flow (since bleed and fuel flow are neglected), u_e is the mixed out exhaust velocity and u_0 is the inlet velocity.

$$\eta_{prop} = \frac{m_{dot}(u_e - u_0)u_0}{m_{dot}(u_e^2/2 - u_0^2/2)} = \frac{2u_0}{u_e + u_0} \tag{2.11}$$

The equation demonstrates that η_{prop} increases as the ratio of exhaust velocity to flight velocity decreases. BPR has this effect, in that it diverts power from the core (and hence core exhaust) to the bypass exhaust, thus lowering the mean jet velocity and increasing the η_{prop}. It has to be noted that while there is an improvement in η_{prop}, there is a decrease in specific thrust. This can be seen in equation (2.12) where F is the net thrust.

$$\frac{F}{m_{dot}} = (u_e - u_0) \tag{2.12}$$

This tradeoff of specific thrust with η_{prop} applies generally to all aircraft engines [5]. So while increasing BPR improves η_{prop}, specific thrust decreases and as a result more mass flow is required for a prescribed net thrust. This increased mass flow would require larger engines, which adds to weight. The increased BPR also adds weight to the engines as there is a larger fan and casing. Weight of high BPR engines has decreased with time in the form of material improvements and as a result it is more viable to operate higher and higher
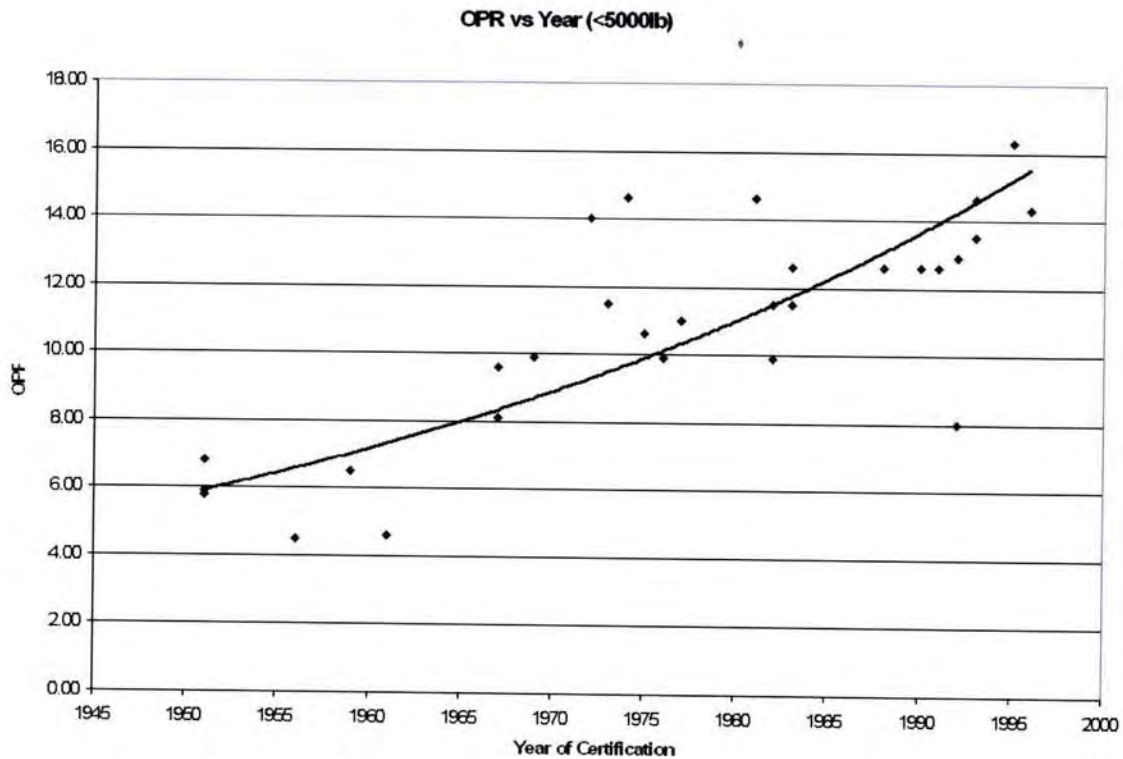
Figure 2-18: OPR vs. Year of Certification for sub-5000lb engines

BPR's, such as the GE-90 (with a BPR of 8.5) [26].

OPR vs. Time

Values of OPR for small engines are considerably lower than those of larger engines. The main explanation is that engines below 5,000lb thrust are constrained in manufacturing cost due to their market and use [6, 11], which makes raising the OPR limited since it is expensive to develop. Further, pressure losses per blade/vane row due to Reynolds number effects enhance the OPR differences between large and small engines.

The scope of distributed propulsion covers this priority currently lacking in small engines. By enabling long-range aircraft capabilities using such engines, SFC becomes more important and therefore OPR as well. So while the OPR capabilities of engines are already increasing by a factor of about 1.5 every 10 years for small engines (figure 2-18), there is opportunity for accelerated improvement if OPR were to become a priority for small engines in the future, which distributed propulsion promises.

2.1.4 Fuel Burn

Recall that the range equation (2.3) relates fuel burn to SFC and weight. While the goal for almost all commercial aircraft is to minimize cost, the manner in which this is achieved in the engines differs considerably. The most important factor for any given mission may vary from $\frac{T}{W}$, to SFC, to cost of development and maintenance. This brings up an earlier point that multiple factors affect fuel burn. However, the breakdown studies of SFC and $\frac{T}{W}$ demonstrate that both are improving with time, and therefore so is fuel burn. This trend of decreasing fuel burn is not quantified, but it suggests that gross weights of aircraft are decreasing due to more efficient and power-dense engines.

2.2 Further Considerations

2.2.1 Economics

With the application of distributed propulsion, the cost landscape can be altered in several ways. The obvious change is that many more engines are used per aircraft. To the furthest extent, it would be possible to produce a "standard engine". This engine would have a set thrust rating and the same engine could theoretically be employed by a number of different aircraft utilizing distributed propulsion. The difference would be the number of "standard engines" in each of these aircraft according to their total thrust requirement. This commoditization of thrust would allow for cost savings in development, manufacturing and maintenance.

Even if the "standard engine" were used in only two airframes, and granted that there would be non-overlapping development costs such as engine integration, it would still equate to one less engine being required for development. Even for small engines, this development cost can be in excess of tens of millions of dollars [27]. Further, for each aircraft, many more engines and spare parts would have to be made which would open up opportunities for manufacturing and maintenance savings through economies of scale.

Table 2.4: In-flight Engine Failure Analysis

	2 engines	4 engines	10 engines	50 engines
Assumed Engine Failure Rate	0.1%	0.1%	0.1%	0.1%
Prob. of 1+ engine failing	0.0020	0.0040	0.0099	0.048
Prob. of 2+ engines failing	$1.0 * 10^{-6}$	$6.0 * 10^{-6}$	$4.5 * 10^{-5}$	$1.2 * 10^{-3}$
Prob. of not meeting FAA regulations (more than half engines failing)	$1.0 * 10^{-6}$	$4.0 * 10^{-9}$	$2.1 * 10^{-16}$	$1.2 * 10^{-64}$

2.2.2 Mission Reliability and Safety

In the context of propulsive systems, mission reliability and safety addresses issues of in-flight shutdowns and aborted missions. A two-engine aircraft must be able to provide an "essential load" (which is the required power supply for functioning under operating conditions of the aircraft) after failure of one of the two engines [32]. For aircraft with three or more engines, essential loads must be provided in the event of two engines failing [32].

A straightforward reliability analysis of a 2-engine configuration, a 4-engine configuration, a 10-engine configuration and a 50-engine configuration shows that a distributed propulsion configuration operating many engines is less likely to have a mission-aborting case due to engine(s) failure. Reliability of engines varies over time, and likely over size (due to manufacturing accuracy, material tolerance, among other factors). The data for this is unavailable, however, so an assumption that engines of all sizes have the same reliability (failure rate) is made. Further, for simplicity assume that this rate is 0.1% per flight. A trial for how likely k number of engines fail out of n engines can be modeled as a binomial (equation 2.13 [33]) where p is the probability of an engine failing and p_X is the probability that event X happens (be it 1 engine failing, 2 engines failing, etc.).

$$p_X(k) = \binom{n}{k} p^k (1 - p)^{n-k}, \quad k = 0, 1, ..., n, \tag{2.13}$$

Table 2.4 shows the probabilities of 1 engine failing, 2 engines failing and the probability that the aircraft loses more than half its thrust (i.e. both engines for the 2-engine configuration, 3 for the 4-engine configuration, 6 for the 10-engine configuration and 26

for the 50-engine configuration). The study assumes that the configurations do not satisfy the essential load when they lose more than half their thrust, which is the same as half their engines.

From the table, it can be deduced that the more engines there are, the greater the likelihood for an engine failure, but it is still orders of magnitude less likely for multi-engine configurations to fail critically, which is to lose half its total thrust. More specifically, compared to the twin-engine configuration, the 4-engine configuration is $O(10^3)$ less likely, the 10-engine configuration is $O(10^{10})$ less likely and the 50-engine configuration is $O(10^{58})$ less likely. While this is an oversimplification for a reliability analysis, it does offer insight into how significant the difference is in probability of critical failure.

One can further argue that even if multiple engines fail in a 50-engine configuration, only a small percentage of total thrust is lost. For example, the probability of 2 engines failing (based on the previous example) is about $1.2 * 10^{-3}$ for the 50-engine configuration, which is less than the probability of 1 engine failing for the twin-engine case ($2.0 * 10^{-3}$). The thrust lost for the 50-engine case would be 4%, whereas for the twin-engine it would be 50%. So not only would 2 engines failing on the 50-engine configuration be less likely to occur, it also loses about 12 times less thrust compared to if the twin-engine configuration were to lose 1 engine. The significance of this is that the twin-engine configuration would have to abort its mission while the 50-engine aircraft would likely satisfy its thrust requirements and complete its mission.

Of greater concern to an aircraft using distributed propulsion is how an engine-out situation in-flight could affect its neighboring engines. This is of higher importance than in a conventional configuration as the engines are inevitably grouped much closer together, and hence have more coupled airflow. These effects are case-dependent on the overall propulsive system and airframe interface. Further, the Federal Aviation Administration (FAA) requires "engine isolation" such that a failed engine would not require the crew's attention nor would it affect the safe operation of the neighboring engines [34]. While, it is extremely likely that the performance of neighboring engines are affected due to their proximity, it is critical that the stability margins of the compressors not be shifted as to affect operability of the engine [30, 31].

2.2.3 Operability, Noise and Emissions

As mentioned earlier in the chapter, operability, noise and emissions are part of performance considerations. Due to lack of data and qualitative aspects of these factors, they are not reviewed in the earlier section regarding trends. A distributed propulsion setup would by nature operate a more complex system, as it incorporates more engines and coupling of these engines with the wing and control surfaces. This puts into question operability since these systems are much less tested, though in theory, physics does not prohibit such a configuration.

Noise would likely be reduced by a distributed propulsion configured aircraft due to the higher degrees of freedom offered for design to make such reductions. Many engines and their coupling with aerodynamics surfaces allow for designs that promote interference that would reduce noise [17].

While smaller engines have poorer performance, improvements in such engines over time coupled with the aerodynamic benefits of distributed propulsion may make the overall aircraft more fuel efficient, resulting in lower emissions. Further, there has been development that suggest emissions from small engines are being lowered significantly, mainly through combustor improvements [20, 21].

2.3 Uncertainty

As can be observed in figures from this section, the data is relatively scattered. Data used in this chapter's analysis is accurate but varies significantly due to many factors. The main reason for this scatter is that the trend analyses are based on two dimensions. Each parameter, however, such as fuel burn has dependence on multiple factors making the methodology flawed.

Different design objectives of each engine also contribute to the scatter. For example, performance parameters of gas turbines can vary between military aircraft and civil aircraft because their missions are so different. A civil engine is likely to be designed to maximize cruise performance whereas a military engine might be designed to maximize $\frac{T}{W}$ with less regard for cruise SFC. This discrepancy in design goals can lead to greatly differing

performance data. For this analysis, civil and military engines are not separated because there lacked data for small civil engines, especially for the early 90's. While there has been development of small civil engines in recent years, their shipments have declined in recent decades until the turn of the century when the economy rebounded [6, p.805] [13].

Another factor that led to more scattered data may be the capabilities of each company or country. A Russian-built gas turbine may have used different technology from one that Rolls Royce built even if they were designed in the same time period.

The date of certification is the best available indicator for the timeline of an engine, but does not necessarily provide a fair comparison of the engines. Redesigns or designs based on existing cores could have been certified at a much later date but may not have employed the newest available technology. Conversely, gas turbines that were conceived several years earlier than their date of certification may have been delayed for non-engineering issues such as government restrictions.

While the data is scattered, the trends expressed in this chapter are clear and indicate the direction in which gas turbine performance is heading. However, the lack of certainty makes it difficult to quantify these trends accurately.

Chapter 3

Small Gas Turbine for a Distributed Propulsion Aircraft

On use of multiple small engines would be to enable short or extremely short takeoff and landings by using the well known interaction of jet exhaust with wing control surfaces to generate such extra lift and drag, and low flight speeds [28].

In order to gain perspective of the extra lift required at takeoff, a comparable class of transport aircraft has a takeoff lift coefficient (C_L) of about 2.5. Such an aircraft requires about 800m to takeoff in its current configuration. Figure 3-1 shows that $\frac{T}{W}$ needs to be increased from 0.2 to 0.9 to achieve the goal of 100m takeoff. However, if the C_L can be increased by a factor of 4 with a fixed wing area (bottom curve of figure 3-1) then a $\frac{T}{W}$ of about 0.35 becomes required, rather than around 0.9 for the original configuration. This minimum C_L of 10 at takeoff is achieved by blowing on the control surfaces.

The airfoil is designed with the engine embedded in the wing (generic engine-wing depicted in figure 3-2). This 2D shape constrains the size of the fan and the length of the engine. Further, the thrust requirement at takeoff along with the span of the wing govern the number of engines and the spacing between each engine. Table 3.1 displays the parameters for the distributed propulsion aircraft and table 3.2 shows the takeoff and cruise conditions. With these constraints and conditions listed, engines with various performances are conceptualized for the aircraft.

This chapter pursues three configurations to determine the feasibility of current engines
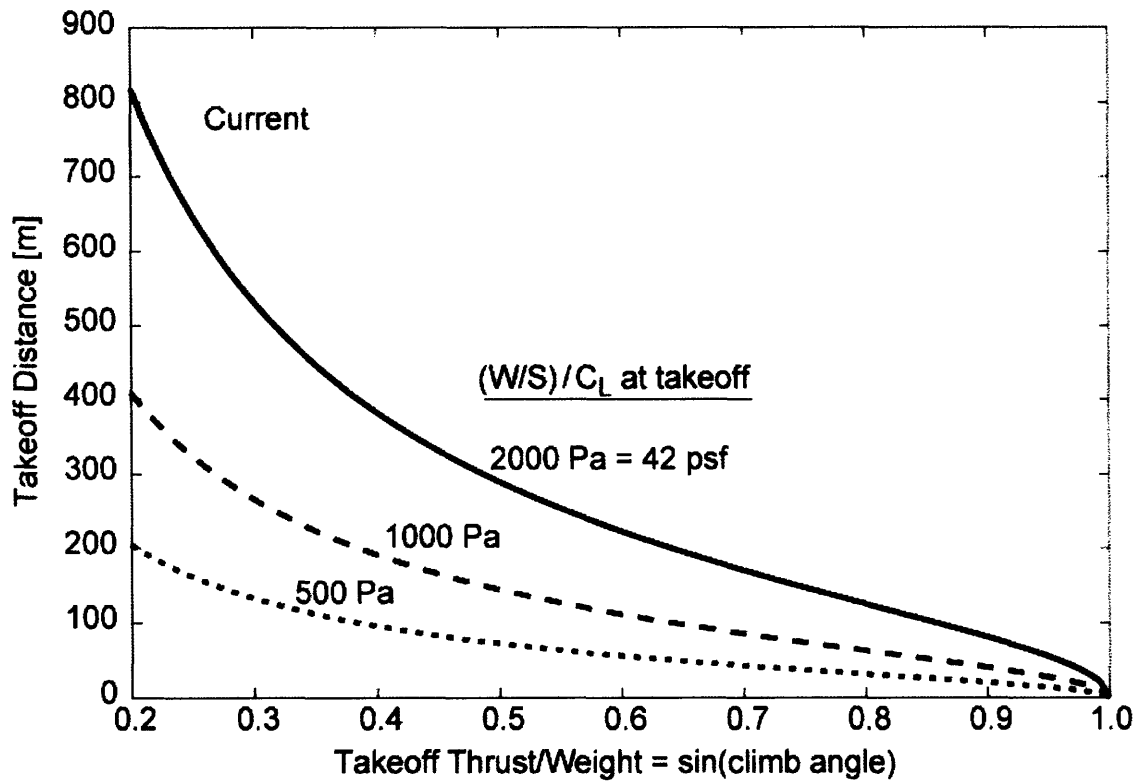
Figure 3-1: Takeoff distance for a 150,000lb class airplane as a function of thrust-to-weight ratio ($\frac{T}{W}$) for different normalized wing loading ($\frac{W}{S}$) to lift coefficient (C_L) ratios
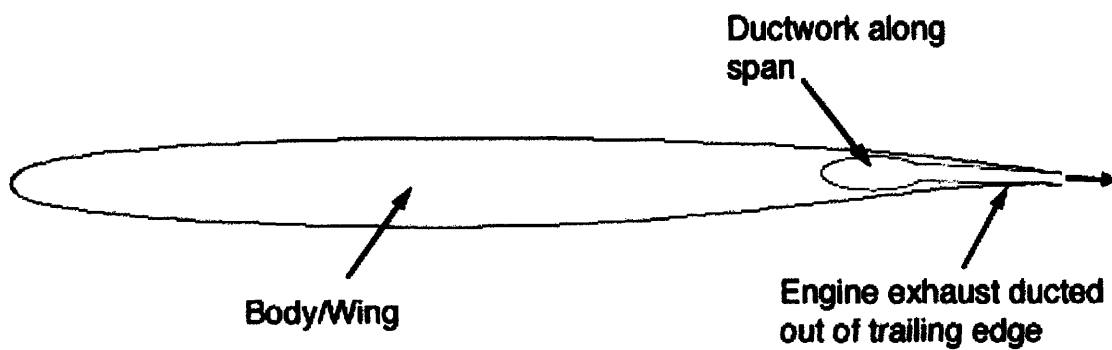
Figure 3-2: Generic airfoil with built-in engine

Table 3.1: Aircraft Parameters

Estimated Takeoff Gross Weight (W)	$70,000lb$
Wing Surface Area (S)	$1076ft^2$
Wingspan (b)	$115ft$
Aspect Ratio (AR)	12.25
W/S	$65psf$
Average Wing Chord ($c_{avg} = \frac{S}{b}$)	$9.61ft$
Average Wing Chord at engines (c_{eng})	$10.80ft$
Span Covered by Engines (b_{eng})	$194.90ft$

Table 3.2: Takeoff and Cruise Conditions for DP Aircraft

	Takeoff	Cruise
Altitude	0	$35000ft$
Air Density (ρ)	$0.737\frac{lb}{ft^3}$	$0.173\frac{lb}{ft^3}$
Static Pressure (p_0)	$2109psf$	$498psf$
Static Temperature (T_0)	$536°R$	$348°R$
Speed of Sound (a)	$1135\frac{m}{s}$	$932\frac{ft}{s}$
Viscosity (μ)	$1.21 * 10^{-5}\frac{lb}{ft-s}$	$9.54 * 10^{-6}\frac{lb}{ft-s}$
Total Thrust Required	$38500lb$	$10104lb$

and hypothetical future engines for use in this high-lift distributed propulsion aircraft. As demonstrated in the last chapter, SFC is most sensitive to variation in BPR at small values of BPR. For a given engine core (gas generator), BPR is limited by the maximum fan diameter of 21 inches (which is constrained by the airfoil design). With a smaller core, it is possible that the limit to BPR is the amount of power that can be extracted from the turbines to power the fan. Future engine cores that employ future technology such as higher TIT's and component efficiencies would be able to provide more power. As such, an engine driving the same-sized fan, a future core could be smaller than a current one and thereby operate at a higher BPR, and hence a lower SFC.

Examining available data for existing engines up to 2008 [1], the maximum BPR is 2.56 for a gas turbine with a fan diameter less than 21 inches. Recall that SFC improves significantly up to a BPR of 8, thus indicating large gains in SFC performance can be obtained through increasing BPR. It is important to note that while increasing BPR improves SFC, it also increases weight, which is detrimental to fuel burn so realistically a tradeoff is

made to minimize fuel burn.

The approach of this research is to begin with a current engine, evaluate its performance operating under the flight conditions of the distributed propulsion aircraft and extend it to the overall performance of the aircraft by coupling it with the aerodynamics. The next step involves developing conceptual engines that operate under the same physical constraints but with enhanced performance capabilities to reflect improvement with time. These future engines are projected as mid-term and far-term. Loosely, mid-term is technology 10 years from now and far-term is technology perhaps 20 years away.

The analysis undertaken in this chapter neglects effects of interference between the engines even though the spacing between engines is less than one fan radius away from each other. However, these parallel compressor effects are ignored at this stage for simplicity as they require 3D analyses.

3.1 Today's Gas Turbine (VLJ1)

The aircraft engine that is examined in this section is modeled as a representative contemporary engine for a very light jet (VLJ). The model used here (VLJ1) is compared to an existing small engine (EE) at flight conditions listed in table 3.2. The engine compared with is selected due to its relatively recent certification and suitable size for the distributed propulsion aircraft. The physical dimensions (fan size, BPR, core size, etc.) are the same for both VLJ1 and EE, but due to the proprietary nature of EE, the dimensions are not listed precisely. Other inputs required for defining VLJ1 include polytropic efficiencies of turbomachinery, combustor efficiency, pressure ratios and maximum TIT. These inputs are approximated and calibrated to match the performance of EE as accurately as possible. The estimated values are realistic when compared to today's technology. The selected turbomachinery polytropic efficiencies between 0.84 and 0.86 are relatively low (compared to ~ 0.9 of the largest modern engines) but since the engine is relatively small, the efficiencies can be expected to be lower due to size effects. The OPR of 18 and maximum TIT of 2280R are also relatively low for the same reasons.

Figure 3-3 demonstrates the accuracy of the cycle model [25] in use for this analysis.
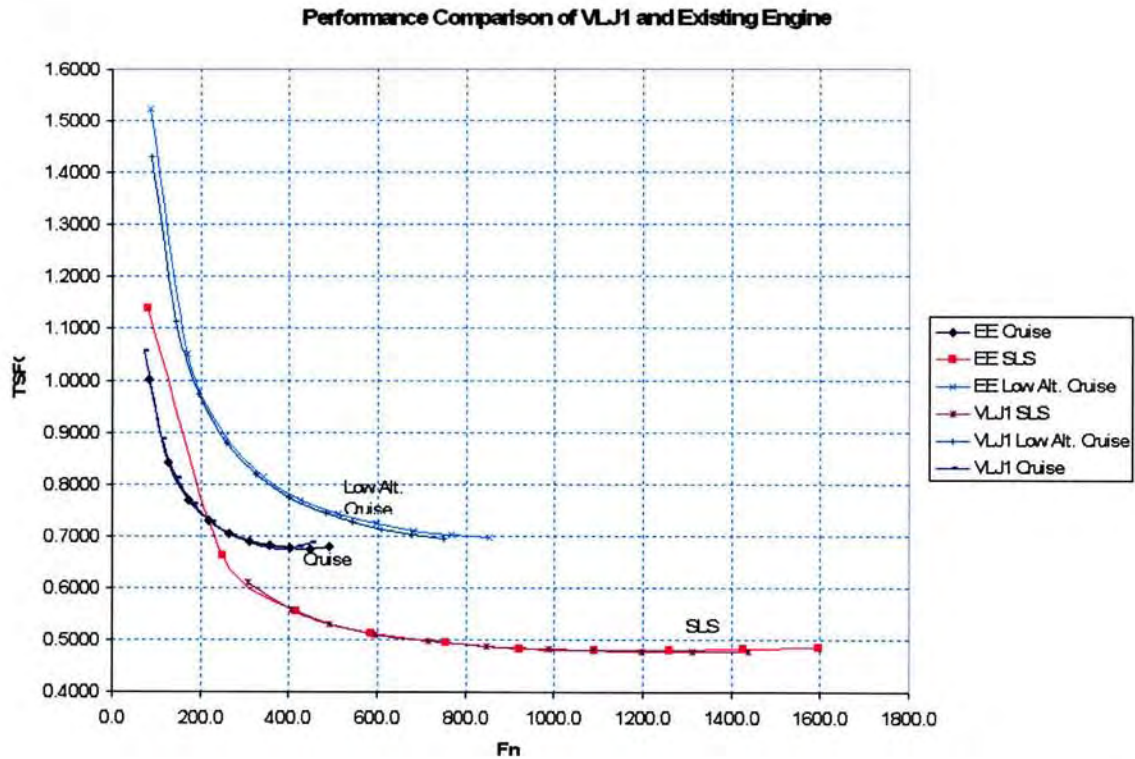
Figure 3-3: Performance comparison between VLJ1 and existing contemporary small gas turbine

In the three operating ranges examined (TO, high altitude cruise and low altitude cruise), the SFC's are within 2% for any given thrust. This suggests that the input parameters used for VLJ1 are realistic and representative of current day small gas turbines.

3.1.1 Satisfying the Distributed Aircraft Requirements

Cruise requires much less thrust due to its high $\frac{L}{D}$ (estimated at 15) of the distributed propulsion aircraft, thus the limiting factor for the number of engines is at takeoff. The $\frac{T}{W}$ required for takeoff is 0.55, which equates to 38,500lb of total thrust needed since the gross weight of the aircraft is 70,000lb. As a result, the number of engines required is 22.4, which is rounded up to 24 to offer a margin for the thrust gap between uninstalled thrust and installed thrust. Furthermore, the number of engines is kept even for balance on both sides of the wing, as the aircraft is not designed to have engines built into the fuselage (see figure 3-4).

55
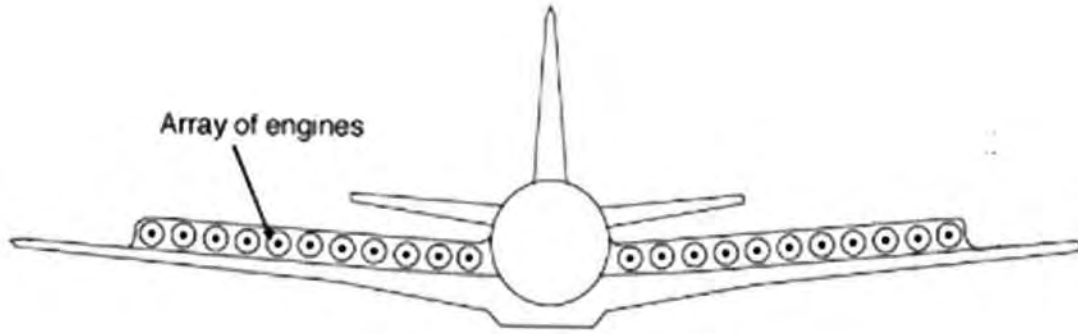
Figure 3-4: Frontal view of conceptual distributed propulsion aircraft, [17]

3.2 Mid-term (VLJ2) and Far-term (VLJ3) Gas Turbines

With the baseline engine VLJ1, the mid-term and far-term engines, VLJ2 and VLJ3, are conceptualized by modifying the input parameters of VLJ1 to account for technology advancement. VLJ2 and VLJ3 are designed to minimize cruise SFC while producing enough thrust for cruise and TO. The number of engines on the distributed propulsion aircraft are kept constant to obtain an appropriate performance comparison between the engines when uninstalled and installed. The design point for these engines is at maximum TIT, 35,000ft altitude and cruising at 0.6 Mach. These inputs, along with cruise and takeoff performance parameters are listed in table 3.3.

3.2.1 Input Choices for VLJ2 and VLJ3

The key differences between the conceptual engines are shown in table 3.3. The initial step taken in developing VLJ2 and VLJ3 is the assumption of OPR, maximum TIT and the turbomachinery polytropic efficiencies (η_{poly}), which are chosen to realistically reflect their improvements with time. The weight of the engines are also kept the same due to the lack of confidence in such estimations as mentioned in the previous chapter.

The time frame of VLJ1, VLJ2 and VLJ3 are about 10 years apart. From chapter 2, the OPR improvement is roughly a factor of 1.5 every 10 years. In the models for VLJ2 and VLJ3, this factor is applied to the high pressure compressors and low pressure compressors (HPC and LPC). The OPR does not reflect this increase exactly because of

56

Table 3.3: Design point, cruise and takeoff performance for VLJ1, VLJ2 and VLJ3

		VLJ1	VLJ2	VLJ3
Design point	Design altitude	$35000 ft$	$35000 ft$	$35000 ft$
	Design M	0.6	0.6	0.6
	FPR	1.90	1.60	1.71
	OPR	18	27	36
	BPR	between 2-3	8	12.5
	TIT	$2280°R$	$2800°R$	$3500°R$
	HPC η_{poly}	0.86	0.87	0.89
	LPC η_{poly}	0.84	0.87	0.89
	HPT η_{poly}	0.86	0.87	0.89
	LPT η_{poly}	0.85	0.87	0.89
Cruise	Thrust	$230 lb$	$230 lb$	$230 lb$
(35k ft, 0.6M)	SFC	$0.723\frac{lb}{lb-h}$	$0.556\frac{lb}{lb-h}$	$0.494\frac{lb}{lb-h}$
	Exhaust velocity V_8	$1065\frac{ft}{s}$	$932\frac{ft}{s}$	$964\frac{ft}{s}$
	Exhaust gas temperature (EGT)	$655°R$	$548°R$	$544°R$
	Inlet Weight Flow (W_2)	$24.0\frac{lb}{s}$	$24.7\frac{lb}{s}$	$24.0\frac{lb}{s}$
Takeoff	Thrust	$1850 lb$	$1860 lb$	$1855 lb$
(0ft. 0.084M)	SFC	$0.49\frac{lb}{lb-h}$	$0.34\frac{lb}{lb-h}$	$0.31\frac{lb}{lb-h}$
	Core size	1.4	0.53	0.27
	V_8	$930\frac{ft}{s}$	$931\frac{ft}{s}$	$931\frac{ft}{s}$
	EGT	$865°R$	$725°R$	$717°R$
	W_2	$64.4\frac{lb}{s}$	$64.5\frac{lb}{s}$	$65.1\frac{lb}{s}$

the lower fan pressure ratios (FPR). Due to lack of knowledge of η_{poly}'s, these are selected conservatively such that VLJ3's η_{poly}'s do not exceed those of large engines today. η_{poly} of 0.89 is a conservative estimate assuming that efficiencies today may be up to 0.91 or 0.92 for state-of-the-art turbomachinery. Further, data suggests that turbine efficiencies are improving at 0.25% per year for small gas turbines [3], which amounts to approximately 2.5% every 10 years.

TIT increase represents approximately 25% for subsequent models, which is considerably more aggressive than OPR and the η_{poly}'s. However, with improving manufacturing technologies, especially thinner blades, it is assumed that the cooling available to large turbine blades will also be available to small turbines in coming decades, or at least the technology gap will close. TIT has increased at a rate of approximately 50°C (90°R) per year [3]. The increase of TIT's for VLJ2 and VLJ3 fall in this range.

Using these assumptions, VLJ2 and VLJ3 are designed to maximize the BPR to achieve better SFC, higher propulsive efficiency (η_{prop}), improved exhaust mixing and lower exhaust gas temperature (EGT). The first three factors directly impact overall performance, while EGT is lowered to relieve heat stresses from the airframe, specifically the control surfaces that the exhaust blows on. Since all models' fans are limited to 21 inches, having a larger BPR means having a smaller core. As a result, with the inputs listed in table 3.3 (other than FPR and BPR), VLJ2 and VLJ3 are designed to have the smallest core that is capable of powering the 21 inch fan. There are several design iterations for VLJ2 and VLJ3 that involve varying BPR and FPR to achieve this maximum BPR while ensuring that the fan did not draw so much power as to adversely affect SFC. In other words, the BPR is incrementally increased every iteration and FPR adjusted accordingly to minimize SFC until there is no more improvement in SFC. While this may not be the ideal design, it is sufficient for a qualitative comparison between these present and future engines. To reiterate an important exclusion, weight variation is not taken into consideration quantitatively in this analysis.
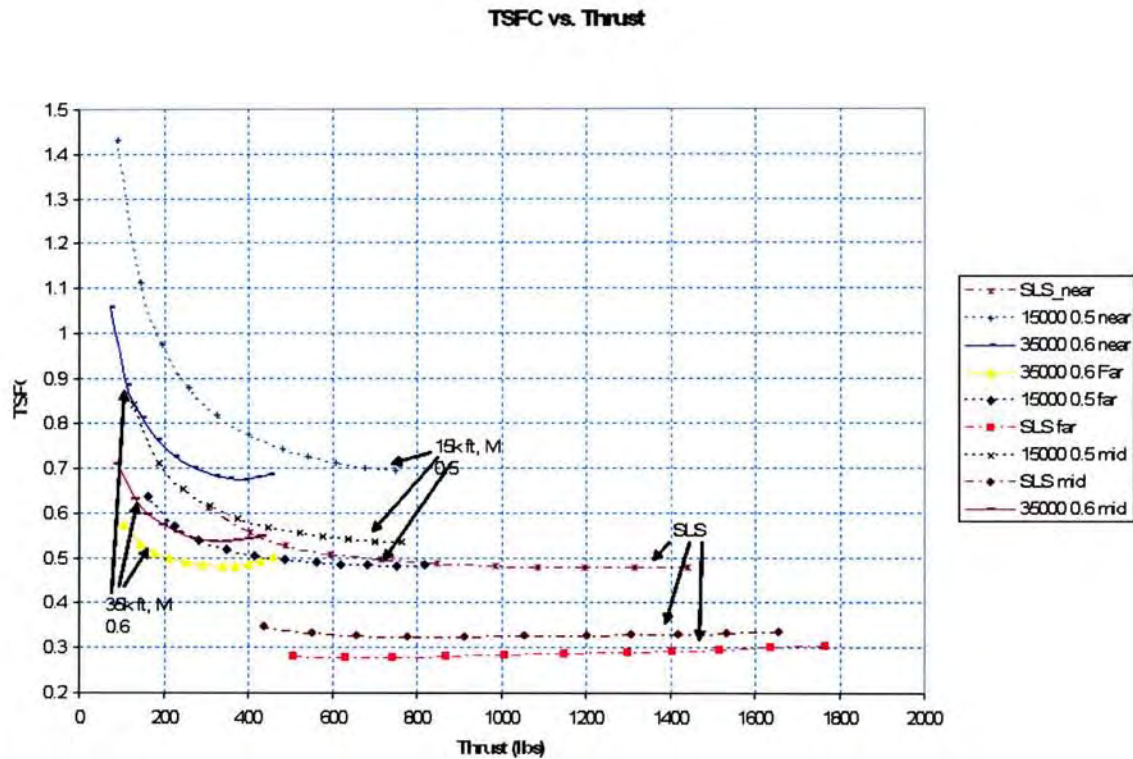
Figure 3-5: SFC vs. Thrust: Operating lines of VLJ1, VLJ2 and VLJ3 at TO, high altitude cruise and low altitude cruise

3.3 Comparison of Current, Mid-term and Far-term Engines

Table 3.3 lists the takeoff and cruise performances of the three models. As expected, there are significant improvements in SFC, especially from current to mid-term (VLJ1 to VLJ2). The cruise SFC of $0.54 \frac{lb}{lb-h}$ for VLJ2 is comparable to that of current large engines (figure 2-2). While this is not an extremely precise performance prediction of a typical 2018 small gas turbine, it does follow the trend of improving SFC and is within the margin of error shown in figure 2-15 (though that margin of error is large).

Further comparison of the models are shown in figure 3-5. The graph shows the SFC versus thrust for the operating spectrum of each VLJ model at takeoff (0.084M at sea level), high altitude cruise (0.6M at 35,000ft) and low altitude cruise (0.5M at 15,000ft). The operating lines consistently demonstrate that there is significant improvement in SFC from

59

VLJ1 to VLJ2 (approximately 20%) and, to a lesser extent, from VLJ2 to VLJ3 (8-10%). This greater improvement from current to mid-term, along with the prediction that the mid-term VLJ2 would have the performance comparable to that of a current large engine, suggest that the technology of small engines necessary for enabling distributed propulsion will be developed within the next decade.

3.4   Parametric Studies

Input parameters are varied for VLJ1 to examine their relative effects. This study determines which factors affect SFC most, and how a parameter constrains another.

3.4.1   Bypass Ratio

From chapter 2, Figure 2-13 suggests that increasing BPR when its value is small has the most significant positive effect on SFC. This figure draws its curve from a Mach number of 0.8 and a (θ_t) of 7.5. Operating under different conditions may dramatically affect whether increasing BPR has the same effect shown in the figure. This prompts the examination of several BPR's with the design inputs of VLJ1 (Figure 3-6).

In this study, TIT and FPR are varied to optimize for SFC. If they are fixed, the study could not be performed since increasing BPR would require more power from the turbine to drive the larger fan but the core of VLJ1 would not be capable of powering such large fans. As a result, either the TIT has to be increased (more power output from the turbines) or the FPR has to be decreased (a weaker fan). In this study, both are varied to achieve the results represented in figure 3-6. More detail will follow regarding the limitation effects of TIT and FPR on BPR.

Decreasing FPR does not represent advancement in technology, but rather a design choice, so such a change is fair for VLJ1 (constant timeframe). Increased TIT on the other hand represents better technology for the configurations operating larger BPR's. Specifically, the TIT is increased from 2280°R for a BPR of 2 to 2900°R for a BPR of 16. Part of the improvement in SFC can be attributed to this increase but more importantly, what increased TIT offers is the enabling of higher BPR's. Without these higher TIT's, the larger
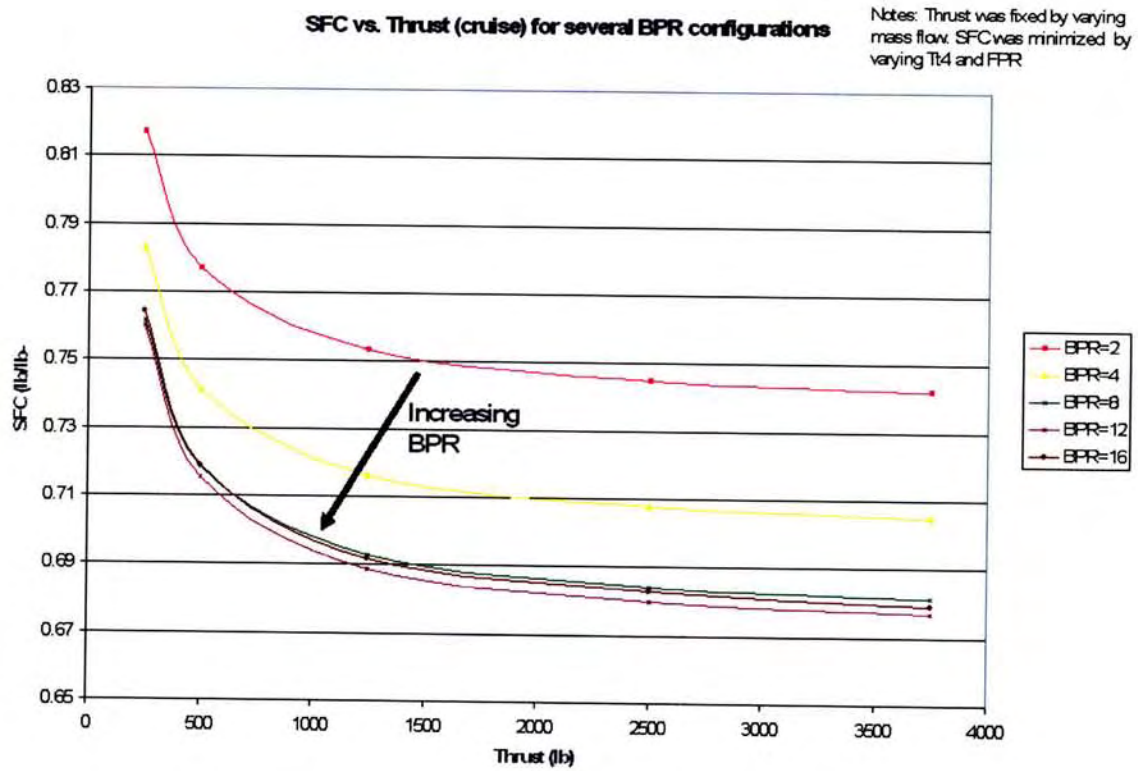
Figure 3-6: Analysis of the effect of BPR on SFC for VLJ1. TIT and FPR not kept constant for this study

Figure 3-7: Parametric study of BPR and TIT

BPR's cannot be achieved with the VLJ1 inputs, unless FPR is lowered unrealistically to approach 1 (effectively having no fan at all).

It can be seen in figure 3-6 that SFC increases most significantly when increasing BPR from 2 to 4 (4%). Subsequent doubling of BPR yield less improvement to SFC (approximately 2.5% from 4 to 8 and less than 0.5% from 8 to 16). This result is consistent with that drawn from figure 2-13, that increases of BPR at small values lead to the most improvement in SFC. While TIT may contribute to this improvement in SFC, the value is selected along with FPR to reflect the lowest SFC for the given BPR and other inputs. Further, previous studies reinforce this observation, that BPR's have to be over 8 in order for small aircraft engines to achieve high fuel efficiencies required for distributed propulsion [22].

3.4.2 Turbine Inlet Temperature

To address the issue of how TIT may be the main factor in lowering SFC in figure 3-6, a parametric study of TIT with BPR for the VLJ1 inputs is performed to demonstrate otherwise.

Figure 3-7 depicts SFC versus thrust for varying TIT and BPR. Thrust is not an impor-

tant factor in this study, as its value can be changed in the model by altering the mass flow. The purpose of this figure is solely to demonstrate how TIT affects BPR, and consequently SFC. For each BPR, it can be seen that there is a minimum SFC, which is achieved at different TIT's. This figure demonstrates that increasing TIT does not necessarily improve SFC, but rather it enables the use of larger BPR's. It can be argued that for a given BPR, the SFC can be improved by changing the TIT (decreasing is also an option). While this is true, the design approach for the VLJ models is based on having a limiting TIT (i.e. fixed), which in turn corresponds to a BPR that minimizes SFC.

3.4.3 Fan Pressure Ratio

The effect of TIT is not as simple as mentioned. Rather, it is coupled with other effects, such as OPR, FPR, η_{poly}'s of turbomachinery. The effect of η_{poly}'s are obvious, the higher the better, which are easily managed when developing the VLJ's since the values are chosen based on what is deemed technologically appropriate. FPR on the other hand, constrains the BPR, since the higher the FPR, the more power required to drive the fan. Compressor pressure ratio also affects the performance since the higher the ratio, the more energy required from the core to drive the compressors, which has the same effect as higher FPR but at a smaller scale (since compressors are smaller than fans). FPR and OPR are analyzed together because the choice of FPR directly affects the OPR.

$$OPR = FPR * \pi_{HPC} * \pi_{LPC} \tag{3.1}$$

Figure 3-8 demonstrates the effect of FPR and HPC pressure ratio (π_{HPC}) on BPR and SFC. Thrust is fixed at 1000lb for each of the data points of the parametric study. Each graph in the figure represents a parametric study of π_{HPC} with BPR. The value of π_{HPC} can be viewed essentially as OPR since equation 3.1 shows that OPR is simply scaled up by FPR and π_{LPC}, which are fixed for both graphs. It can be further deduced that each FPR-OPR combination (each curve of fixed π_{HPC}) has a corresponding BPR that minimizes SFC.

As π_{HPC} increases, SFC improves for a given BPR up to a point but then starts de-

THRUST=1000lb

FPR=1.2
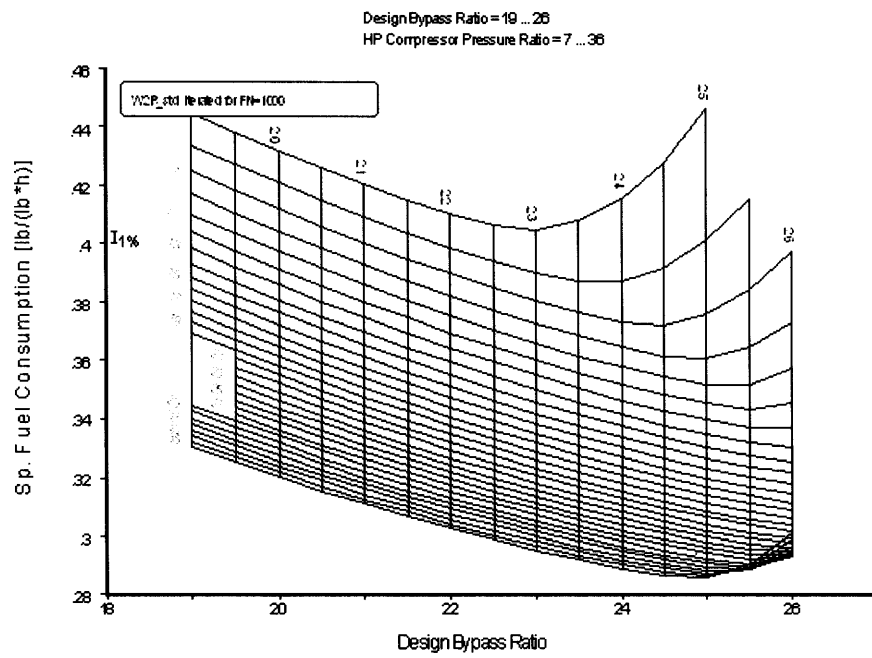
(a)

FPR=1.8

(b)

Figure 3-8: Effect of OPR and BPR on SFC for two FPR's. (a) FPR=1.2 (b) FPR=1.8

teriorating. This occurs because the core no longer provides enough power to drive the compressors (HPC, LPC and fan) efficiently. This suggests that for a given OPR, which in this distributed propulsion study refers to technology level, there is a corresponding optimal BPR if other inputs (TIT, FPR) are fixed.

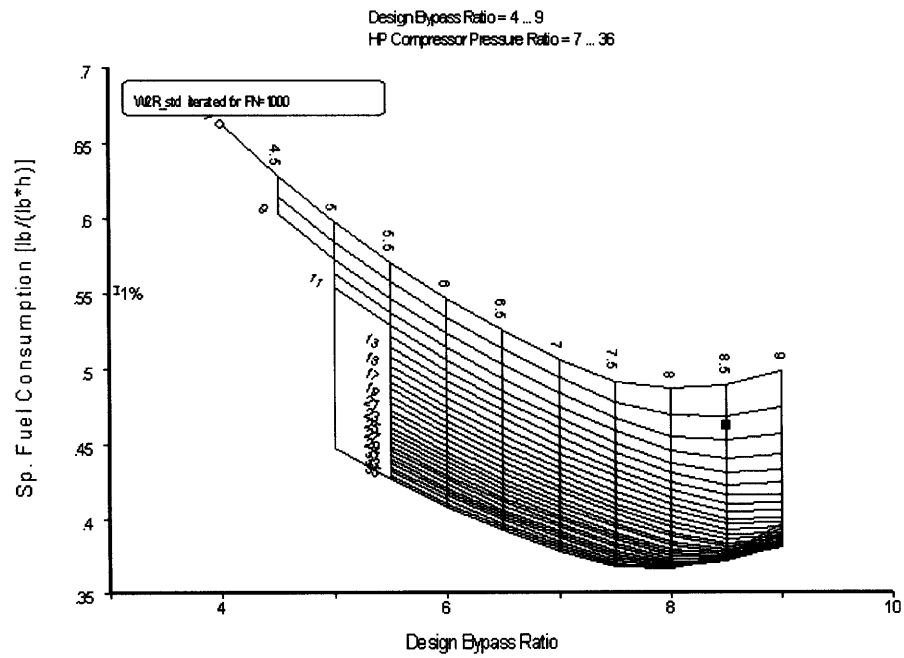While TIT, OPR and FPR are parameters that affect SFC for a given BPR, they can also be viewed in reverse, where TIT, OPR and FPR enable a certain BPR, which in turn affects the SFC. VLJ2 and VLJ3 are designed in this way since TIT and OPR have fixed design values, whereas FPR and BPR are varied to minimize SFC. Parametric studies depicted in figures 3-6 and 3-8 help with this optimization.

3.4.4 Polytropic Efficiencies of Turbomachinery

Fan η_{poly}'s effect on SFC varies depending on the size of the fan (BPR). It is clear that the higher the BPR, the greater the effect of the fan η_{poly} since an efficient large fan has more impact on the overall performance (SFC) than an efficient small fan. Figure 3-9 is an example of how significantly the fan η_{poly} affects SFC. For a BPR of 2, a 1% change in fan η_{poly} leads to a 0.2% change in SFC. For a BPR of 3 however, a 1% change results in approximately a 1% change in SFC, which is a factor of 5 difference.

The sensitivity of SFC to fan η_{poly} at high BPR's shows the importance of improving fan designs with time since VLJ2 and VLJ3 both operate at significantly higher BPR's. Similar studies for the HPC, LPC, HPT and LPT demonstrate similar trends, but not to the extent that the fan demonstrates. While figure 3-9 is quantitatively specific to VLJ1 settings, the effect of SFC being sensitive to polytropic efficiency at larger BPR's applies more generally. Thus, a small uncertainty in the fan η_{poly} could lead to very different SFC's, which is important to note for the VLJ2 and VLJ3 configurations.

3.4.5 Combustor Pressure Drop

Pressure drop across the combustor is kept constant for the VLJ's at 0.97 (Gasturb default [25]). This drop is designed in for combustion stability and does not vary with engine size [22]. This constraint eliminates a parameter that has influence on the OPR and SFC. Com-
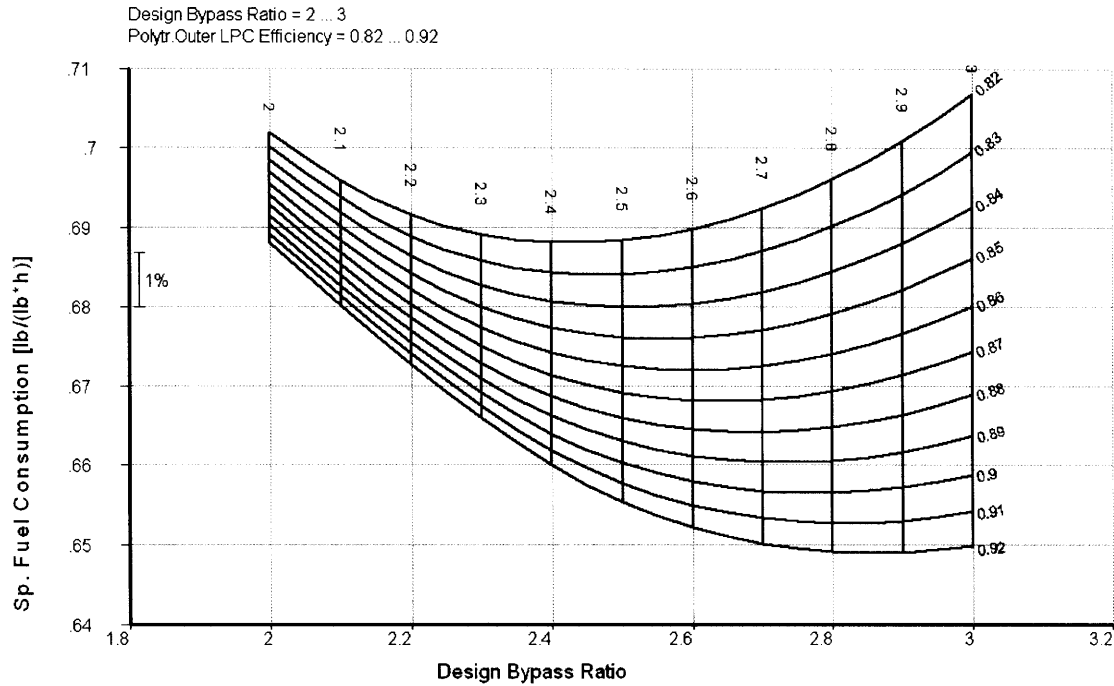
Design Bypass Ratio = 2 ... 3
Polytr.Outer LPC Efficiency = 0.82 ... 0.92

Figure 3-9: SFC vs. BPR: Parametric study of the effects of fan η_{poly} and BPR on SFC

bustor technology is not studied as a trend and no predictions are made for its improvement with time. The effects of varying combustor pressure drop with BPR and turbomachinery efficiencies are studied for the VLJ1 configuration. This is performed to provide insight to how improving combustor technology may affect the SFC even though it is not implemented for the VLJ's. Figure 3-10 demonstrates the effect of the combustor pressure drop (π_{comb}) in conjunction with the HPC η_{poly}. It can be seen that with increasing efficiency of the HPC, improvement of the combustor has less effect on the SFC. This relationship can be similarly demonstrated for the other components of turbomachinery. This indicates that combustor improvements in the nearer term would be more effective in improving performance (i.e. for VLJ2 more so than VLJ3).

Figure 3-11 shows the effect of π_{comb} with BPR. The SFC minimums for each curve in the figure exist because the TIT and FPR are optimized for that particular BPR, so no conclusion should be drawn from these minimums. The figure shows that for higher BPR's, improvement in combustor technology provides greater gains in SFC. Specifically, a 0.01 point gain in π_{comb} (approximately 1%) for a BPR of 2 results in approximately a 0.3% decrease in SFC. For a BPR of 3 however, a similar improvement in π_{comb} results in a 0.6%
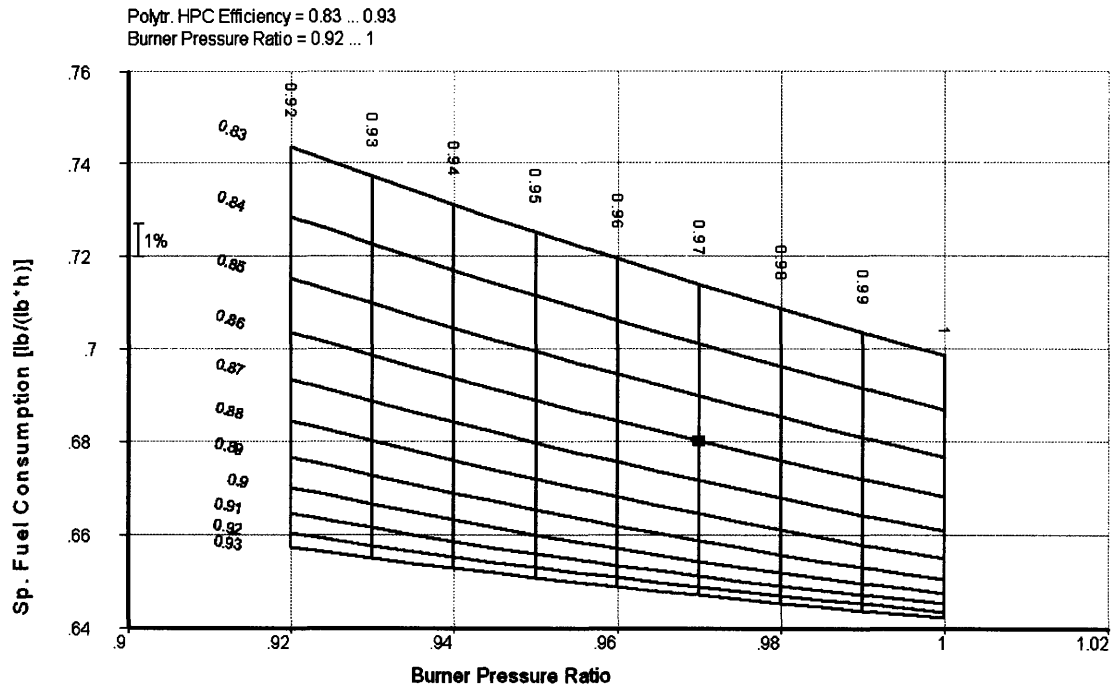
Figure 3-10: Parametric Study of Burner Pressure Ratio with HPC η_{poly}

decrease in SFC, which is twice that of BPR of 2. This result indicates that improving combustor technology is most beneficial to cycle efficiency with high BPR's, which the later VLJ's operate.

3.5   Performance of Aircraft with Installed Engines

VLJ1 is designed to represent an engine with today's technology and is capped at 21 inches for fan size. The amount of takeoff thrust is calculated for VLJ1 and the number of engines determined for the distributed propulsion aircraft with this. VLJ2 and VLJ3 are designed to represent future engines that have the same size and thrust capacity as VLJ1, albeit with better fuel efficiency. Ultimately though, the airflow that the aircraft sees from operating VLJ1, VLJ2 and VLJ3 are similar because the inlet design Mach numbers are the same (0.5M), the engines are physically identical in length and fan diameter, and the mixed out exhaust is projected to be similar (V_8's are almost equal and EGT at such low temperatures present no issues for the control surfaces). The main difference the distributed propulsion aircraft experiences is improved cycle efficiency, which equates to a combination of lower
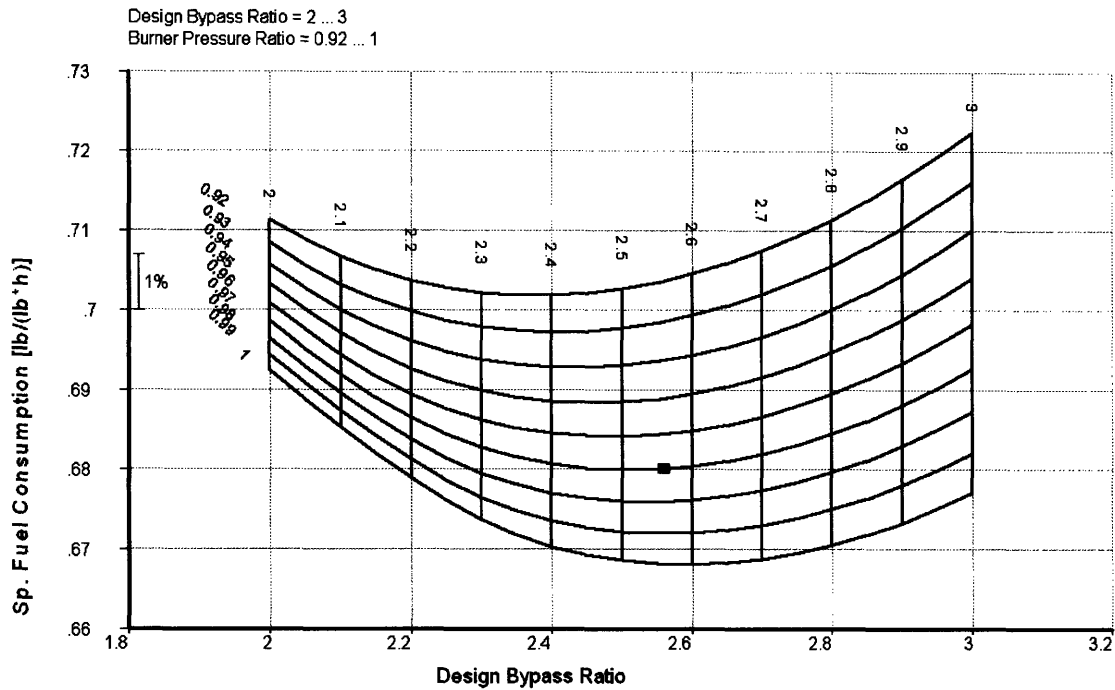
67

Figure 3-11: Parametric Study of Burner Pressure Ratio with BPR

gross weight (less fuel) and longer range. Since the exhaust is mixed out within the nozzle, there are no propulsive efficiency gains associated with higher BPR's of VLJ2 and VLJ3 as this is taken into account in the SFC. Higher BPR's would normally be associated with heavier engines, but with VLJ2 and VLJ3, the fan sizes are the same as VLJ1 due to the airfoil constraint. Further, VLJ2 and VLJ3 have smaller cores which would likely mean lighter engines. Fuel burn is thus improved for later versions of VLJ (recall the range equation [2.3]) due to this lower gross weight and SFC.

VLJ2 and VLJ3 are designed with the constraints of 24 engines, which meant that the design thrust (421lb at 35,000ft, 0.6M, table 3.3) is also constrained. This constraint is kept to offer a better comparison between the engines used in the distributed propulsion aircraft (the VLJ's). While this is the design point, it is not necessarily the only design option. The number of engines could be different (if the same airframe is kept, this number could only be lower), which would offer a degree of freedom to design more power-dense engines. For example, VLJ3 operates at a BPR of 12.5, which from figure 3-6, is deduced to have not much BPR-induced SFC improvement (recall that SFC gains are greatest up to an of BPR of 8). An alternative for the design of VLJ3, is for the design BPR to be the same as that of

68

VLJ2. Keeping the BPR at 8 would mean having a more powerful core compared to VLJ2 and would therefore open up opportunities such as higher FPR and higher thrust.

Lundbladh and Gronstedt [22] studied the effects of varying the number of engines. For their specific case of changing the number of engines from 2 to 8 for a 250-passenger aircraft, the effect is a 4% gain in fuel efficiency. If this holds true more broadly to include this distributed propulsion aircraft, it suggests that lowering the number of engines (less distributed airflow) may be detrimental to fuel efficiency. However gains in engine performance by using less engines may balance this effect.

3.5.1   Installation Efficiency

Embedding the engine into the wing affects the performance of the engine, mainly through the inlet and exhaust. The 3D installation drag is not accounted for in this analysis. 3D CFD analysis of the model would be able to determine such drag. Further concerns are discussed in [23, 24].

3.6   Propulsive System Analysis for a Distributed Propulsion Aircraft Mission

The purpose of this example is to quantitatively compare the VLJ models when operating the distributed propulsion aircraft for a simple mission. The focus of the study is on fuel burn and as such, only the climb and cruise situations are analyzed. The mission is split into these two respective legs.

3.6.1   Climb

For purposes of comparison, the climb path for each VLJ configuration is modeled as closely to each other as possible, however a perfect match proved difficult due to factors such as excess thrust and aircraft weight at any given time (from varying fuel burn rates).

Climb Model

The model is based on the total energy approach [5, 35]. At any given point during the climb, there is an energy level (E) associated with the aircraft. This E is defined by equation 3.2 where m is the aircraft mass, g is the gravitational acceleration, h is the aircraft altitude, V is the flight velocity.

$$E = m(gh + \frac{V^2}{2}) \qquad (3.2)$$

The first term on the right hand side represents the potential energy (PE) of the aircraft, and the second term represents the kinetic energy (KE). This E is known at the beginning of climb and at cruise. Starting from a E of virtually 0 at the beginning of climb to a maximum E at cruise, any path through increasing h and V can be taken. Two popular methods for optimizing the path exist, which are minimizing for climb time or minimizing for fuel burnt [5]. Realistically however, a typical climb path is in between these maximum rate and maximum energy schedules [35].

Energy required to accelerate and climb stems from excess thrust (T_{ex}) produced by the engines. This T_{ex} can be calculated via equation 3.3, where T_{net} is the net thrust of the aircraft (of all 24 engines) and D is the aircraft drag. Drag (defined in equation 3.4) in this model has a constant coefficient (C_D) of 0.04 and since the wing surface area (S) is fixed (table 3.1), D is only dependent on the dynamic pressure (q_∞) which is a function of h and V.

$$T_{ex} = T_{net} - D \qquad (3.3)$$

$$D = C_D q_\infty S \qquad (3.4)$$

The climb path can be broken into increments to find the energy gain in an incremental time step (Δt), given by equation 3.5. In this equation, ΔE_{ex} is the 'excess energy' obtained from T_{ex} at V for a time period Δt.

$$\Delta E_{ex} = \int_{t_1}^{t_2} F_{ex}\, dt \approx F_{ex} V \Delta t \tag{3.5}$$

This ΔE_{ex} can then be applied to either accelerate the aircraft or climb. Substituting equation 3.2 into equation 3.5 yields equation 3.6:

$$\Delta E_{exi} = g(m_{i+1}h_{i+1} - m_i h_i) + \left(\frac{m_{i+1}V_{i+1}^2 - m_i V_i^2}{2}\right) \tag{3.6}$$

The subscripts i and $i + 1$ are indices for the step number, allowing for the calculation of the next step (at time $t + \Delta t$). A choice is made for how this ΔE_{ex} is distributed to PE and KE. This choice of distribution affects the h and V, and therefore the climb path. A weighting factor is used to distribute the ΔE_{ex} at each time step, according to priority based on the climb path.

The rate of change of altitude ($\frac{dh}{dt}$) is computed using equation 3.7 at each time step. This $\frac{dh}{dt}$ is used to estimate the flight angle (γ) at each time step as a sanity check for realistic flight paths (equation 3.8). The maximum γ's for the VLJ configurations are found to be 12.2°, 15.1° and 15.5° respectively. Angles of 15° are relatively high, but when the zero-lift angle of attack ($\alpha_{L=0}$) is factored in for this high lift aircraft, the actual maximum α is closer to 12°, which is below stall for most wings (a NACA 2412 stalls at 16° α for example [14]).

$$\frac{dh}{dt}_i \approx \frac{h_{i+1} - h_i}{\Delta t} \tag{3.7}$$

$$\sin \gamma_i \approx \frac{\frac{dh}{dt}_i}{\frac{V_{i+1} - V_i}{2}} \tag{3.8}$$

In summary of the model, the state is known at index i (with $i = 0$ being the start of climb). This state includes h_i and V_i. F_{net} is obtained via input of these states into the cycle model of the VLJ's [25]. Equation 3.3, 3.5 and 3.6 are then applied to acquire the new energy level at $i + 1$, and hence h_{i+1} and V_{i+1}. For each time step, the fuel consumption is measured and weight of the aircraft updated accordingly.
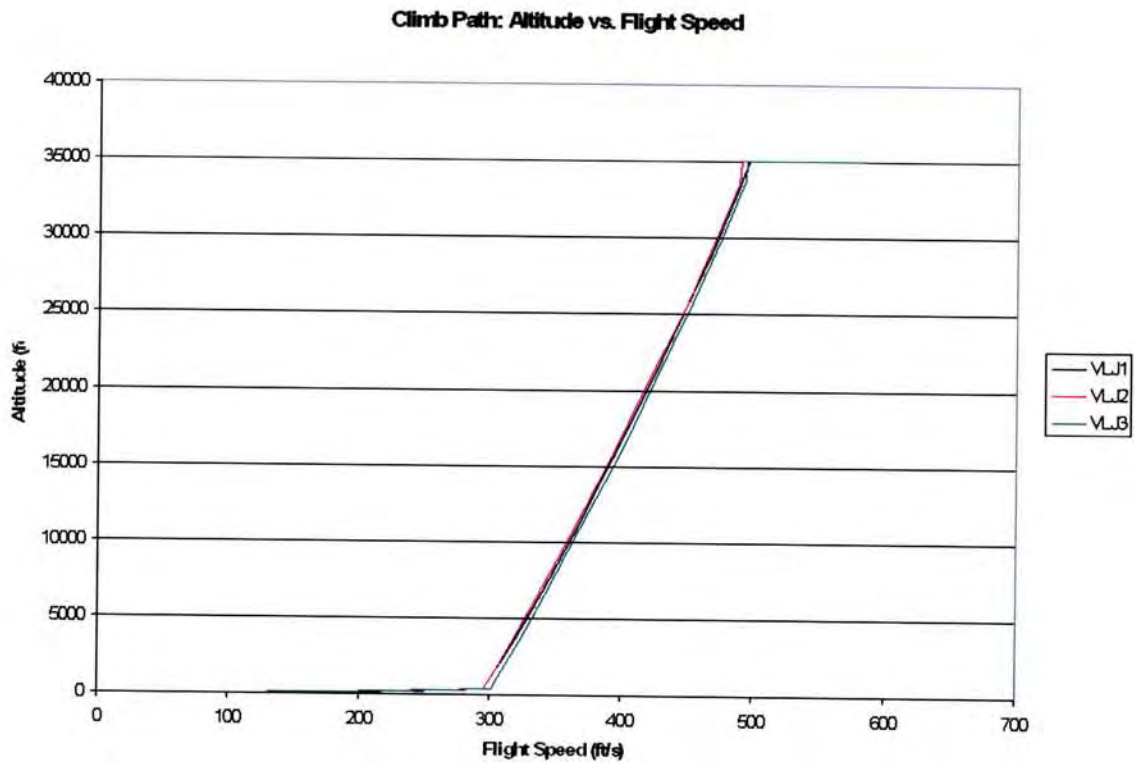
Figure 3-12: Climb Schedule Comparison: Altitude vs. Flight Velocity

Climb Path

The takeoff roll for the aircraft is at 30m/s (98.4ft/s) and at sea level. It is deemed important for the aircraft to increase its speed early during the climb due to its nature. This 'safe' speed, is chosen as 300ft/s, approximately half the cruise speed. Initial attempts to boost flight speed to its cruise speed before climbing failed due to the lack of excess thrust at high flight speeds. The weighting factor, mentioned in the model, is set such that 80% of the excess thrust is used to accelerate the aircraft, while the remaining 20% is used to increase altitude. This factor is arbitrary, but correctly reflects the priority of the aircraft at this stage of the climb. Once the speed of 300ft/s is obtained, the aircraft shifts its priority to climb, but for simplicity and smoothness of path, at a constant ratio of $\frac{dh}{dt}$ to $\frac{dV}{dt}$ (ratio of altitude gain rate to acceleration). These constraints are set such that the aircraft obtains cruise altitude at a Mach number of 0.5, or approximately 495ft/s. As part of the climb schedule in this study, the aircraft then accelerates to cruise speed of 584ft/s (M=0.6). The aircraft does not reach its cruise speed at top-of-climb because, as before, the $\frac{dh}{dt}$ is too low when
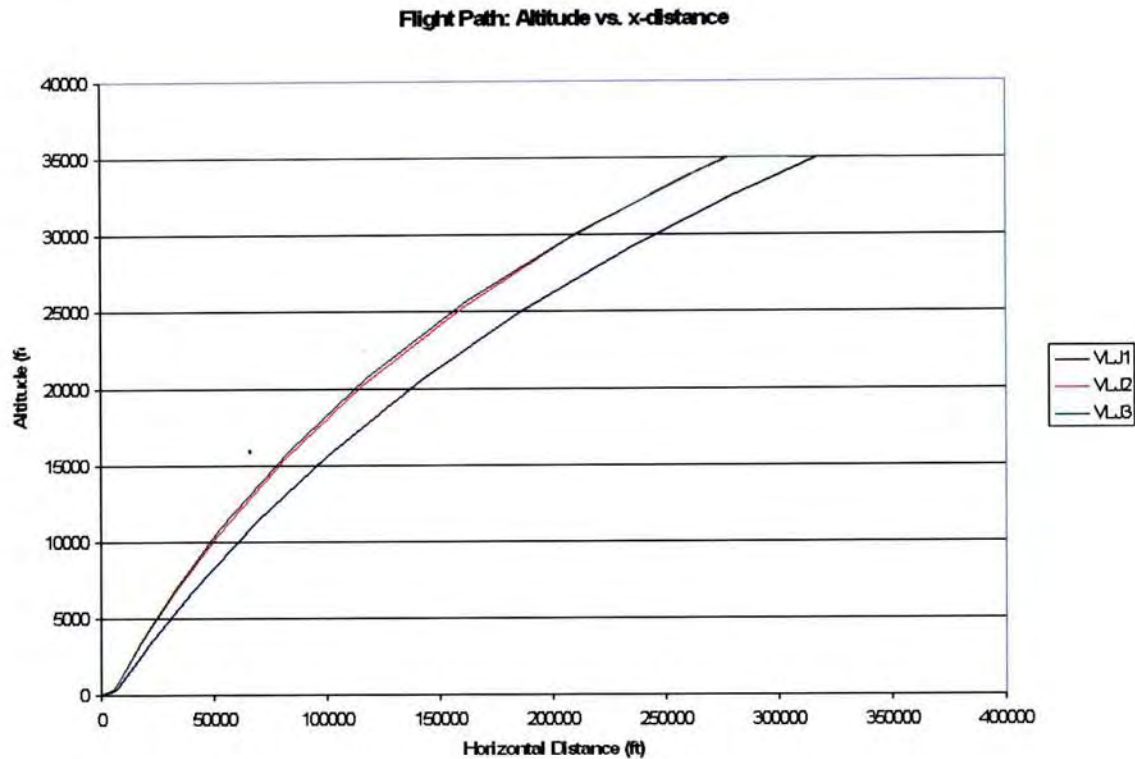
72

Flight Path: Altitude vs. x-distance

Figure 3-13: Climb Path Comparison: Altitude vs. Horizontal Distance

climbing at high flight speeds.

Climb Schedule Results

Figure 3-12, a plot of altitude versus flight velocity, demonstrates the similar climb sched-
ules of the three configurations, which shows the reliability of the model to create such a
schedule. While these climb schedules are similar, the actual path taken by the aircraft for
each configuration is different, as shown in figure 3-13. This difference can be attributed to
variation in excess thrust of the engines, which is explained later in the section.

At increasing energy levels, cycle performance deteriorates, as can be expected, from
gains in altitude and flight velocity. Comparisons of how each VLJ model's SFC varies with
the energy level is shown in figure 3-14. The kinked shapes at the ends of each curve depict
the change in priority in climb path as described previously. Figure 3-14 demonstrates
no clear distinction between each configuration for efficiency degradation with increasing
energy level. This helps to explain the shape of the cumulative fuel burn chart shown in
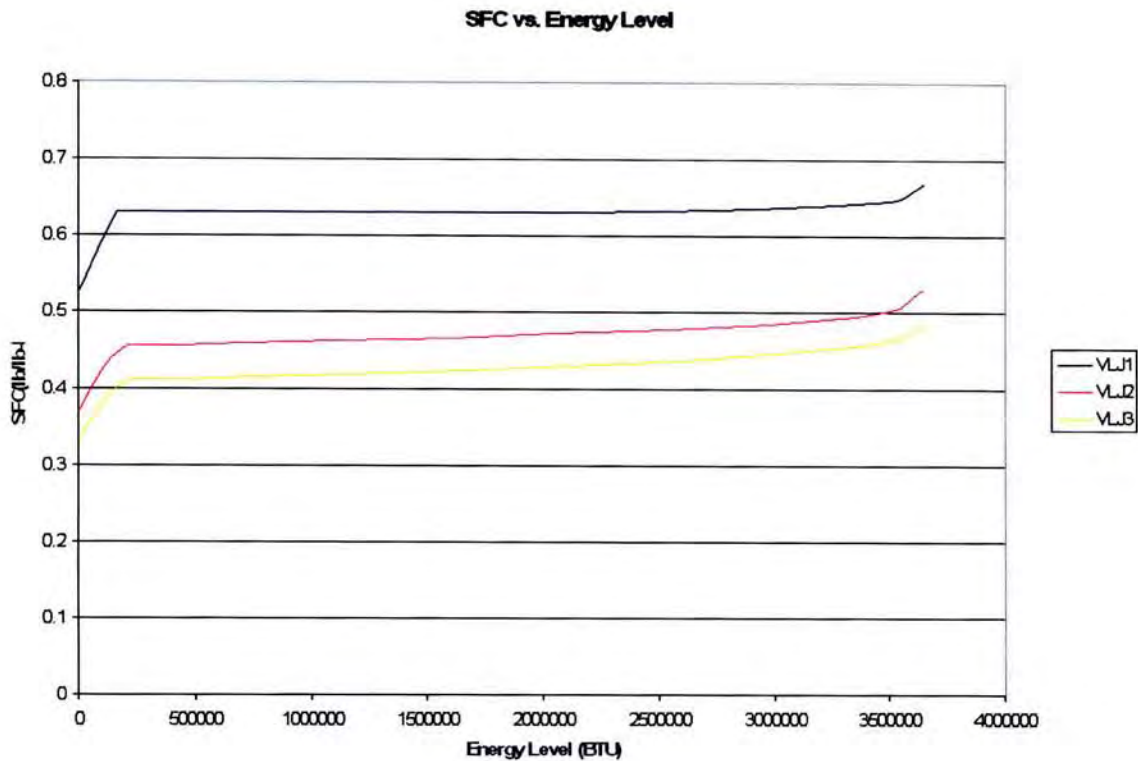
SFC vs. Energy Level

Figure 3-14: Comparison of SFC vs. Energy Level for VLJ models

figure 3-15. The curves of cumulative fuel burn diverge because the efficiencies of the later VLJ's remain consistently higher, meaning that at each time step, the newer VLJ's are always burning less fuel. This is mitigated slightly by the extra loss in aircraft gross weight of the less efficient models.

Figure 3-15 shows that the greatest gains in performance (in this case, burning of less fuel) is from VLJ1 to VLJ2, which is consistent with analysis performed earlier in the chapter with the uninstalled engines. By the time the configurations reach cruise conditions, VLJ2 burns approximately 30% less fuel than VLJ1 (with respect to VLJ1) and VLJ3 burns approximately 9% less fuel than VLJ2. Not only do newer VLJ configurations burn less fuel, they also reach cruise conditions faster. Notice from the figure that the time lapse difference between VLJ2 and VLJ3 is much smaller than that of VLJ1 and VLJ2. Shorter time spent for climb results in less time burning fuel. The fact that VLJ1 spends significantly longer climbing, and is significantly less efficient than VLJ2 explains why the cumulative fuel burn margin between the two is so great. A similar comparison of VLJ2
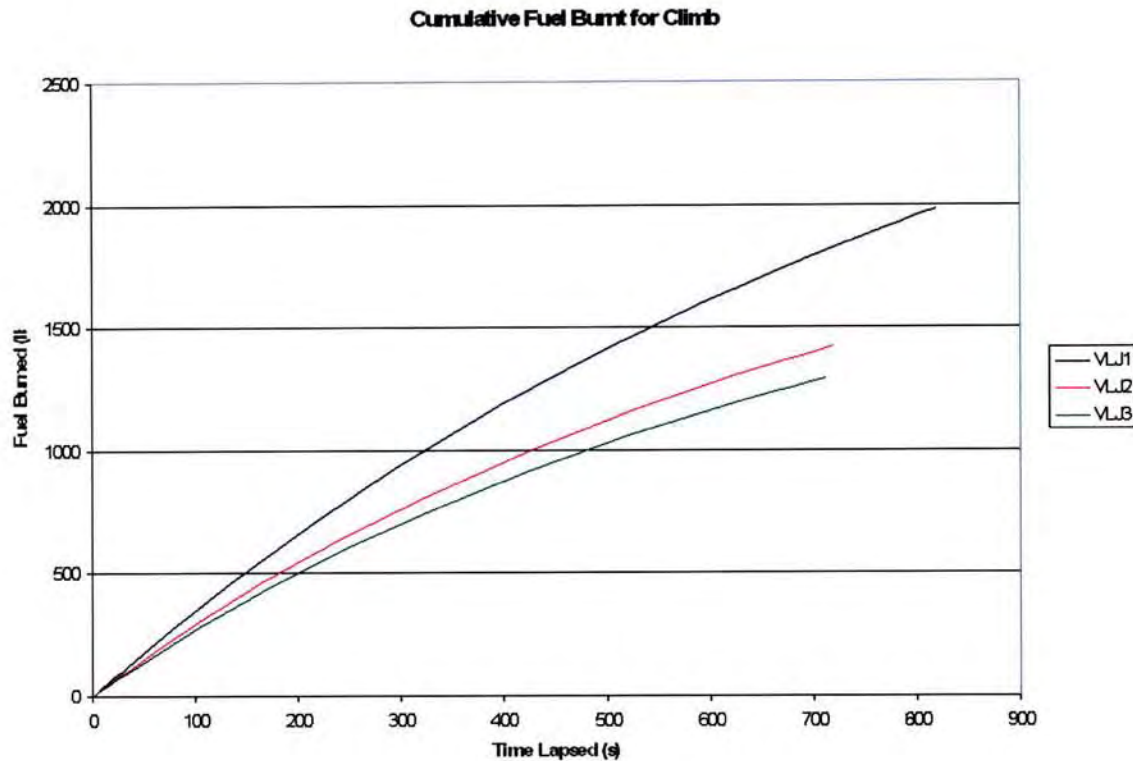
74

Figure 3-15: Cumulative Fuel Burn vs. Time

and VLJ3 explains the more modest fuel burn differential between these two configurations.

VLJ1 requires more time to climb because it produced less excess thrust than VLJ2 and VLJ3. Figure 3-16 demonstrates this. This plot shows that the excess thrust curves between VLJ2 and VLJ3 throughout the climb schedule are very similar, and in fact the gap closes at higher energy levels. Conversely, the gap between the excess thrust of VLJ1 and VLJ2 for a given energy level is much greater. This excess thrust gap narrows as energy level increased, but this effect is not seen in fuel burn since it is more than balanced out by the longer climb time and lower efficiency.

3.6.2 Cruise

Following the climb schedule, the weight of the aircraft at the beginning of cruise can be adapted by taking into account the fuel burned. While there are differences in horizontal distance traveled during climb, this distance is neglected since it is small compared to the intended range of the aircraft. For purposes of determining fuel burn and range of the
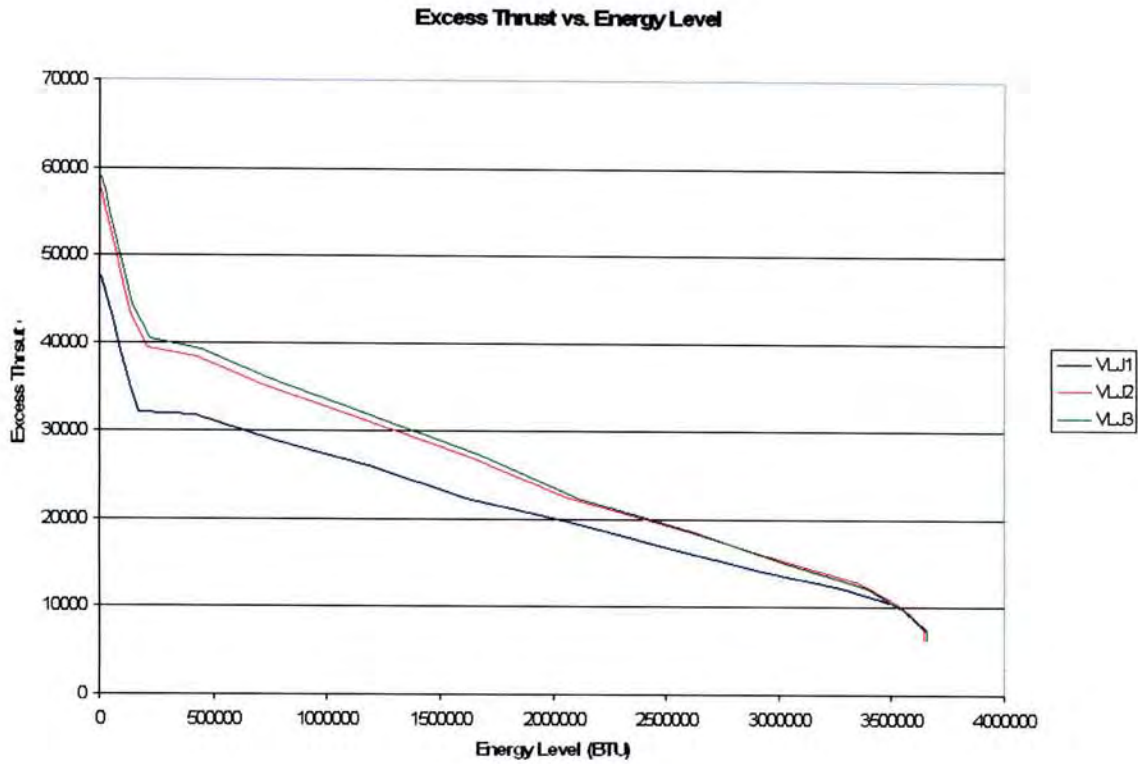
Figure 3-16: Comparison of Excess Thrust for VLJ's: Excess Thrust vs. Energy Level

aircraft, the model used for cruise is the Breguet Range Equation (2.3). For convenience:

$$Range = \frac{1}{gSFC}u_0\frac{L}{D}ln\frac{W_g}{W_g - W_f} \tag{3.9}$$

Instead of ISP, SFC is substituted in directly in equation 3.9. Recall from table 3.1 that the $\frac{L}{D}$ at cruise is 15, the flight speed u_0 is 584ft/s. Since all VLJ configurations take off at maximum gross weight, it is assumed that they start with maximum fuel capacity, which is 18,000lbs. After deducting the weight of fuel for climb, it is insightful to determine the range and endurance of each configuration. Further, for completeness of the flight envelope, two cruise missions are performed, one requiring cruise of three hours, and one of five hours. It is likely that missions may require cruise at different altitudes, but for simplicity, only the design cruise altitude and speed are examined. Also, it is assumed that landing would require a negligible amount of fuel and that the 'empty weight' of the distributed propulsion aircraft accounts for fuel reserves required in emergency situations.

Table 3.4 shows the results of this analysis. Consistent with results from earlier in the

76

Table 3.4: Cruise Comparison of VLJ Configurations (accounting for climb)

	VLJ1	VLJ2	VLJ3
Fuel burned during climb (lb)	1984.7	1420.7	1290.9
Fuel remaining for cruise (lb)	16015.3	16579.3	16709.1
Weight at beginning of cruise (lb)	68015.3	68579.3	68709.1
Cruise SFC (lb/(lb-h))	0.680	0.541	0.495
Range (nmi)	2048.5	2654.0	2920.5
Endurance (hours)	5.92	7.67	8.44
Total fuel burn: 3 hour cruise(lb)	9562.9	7364.9	6704.3
Total fuel burn: 5 hour cruise(lb)	15219.1	11700.6	10622.8

chapter, greater improvement is found from VLJ1 to VLJ2 than from VLJ2 to VLJ3. VLJ2 has a range and endurance almost 30% greater than that of VLJ1 while VLJ3 has a range and endurance about 10% greater than VLJ2.

The results from this study reinforce the notion that improvement in the next 10 years, from VLJ1 to VLJ2, will yield the most improvement in engine performance for small engines.

3.7 Summary of Technology's Effect on the Distributed Propulsion Aircraft

What newer technology offers the distributed propulsion aircraft is improved fuel efficiency, mainly through the enabling of larger BPR's. In the study of uninstalled engines, it is found that higher OPR, turbomachinery η_{poly}'s and TIT offer the improved engines VLJ2 and VLJ3 opportunity to operate larger fans, which in turn greatly reduce SFC up to a BPR of about 8. Further, new technology allows the distributed propulsion aircraft to demand more from the engines, be it through fuel efficiency or thrust density. The study of installed VLJ engines demonstrates that reduction in fuel burn is most significant from VLJ1 to VLJ2 ($\sim$ 30%), and less effective from VLJ2 to VLJ3 ($\sim$ 10%).

Chapter 4

Conclusion and Future Work

Conceptual engines for current, mid-term and far-term are developed for a distributed propulsion aircraft. The performance analyses of these engines demonstrate significant improvement in fuel efficiency, mostly from current to mid-term (approximately 20%) such that the mid-term engine SFC is comparable to that of a current state-of-the-art large engine. The inputs for these conceptual engines are justified by the historical trends observed. Parametric studies determined that SFC improves most by increasing BPR up to 8 and that TIT, FPR, OPR, and turbomachinery η_{poly} advancement enabled larger BPR's and lower SFC's. Installed performance of the conceptual engines are examined, which confirm the uninstalled findings that gains are most significant from the current to mid-term.

Finally, these results and the observation that the mid-term engine performance is comparable to that of a large, current state-of-the-art engine suggest that the technology of small engines required for commoditized and distributed propulsion will likely be developed in the next decade.

4.1 Future Work

Of particular concern to this distributed propulsion aircraft is the effect of an engine shutting down while operating under various flight conditions. When such an event occurs, the inlet flow of the neighboring engines is distorted, which is detrimental to performance but more importantly, lessens the stable flow range of the fan [19, 30].

3D CFD analysis of the distributed propulsion aircraft with an engine-out would determine whether inlet distortion to neighboring engines would lead to instability in the compressors. Such a case is important as instability in neighboring engines would indicate potential failure in many engines along the wing. The FAA also requires there to be no such instability caused to neighboring engines [34].

For development of trends, it may be useful to separate engine data by their mission requirements (maximizing $\frac{T}{W}$, range or fuel efficiency for example). More informative and reliable data on weight for engines may allow a revisit of weight estimation. Such a study would provide improved installed-engine performance analysis since the aircraft gross weight and fuel weight can be estimated and incorporated more accurately.

Finally, a study of economics of commoditized and distributed propulsion would provide another dimension in analyzing the viability of its applications today, and in the future.

Bibliography

[1] Daly, M., Gunston, B., Jane's Aero-Engines, ISSN-1748-2534, Issue 22, September 2007.

[2] Drela, M., Protz, J. M. and Epstein, A. H., The Role of Size in the Future of Aeronautics, AIAA-2003-2902, 2003.

[3] Moustapha, H., Small Gas Turbine Technology: Evolution and Challenges, AIAA-2003-2559, 2003.

[4] Cumpsty, N. A., Compressor Aerodynamics, Krieger Publishing, 2004.

[5] Kerrebrock, J., Aircraft Engines and Gas Turbines, The MIT Press, 1992.

[6] Leyes II, R. A. and Fleming, W. A., The History of North American Small Gas Turbine Aircraft Engines, The Smithsonian Institution, 1999.

[7] Wassell, A. B., Reynolds Number Effects in Axial Compressors, Trans ASME Journal of Engineering for Power 90: 149-56, April 1968.

[8] Schäffler, A., Experimental and Analytical Investigation of the Effects of Reynolds Number and Blade Surface Roughness on Multistage Axial Compressors, Trans ASME Journal of Engineering for Power, Paper no.: 79-GT-2, 1979.

[9] CFM56 website, http://www.cfm56.com

[10] Boeing website, http://www.boeing.com/commercial/737family/pf/pf_600tech.html

[11] Franz, A., Some Experiences in the Development and Application of Lycoming's T_{53} Gas Turbine Engine, American Helicopter, Vol. 46, No. 4, March 1957.

[12] Wallner, L. E. and Fleming, W. A., Reynolds Number Effects on Axial-Flow Compressor Performance, NACA Lewis Flight Propulsion Laboratory, Cleveland, Ohio, 1949.

[13] "Civil Aircraft Shipments-Calendar Years 1972-1995," World Aviation Directory, Washington, D.C.: McGraw-Hill, Summer 1995, X-41.

[14] Anderson Jr., J. D., Fundamentals of Aerodynamics, McGraw Hill, 2001.

[15] Matsunuma, T. Effects of Reynolds Number and Freestream Turbulence on Turbine Tip Clearance Flow, *Journal of Turbomachinery*, 128:166–177, January 2006.

[16] Gregory, A. T., Small Turbojet Engines- A Big Factor in Aviation, SAE Paper No. 499, 1955.

[17] Ko, Andy., Schetz, J. A. and Mason, W. H., Assessment of the Potential Advantages of Distributed-Propulsion for Aircraft, ISABE-2003-1094, 2003.

[18] Ko, A., Leifsson, L . T., Schetz, J. A., Grossman, B. and Haftka, R. T., MDO of a Blended-Wing-Body Transport Aircraft with Distributed Propulsion AIAA-2003-6732, 2003.

[19] NASA Aeronautics Blueprint: Toward a Bold New Era in Aviation, NASA, http://www.aerospace.nasa.gov/aero_blueprint/cover.html

[20] Esler, D., A New Engine Class Emerges: 'The 10K's', p38., Aviation Week, 08/01/2007.

[21] Sampath, P. and Verhiel, J. and McCaldon, K., Low Emissions Technology for Small Aviation Gas Turbines, AIAA-2003-2564, 2003.

[22] Lundbladh, A. and Gronstedt, T., Distributed Propulsion and Turbofan Scale Effects, ISABE-2005-1122, 2005.

[23] Kim, H. D. and Saunders, J. D., Embedded Wing Propulsion Conceptual Study, NASA/TM-2003-212696, 2003.

[24] Rodriguez, D., A 3D Multidisciplinary Design Method For Boundary Layer Ingesting Inlets, AIAA-2000-0424, 2000.

[25] Kurzke, J., GasTurb 10 User's Manualm A Program for Gas Turbine Performance Calculations, 2004.

[26] Masaki, S. and Mijiya, A., Advanced Materials for Aircraft Engine Applications, Proceedings of Aircraft Symposium. 36: 369-372, 1998.

[27] Walsh, P. P. and Fletcher, P., Gas Turbine Performance, Second Edition, Blackwell Science Ltd., 2004.

[28] Englar, R. J., Circulation Control Pneumatic Aerodynamics: Blown Force and Augmentation and Modification; Past, Present & Future AIAA-2000-2541, June 2000.

[29] Englar, R., J., Overview of Circulation Control Pneumatic Aerodynamics: Blown Force and Moment Augmentation and Modification as Applied Primarily to Fixed-Wing Aircraft, NASA CP 2005-213509, 2005.

[30] Longley, J. P. and Greitzer, E. M. Inlet Distortion Effects in Aircraft Propulsion System Integration AGARD Lecture Series 183.

[31] Korn, J., Compressor Distortion Estimates Using Parallel Compressor Theory and Stall Delay, Journal of Aircraft, Vol. 11, No. 9, 1974.

[32] US FAA. 25.1310 Power source capacity and distribution, Part 25- Airworthiness Standards: Transport Category Airplanes, Amdt. 25V123, 72 FR 63405, Nov. 8, 2007

[33] Bertsekas, D. P. and Tsitsiklis, J. N., Introduction to Probability, Athena Scientific, 2002.

[34] US FAA. 25.903 Engines, Part 25- Airworthiness Standards: Transport Category Airplanes, Amdt. 25V100, 65 FR 55854, Sept. 14, 2000.

[35] Gallagher, G. L., Higgins, L. B., Khinoo, L. A. and Pierce, P. W., Fixed Wing Performance: Chapter 7: Climb Performance Naval Test Pilot School Flight Test Manual USNTPS-FTM-No.108, 30 September 1992.

[36] Kuchemann, D., On the Possibility of Connecting the Production of Lift with that of Propulsion, M.A.P. Volkenrode, Reports and Translations No. 941, November 1947.